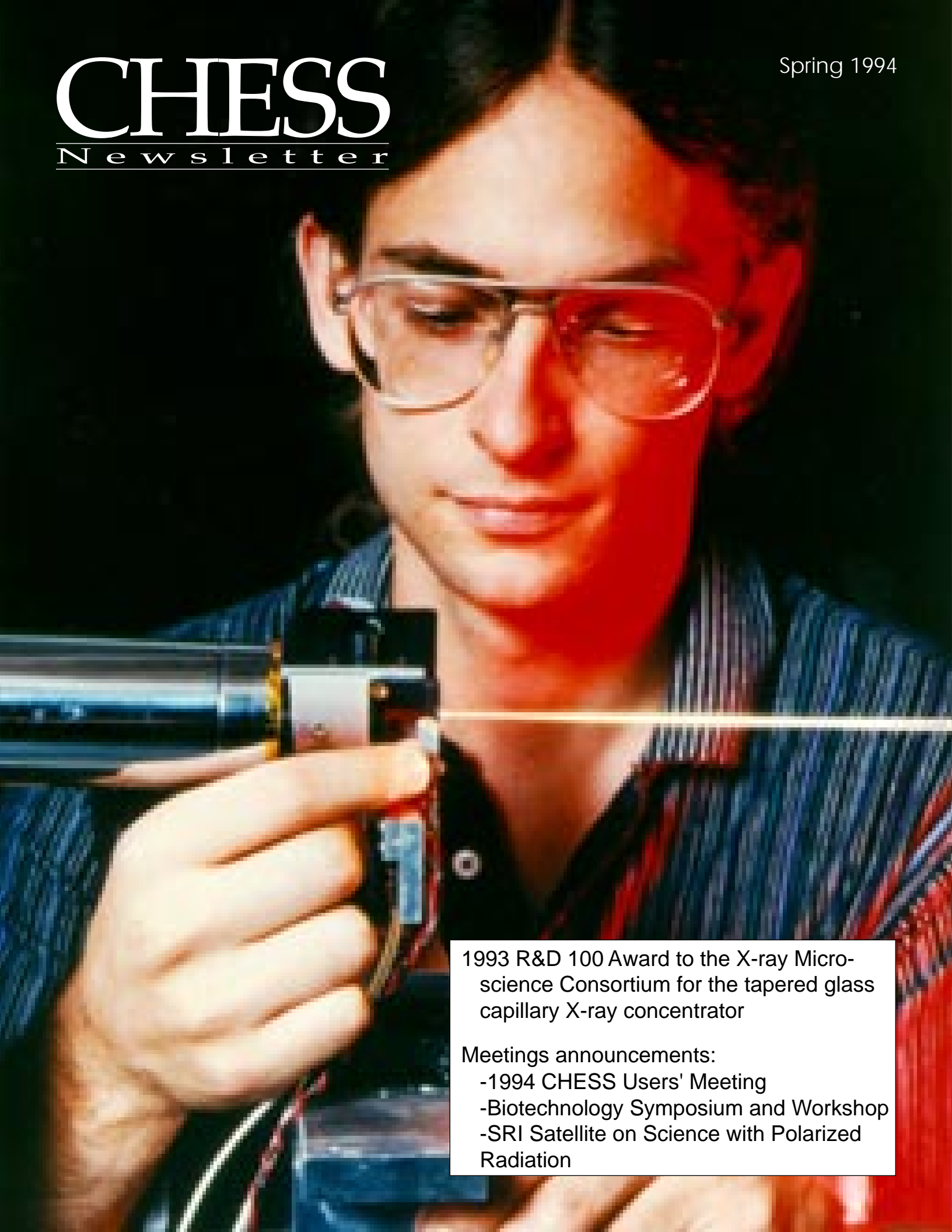


# CHESS

Newsletter

Spring 1994



1993 R&D 100 Award to the X-ray Micro-science Consortium for the tapered glass capillary X-ray concentrator

Meetings announcements:

- 1994 CHESS Users' Meeting
- Biotechnology Symposium and Workshop
- SRI Satellite on Science with Polarized Radiation



(Cover photo) Dan Thiel aligns a fiber optic taper using a visible light source. A 1993 R&D 100 Award was given to the X-ray Micro-science group at CHESS for developing tapered capillaries that can deliver hard x-ray beams smaller than 1 micron. See article page 8. (Photo: Charles Harrington, Cornell University Photography)

# CORNELL UNIVERSITY

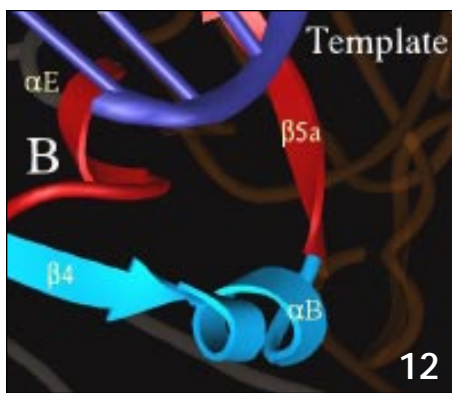
The purpose of this Newsletter is to inform the scientific community of the technical developments within the Cornell High Energy Synchrotron Source (CHESS) that could enhance their research programs and to showcase the scientific results of our users. Comments are welcomed; contact Ernie Fontes at (607)255-2959, or E-mail: ef11@cornell.edu.

## GENERAL INFORMATION

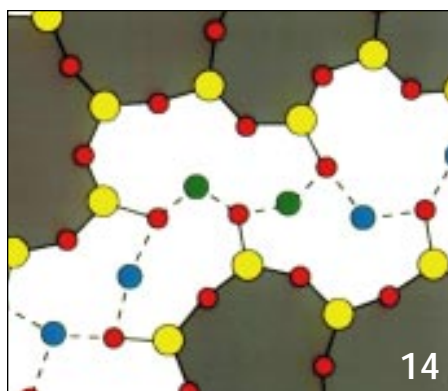
- CHESS Director's message 1
- MacCHESS Director's report 2
- CHESS Users' Meeting 3
- May Biotechnology Symposium and Workshop 4
- SRI Satellite Meeting on X-ray Science with Polarized Radiation 5
- Contacting CHESS staff 5
- Operations and scheduling 6
- New CHESS Facility Description 7

## SCIENCE

- Cornell researchers set record for smallest hard X-ray beam 8
- CHESS gives researchers a nondestructive look at calcium stores in swallows 11



12

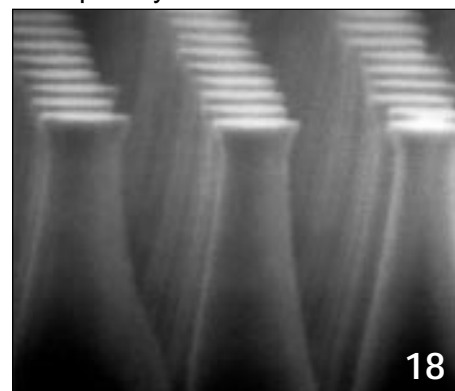


14

- Bombarding the AIDS virus Reverse Transcriptase with synchrotron radiation at CHESS 12
- Silver/sodium ion exchange in optical glasses: an XAFS study 14
- Probing surface grating structures of 300 nm periods with 1 Å X-rays 18
- Transient structure of a driven charge-density wave in NbSe<sub>3</sub> 20
- MAD phasing on F2: crystallographic results and station developments 22
- Muscle diffraction at CHESS 24
- Circular magnetic X-ray dichroism in crystalline and amorphous GdFe<sub>2</sub> 26
- Energy dispersive XAS and diffraction 28
- An atomic monolayer of Ag on the Si(111) surface 30

## DEVELOPMENTS

- X-ray collimation by multiple beam diffraction 32
- Elliptically polarized x-rays from a standard undulator 34
- High pressure facility report 35
- New CCD detector for macromolecular diffraction data 36
- A multipurpose polarimeter for x-ray studies 38
- MacCHESS data reduction capability 40



18

- An infrared thermometer for x-ray windows 42
- Crystal optics for 0.3 eV energy resolution 43
- Shock freezing of macromolecular crystals at MacCHESS 44
- 1993 publications from work done at CHESS 46
- Customized data collection and handling at CHESS 47

# CHESS Director's message

Bob Batterman

1993 was a watershed year for CHESS. Over the course of the year, we completed a 3 year funding cycle with the National Science Foundation and submitted, for the first time, a five year competitive renewal. Also spanning the course of the year, a major decision about the construction of a B-factory at either Cornell or Stanford was imminent. Needless to say, CHESS's future direction and makeup were pivotally connected to these two events.

Our NSF site visit went well, and it was recommended to the National Science Board that our funding continue, at a modest increase - subject to a decision on the B-factory. In the fall, the B-factory decision of the DOE was finally handed down - Stanford was chosen.

This news was received at CHESS with mixed feelings. On one hand, we lost the chance to build a new x-ray laboratory with continuously operating undulators and wigglers, and prospects of more than an order of magnitude increase in available flux. On the other hand, we have avoided the inevitable shut-down of two to three years for construction and commissioning.

Arguably, the loss of the B-factory may be no loss for CHESS users. Wilson Laboratory has received \$36 million from the NSF to substantially upgrade the high-energy physics program. We expect, over the next five years, a systematic increase in CESR beam currents by up to a factor of five. With increased beam currents and only short term interruptions for equipment improvements, CHESS users can continue to depend on high-flux high-intensity x-ray beams for their scientific programs.

In short, by the end of 1993, CHESS funding for the next five years had been approved by the National Science Board. In addition, MacCHESS had also completed a successful 5-year competitive renewal through the NIH.

**On the experimental floor**, the construction of the new A-line is now finished. The A1 station receives half of the radiation from our new 24 pole 1.2 T wiggler and is tunable from 5-14keV with both vertical and horizontal focussing. Measured fluxes are even greater than our premier F1 station.

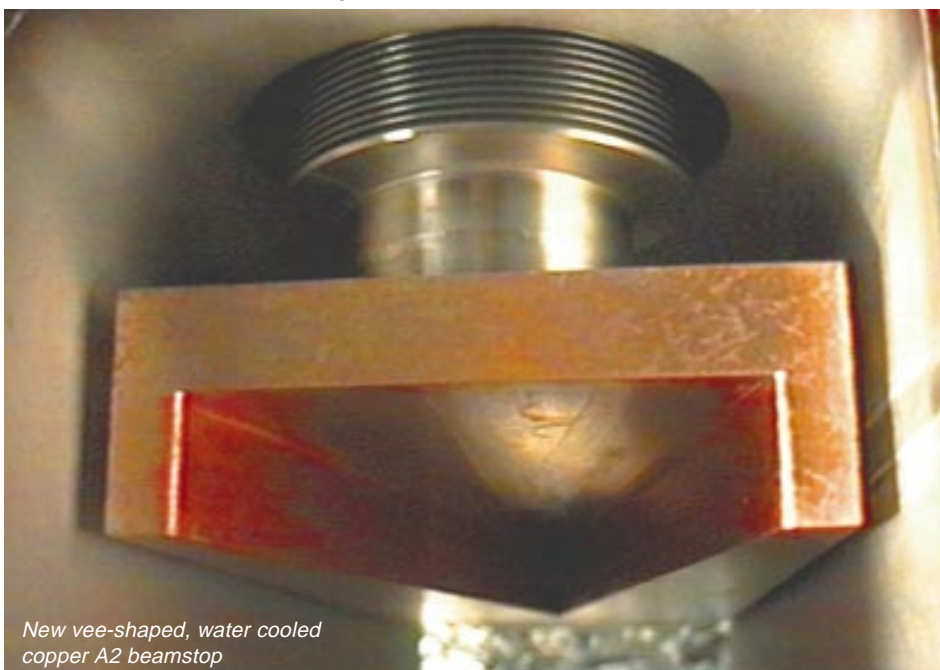


A2 receives the other half of the wiggler beam. The hutch is much larger than its predecessor. It provides a tunable high-angular resolution beam from an extremely flexible vacuum monochromator housing. Two A2 mirrors are being designed and constructed under a joint project with the APS. The double-focussing toroidal white beam mirror will provide unprecedented photon intensities and be used by APS staff as a high-heat-load test facility for optics and machine components.

**Looking ahead**, we plan a major new effort to design and construct CCD two-dimensional x-ray detectors. An ongoing collaboration with Professor Sol Gruner of Princeton University has led to the development of CCD detectors for protein crystallography at CHESS. With MacCHESS funding, we now have a 1K x 1K CCD detector. Initial runs on F1, F2 and A1 have produced data of exceptional quality (see page 36).

From this initial success, it is clear that CHESS users could benefit greatly if a variety of CCD detectors were available for all experimental stations. To this end, we plan to use part of a Keck Foundation grant to MacCHESS, and other pending support, to form a detector construction and support group within CHESS.

**In conclusion**, over the next five years we anticipate higher beam currents, more stable beam positions, and a CCD development program that provides new capabilities in x-ray imaging, diffraction, and time-resolved studies. Among others, we hope that these factors will significantly enhance the scientific programs of CHESS users.



New vee-shaped, water cooled copper A2 beamstop

# MacCHESS Director's report

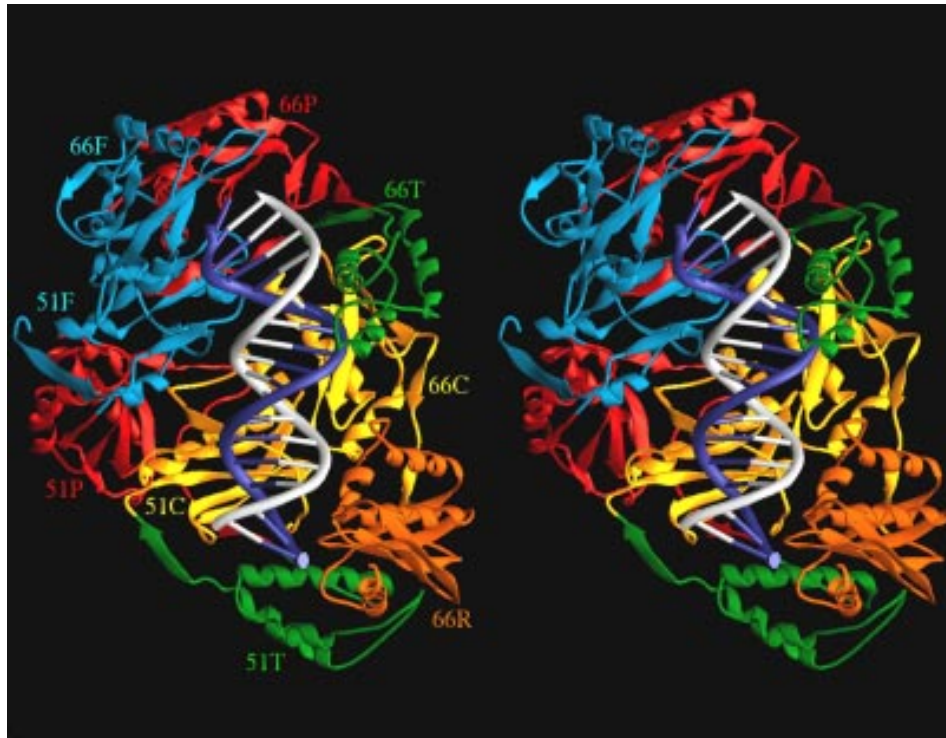
Steven Ealick

Activities in structural biology continue as a strong component of the overall research program at CHESS. After successfully competing for a five year renewal of the MacCHESS NIH Research Resource grant we have now set our sights on a research and development program that will benefit from a significant increase in our equipment budget. We have also received a generous award from the W.M. Keck Foundation and several other funding requests are pending. These new funds, coupled with the recent upgrade of station A-1, will provide substantial new capabilities for the macromolecular crystallography user community.

Currently, stations A-1 and F-1 are routinely used for macromolecular crystallography, while station F-2 has been used to develop capabilities for MAD phasing experiments. Station A-1 is now a doubly focused, tunable station and the beam intensity (as measured through a 0.3 mm collimator) is at least as high as that of station F-1. It is anticipated that a large fraction of the time on station A-1 will be available for structural biology.

Demand for beam time from macromolecular crystallographers remains high both from regular proposals and express mode proposals. The considerable back log of user requests that accumulated during the A line construction period has begun to show signs of letting up now that the A-1 station is fully operational. Nevertheless, new structural biology proposals are arriving at a record pace and it is likely that additional new resources will be needed to fully satisfy all of our user requests.

We have now added a second FUJI BAS-2000 image plate scanner, primarily for use on station A-1. With this addition we can now finally phase out the Kodak scanner and the PDP-11 computer which was required to control it. We will continue to provide 8" x 10" image plates,



Stereoview of HIV-RT taken by the Arnold group at Rutgers. See article on page 12.

however users are encouraged to purchase their own personal set to ensure the highest quality data. It seems that FUJI image plates are one item that we have not been able to make user proof. We have also purchased a Molecular Structure Corporation flash freezing system and a second MSC device has now been ordered (see article on shock freezing on page 44). We strongly encourage users to freeze crystals and will provide training and guidance to those who need assistance.

During the next few years the main MacCHESS development efforts will be in three areas: (1) CCD-based detector development, (2) MAD phasing and (3) on site data reduction. The CCD detector work is carried out in collaboration with Dr. Sol Gruner at Princeton University and has already paid off in the form of a 1K x 1K detector which is currently installed on the A-1 station (see separate article in this report by Rick Walter, page 36). Future plans include the construction of a 2K x 2K

detector and a 16 module mosaic detector.

We have now used station F-2 for several MAD phasing runs which have resulted in three new structures with several others in progress (see MAD article on page 22). Although we plan additional developments, we urge users to submit proposals for MAD phasing experiments which require the flux and energy resolution provided by station F-2.

Finally we have taken steps to ensure that users can more efficiently process the data collected at CHESS (see page 40). We now have two DEC Alpha workstations on site and plan to add additional workstations as funds become available. Both the DENZO (now DENVIEW) and MOSCO packages are implemented and users are encouraged to process their data before returning home. Drs. Wladek Minor and Zbyszek Otwinowski have kindly agreed to provide a temporary site license for those users who need to process CHESS data in the home laboratory

CONTINUED ON PAGE 4

# CHESS Users' Meeting

R.A. Bubeck (CHESS Executive Committee Chair)  
The DOW Chemical Company

The 1993 Cornell High Energy Synchrotron Source Users' Meeting was held in Clark Hall on the Cornell campus on June 22 and 23. The activities of this annual review include: highlights of current synchrotron technology and synchrotron-based studies; the fostering of improved experimental practice through topical "workshops"; promoting technical exchange between users through the use of poster sessions and one-on-one contact; and the soliciting of feedback on the facility operations from the users.

Facility reviews included status reports on CESR from Karl Berkelman, on CHESS from Bob Batterman, and on MacCHESS from Steve Ealick. The developments in A1 and A2 stations were covered by Ken Finkelstein and Joel Brock, respectively. Of course, the big development in 1993 is the coming back on line of completely rebuilt A1 and A2 beamlines and hutch facilities with enhanced light source intensity and tunability. Three CHESS initiatives were also reported upon in the areas of real-time crystal growth, X-ray microbeam science, and heat loading of X-ray optics. The intent behind these initiatives is to create critical masses of experimental expertise and capabilities for general areas of investigation that are beyond a single users' resources to develop. They also help expand general synchrotron-based experimental capabilities. For example, the X-ray optics heat load effort will benefit not just CHESS but also the Advanced Photon Source of Argonne.

The principal topic of discussion and concern during the User Group discussion was the state of current and future computer capabilities at CHESS. Virtually everyone present has been very pleased with the intensity and quality of support from the CHESS staff.

The workshop for this meeting provided a thorough coverage of the current state of the technology of 2-

dimensional detectors, which is a critical issue for the future of synchrotron-based scattering experiments. Although high-intensity x-ray sources are becoming increasingly available, many potential experiments of significant value will be limited by the availability, capabilities, and software data handling of X-ray detectors.

Both the invited talks and poster presentations covered topics related to advanced hardware, microbiology, polymer scattering, scattering from



inorganic systems, and dynamic structure studies, all of which attest to the very high level and quality of the work afforded by having CHESS as a user-friendly facility.

All are encouraged to attend the next CHESS users' meeting, scheduled for June 21 and 22, 1994.

A large graphic for the CHESS Users' Meeting 1994. It features the text "CHESS Users' Meeting" in a serif font, with "1994" in a diamond shape below it. The graphic is composed of several images: a close-up of a synchrotron component, a person's face, and a schematic diagram of the facility. The text "June 21-22, 1994" and "Cornell University" is at the bottom right.

CHESS  
Users'  
Meeting

1994

June 21-22, 1994

Cornell University

with DENVIEW. We have also entered into a collaboration with the Cornell Theory Center with the ultimate goal of real time data processing. We plan to use an IBM SP-1 scalable parallel computer for data management and processing.

Now that our funding is secure for the next five years, the Mac-CHES staff is beginning a process of refurbishment and development. Our goal is to have reliable station hardware for stations A-1, F-1 and F-2 with at least one backup for every key component. We have also begun to assess documentation. Much of the station documentation is out of date and new developments have made additional documentation necessary. As part of this process, we are developing a troubleshooting guide which will be available to users on each station.

I would like to close this report by stating that macromolecular crystallography is alive and well at CHES. New funding, new staff and new development initiatives are providing opportunities both for our user community and Cornell research programs. With announced plans to increase ring currents to 500 mA, the intensity of the CHES wiggler beams will be comparable to those of the APS wigglers. It is my belief that if our current progress continues, CHES will remain a leader in structural biology for many years to come.

## May Biotechnology Symposium and Workshop

For further information, call or write:  
Professor Steven Ealick  
Cornell University  
Biochemistry Department  
207 Biotechnology Building  
Ithaca, NY 14853 USA  
phone: (607)255-7961 (-2428 FAX)

### NEW FRONTIERS IN SYNCHROTRON RADIATION RESEARCH AND STRUCTURAL BIOLOGY

MAY 2-3, 1994  
CORNELL UNIVERSITY  
ITHACA, NY USA

The use of synchrotron radiation to record diffraction patterns from crystals of macromolecules has played an important role in structural biology. New advances in synchrotron radiation research promise to further enhance our capabilities for structural analysis. The symposium will highlight recent accomplishments in macromolecular crystallography using synchrotron radiation. Invited speakers will present structural results describing a variety of molecules including viruses, DNA binding proteins, enzymes and others. In addition, speakers will address future developments in synchrotron radiation including new beamlines, X-ray optics, X-ray detectors and third generation synchrotron sources. The symposium is intended for both specialists in structural biology and the general scientific community interested in structural results.

SPONSORED BY  
The Program in Molecular Structure  
Division of Biological Sciences  
and  
The Center for Advanced  
Technology  
(Biotechnology)

### WORKSHOP ON SYNCHROTRON RADIATION AND STRUCTURAL BIOLOGY: MEASURING AND PROCESSING X-RAY CRYSTALLOGRAPHIC DATA

MAY 3-6, 1994  
CORNELL UNIVERSITY  
ITHACA, NY USA

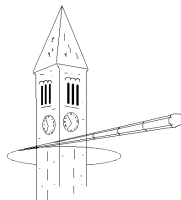
The workshop is planned as an intense three day event that is designed to familiarize the participants with all aspects of synchrotron data collection and processing as applied to macromolecular crystallography. Eight instructors will cover topics such as cryocrystallography, experimental design, X-ray detectors, data processing and data scaling. Each participant will receive hands-on training in data collection and processing. The workshop will consist of lectures, training sessions for crystal freezing and data processing, and live data collection using stations A-1 and F-1 at CHES. Participants are encouraged to bring crystals for data collection, data sets for processing or other crystallographic problems for discussion. To ensure the effectiveness of the workshop, the number of participants will be limited to 16. The participants will be selected from the applicants in order to maximize the benefit to the crystallographic community.

SPONSORED BY  
The Program in Molecular Structure  
Division of Biological Sciences  
The Center for Advanced  
Technology (Biotechnology)  
Center for Theory and Simulation  
in Science and Engineering (Theory  
Center)  
Digital Equipment Corporation

# SRI Satellite Meeting on X-ray Science with Polarized Radiation

July 24-25, 1994

Cornell University, Ithaca, NY. 14853, USA.



**MEETING** The Satellite Meeting on *X-ray Science with Polarized Radiation* will take place from 9 a.m. Sunday July 24 to 12:30 p.m. Monday July 25, 1994, at the Cornell University campus located in Ithaca, New York. The meeting is a satellite symposium of the 5th International Conference on Synchrotron Radiation Instrumentation (SRI-94). The purpose of the meeting is to bring together scientists and experts to communicate and discuss new developments and applications in theory, experiments and instrumentation related to x-ray polarization studies.

**TOPICS** The meeting will complement the SRI Conference with a variety of topics including:

- Magnetic scattering;
- Circular dichroism and optical activity;
- Resonant absorption and emission;
- Applications with soft x-rays;
- Resonant elastic/inelastic scattering;
- Special insertion devices;
- Optics and phase plates;
- Polarization characterization and polarimetry;
- Magnetic Compton scattering;
- Mössbauer diffraction and scattering.

**PRESENTATIONS** There will be invited talks and a poster session, with plenty of time for informal discussions.

For more information about the meeting, please contact CHESS Staff Scientists: Qun Shen at (607) 255-0923 (qs11@cornell.edu), or Ken Finkelstein at (607) 255-0914 (kdf1@cornell.edu).

## Contacting CHESS staff

Information: 607-255-7163  
FAX: 607-255-9001

Format: Name (EEEE) -XXXX  
Phone: 607-255-XXXX  
E-mail: EEEE@cornell.edu

Bob Batterman (bwb1)  
Director, CHESS -0917  
Don Bilderback (dbh2)  
Assoc. Director, CHESS -0916  
Assoc. Director, MacCHESS  
Virginia Bizzell  
Administrative Manager -0922  
Keith Brister (kb22)  
Staff Scientist -0920  
Park Doing  
Assist. Ops. Manager -0942  
Steve Ealick (see3)  
Director, MacCHESS -7961  
Ken Finkelstein (kdf1)  
Staff Scientist -0914  
Ernie Fontes (ef11)  
Staff Scientist -2959  
Randy Headrick (rlh6)  
Staff Scientist -0919  
Qun Shen (qs11)  
Staff Scientist -0923  
Lana Walsh (llw3)  
Proposal Administrator -7163  
Jeff White (jaw7)  
Operations Manager -7163

The CHESS and MacCHESS  
Staff includes:

Neil Ashcroft	Joe Navaie
Bob Batterman	Gary Navrotski
Basil Blank	Reinhard Pahl
Don Bilderback	Vic Pollock
Virginia Bizzell	Walt Protas
Keith Brister	John Quillinan
Ben Clark	Peter Quigley
Park Doing	Dana Richter
Steve Ealick	Sarvjit Shastri
Ken Finkelstein	Qun Shen
Ernie Fontes	Mike Sloand
Randy Headrick	Karl Smolenski
Chuck Henderson	Chris Staffa
Mark Keefe	Marian Szebenyi
John Kopsa	Dan Thiel
Jim Laluppa	Lana Walsh
Matt Marston	Jeff White

# Operations and scheduling

Jeff White

For much of 1993, the CHESS West Area was involved in a large construction project to replace the A-line and the experimental stations A1 and A2. The new A1 station has been in use since fall of '93 (except for during the dedicated undulator run) and has proven to be quite successful. The A2 station is just coming into full operation. With the reintroduction of these improved experimental facilities, we hope to start alleviating the backlog in scheduling due to construction. Although there will continue to be further upgrades of CHESS and MacCHESS equipment throughout the year, we see this time period as an opportunity to concentrate more on user assistance and we expect this will be reflected in a more efficient use of upcoming beam time.

In an effort to calibrate our own efficiency, the bar graph on the opposite page compares the beam time provided to users on each experimental station to the time which was originally scheduled. The overall delivery rate is 75%; the 25% loss was due to unscheduled equipment failures. Although we try to minimize problems, they do occasionally arise, either within CESR or our own station equipment.

Over the past two years, the majority of CESR failures were related to problems encountered with the old 14-cell RF cavity systems that power the stored particle beams. At the beginning of last year there was an extended down period due to the failure of one of those two cavities. Since then CESR has replaced all the old cavities with upgraded 5-cell cavities, and they even have the luxury of having one as a spare. Accelerator personnel have also been working hard on replacing the old style horizontal separators which caused frequent beam dumps during voltage sparkovers. The immediate benefit of these two upgrade programs is that CESR is now running with high-

er starting beam currents, typically 120 mA per particle beam, and better reliability. Further current increases are soon to come.

On the CHESS side, one of the ongoing problems with the experimental stations is the problem of x-ray beam position stability. During the October undulator run, a prototype feedback scheme was installed, which stabilized the x-ray beam position in the A2 hutch to better than 10

microns over the 3-4 hour fills. We are currently developing a feedback system that can be used during normal operations, which we hope to have in place in the near future. We are confident that the ongoing information exchange between CESR staff, CHESS staff and the CHESS users will lead to an improvement in the x-ray delivery statistics.

Below we show a Tentative 1994 CHESS Operations Schedule. Note

## Tentative 1994 CHESS Operations Schedule

January	<b>Normal Operations</b>
February	<b>Normal Operations</b>
March	Two week shutdown for general CESR maintenance
April	<b>Normal Operations</b> Proposal Submission Deadline (end of month)
May	Shutdown for Superconducting Radio-Frequency Cavity Test <sup>1</sup> Symposium May 2-3 "New Frontiers in Synchrotron Radiation Research and Structural Biology" Workshop May 3-6 "Workshop on Synchrotron Radiation and Structural Biology: Measuring and Processing X-ray Crystallographic Data"
June	<b>Normal Operations</b> following Machine Start-up CHESS Users' Meeting June 21-22
July	<b>Normal Operations</b> SRI Satellite Meeting July 24-25 "X-ray Science with Polarized Radiation"
August	<b>Normal Operations</b>
September	Shutdown for Silicon Vertex Detector in CLEO <sup>2</sup>
October	Shutdown for Silicon Vertex Detector in CLEO <sup>2</sup> Proposal Submission Deadline
November	Shutdown for Silicon Vertex Detector in CLEO <sup>2</sup>
December	<b>Normal Operations</b> following Machine Start-up

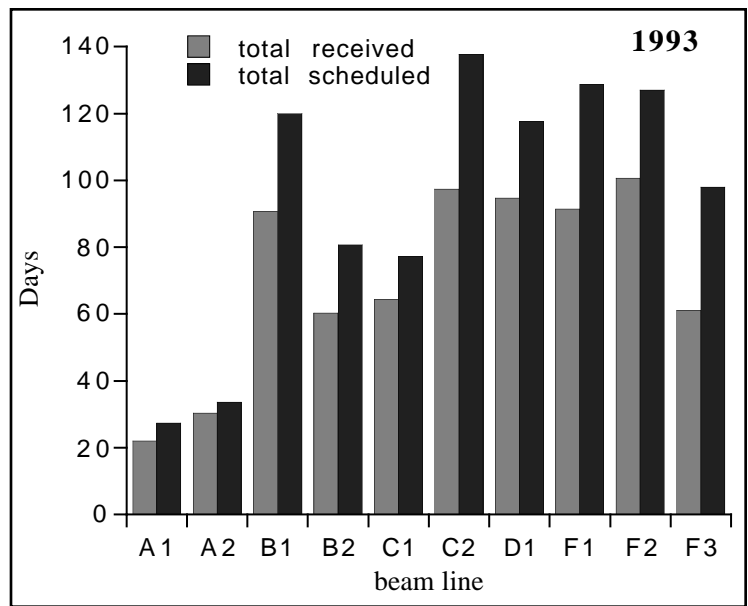
<sup>1</sup>The shutdown for the SRF test may be slightly delayed

<sup>2</sup>The shutdown of the SVX detector is *very* tentative

the long shutdown at the end of the year for the installation of a Silicon vertex detector in CLEO. This project is part of an overall plan to upgrade the high-energy physics program. During that time, and prior to the shutdown, CHES will also be working on methods to further accommodate higher beam currents and to provide higher x-ray fluxes into the experimental stations.

In order to see that the needs of the incoming user are met, we have promoted Park Doing to Assistant Operations Manager.

*A comparison of the number of days that CHES users were scheduled for beam versus the number of days received, by beam-line. The loss of time was due to unscheduled equipment failures. Note that the A-line was down for construction for most of the year, and that the east beam-lines (D and F) were not scheduled during the October dedicated undulator run. (data compiled by Lana Walsh.)*



## New CHES Facility Description

Ernie Fontes

A new CHES Facility Description is almost complete. When done, it will be distributed to all CHES users and prospective users.

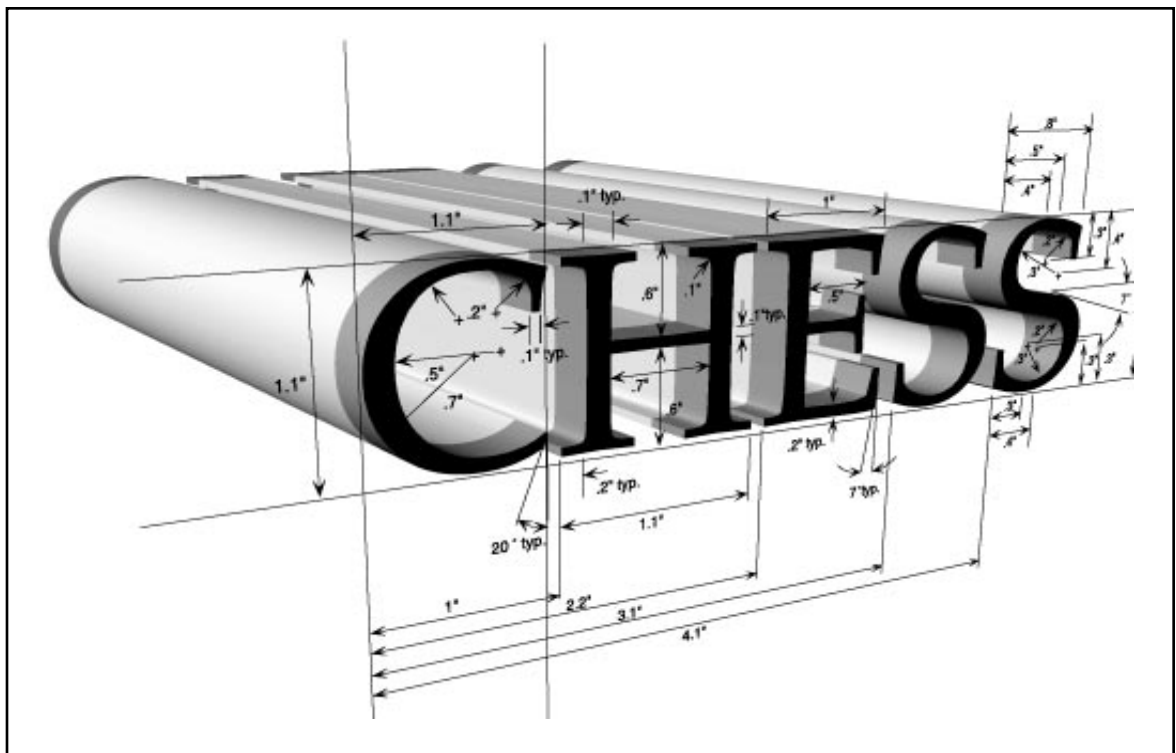
Our goal is to include enough information in the description to assist in the design of x-ray experiments.

The contents include mechanical drawings of the experimental hutches, including floor plans with heights of ceilings and door clearances, the locations of utilities (electricity, gas, vent lines, signal and high-voltage patch panels, etc.) and the overall user space around the hutches. We include x-ray flux information for the hard-bend magnet and wiggler sources, and the availability of diffractometer components, with specimen goniometer dimensions.

We also list the available support facilities (darkroom, machine shop, stockrooms), and a description of special research programs and facilities (MacCHES, High-pressure, etc.). Last but not least, we include a map to navigate from the local air-

port, local air carriers, a brief road map, and a complete list of local hotel and motel accommodations.

Any suggestions for improving the format or content are welcomed. Contact Ernie Fontes at (607)255-2959 or ef11@cornell.edu.

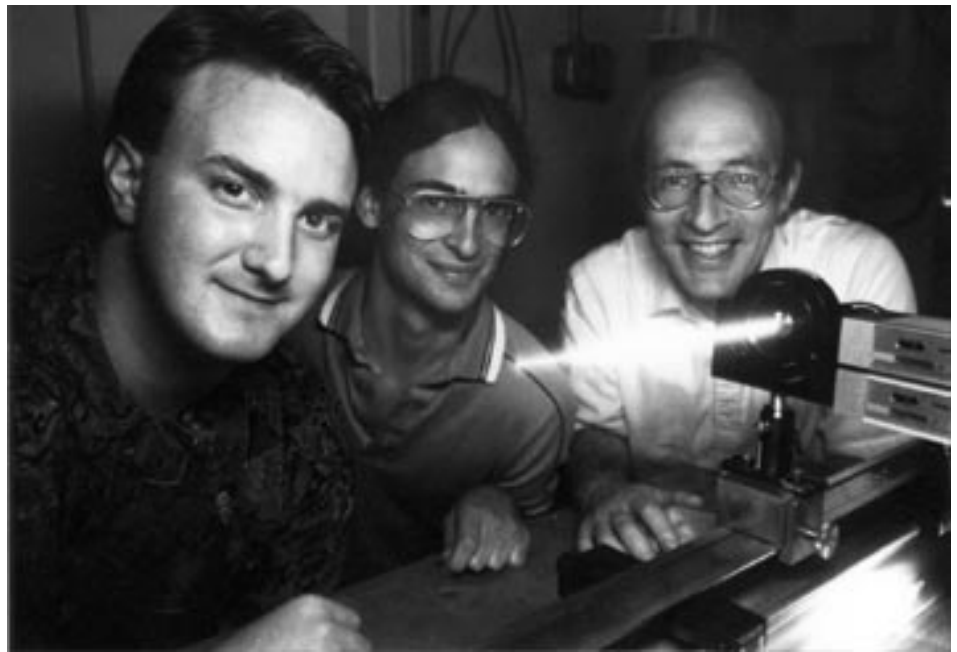


# Cornell researchers set record for smallest hard X-ray beam

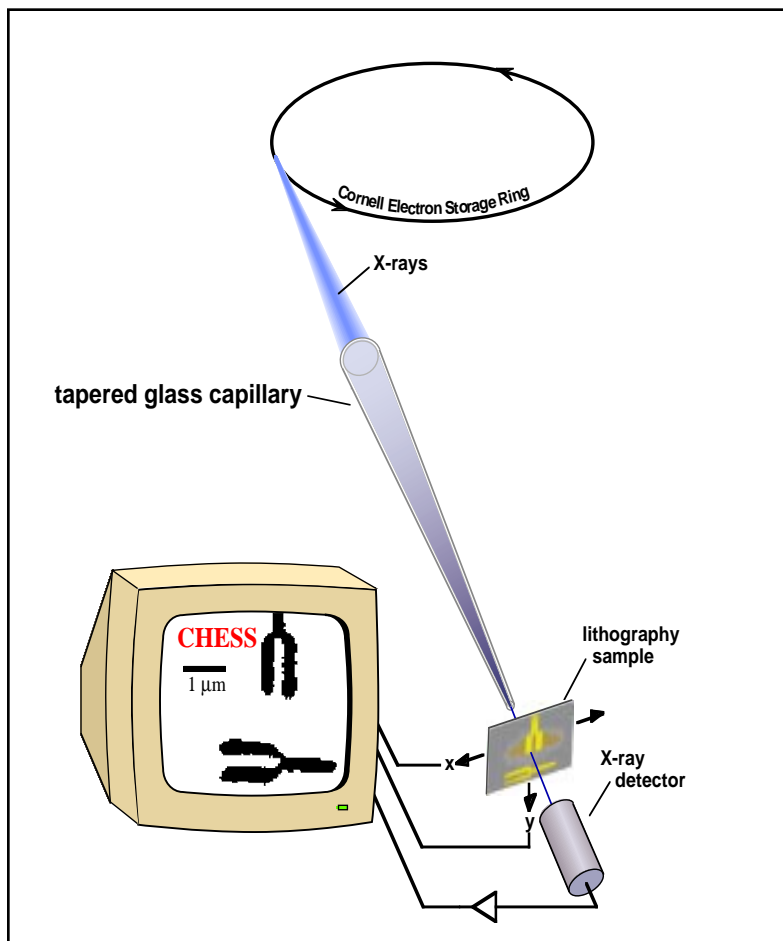
Donald Bilderback, Stephen Hoffman\*, and Daniel Thiel

Cornell staff members Donald Bilderback, Stephen Hoffman\*, and Daniel Thiel have recently developed tapered glass capillaries that compress x-rays down to a size less than one-thousandth the diameter of a human hair - the smallest beam diameter ever achieved for hard (high-energy) x-rays. X-rays confined on such a small scale have yielded the highest resolution image ever obtained with hard x-rays, with an observed spatial resolution<sup>1</sup> of 50 nanometers.

These beams can be used for the characterization of materials at an unprecedented resolution. Glass capillaries<sup>2,3,4</sup> offer significant advantages in x-ray microdiffraction studies because they can concentrate wide-band polychromatic as well as



(Above) From left, Stephen Hoffman, Daniel Thiel and Donald Bilderback, with their glass capillary at Wilson Lab. (Photo: Peter Morenus/Cornell University Photography)



(Left, Figure 1 a). Conceptual view of the imaging experiment. Wide bandwidth synchrotron radiation from a CHES bending magnet is first squeezed into a small size by a tapered capillary, then directed onto a lithographically prepared test sample consisting of a 100 nm thick gold pattern deposited on a 200 nm thick silicon nitride substrate. The absorption of x-rays in the thin gold layer produces the contrast seen as the specimen is scanned in the x-y plane. (Drawing by Chris Staffa)

monochromatic x-rays. At this time, tapered capillaries are the only x-ray optical component producing nanometer spatial resolution with high energy x-rays. Other components such as phase zone plates<sup>5</sup>, Bragg-Fresnel lenses<sup>6</sup>, and Kirkpatrick-Baez mirrors<sup>7</sup> are producing focused, nearly monochromatic x-ray beams on a length scale 10 to 100 times larger.

The leaded glass capillary takes the x-ray beam generated at CHES and compresses it because the glass is tapered to a fine point. The glass tubes, which can be made to a variety of diameters, act as a funnel for the beam of x-rays, successively bouncing x-rays off the smooth inside wall by total reflection as they pass down the length of the tube. The beam leaving the capillary is smallest in size right at the tip and has a divergence of a few milliradians.

Virtually all of the traditional methods of studying the nature of a sample with x-rays such as x-ray dif-

fraction (monochromatic and Laue, wide- and small-angle scattering, etc.), elemental fluorescence mapping, near and extended edge absorption spectroscopy, tomography, radiographic imaging, etc., are usable with tapered capillaries. Recent experiments in imaging and Laue diffraction serve to illustrate how capillaries can be applied to the emerging field of x-ray microscience.

A record-setting spatial resolution of 50 nm was observed in an imaging experiment on the CHESS B2 bending magnet station ( $E_{\text{crit}}=10\text{keV}$ ,  $E=5.3\text{GeV}$ ,  $I=80\text{mA}$ ) with a test sample placed a few microns away from the tip. The 4 cm long monicapillary was drawn by Dan Thiel. The sample consisted of a 100 nm thick gold stripe pattern prepared on a silicon nitride wafer 200 nm thick. Figure 1 shows the conceptual outline of the imaging experiment. A flat total-reflection mirror upstream of the capillary (not shown) set an upper energy cutoff of 8 keV. The lower end of the bend magnet spectrum was approximately 5 keV and was determined by the length of the air path and the thickness of the beryllium windows on the beamline. The contrast in the image (figure 2) was obtained from x-rays being absorbed by an extra 4% as the beam was scanned over the 100 nm thick gold portion of the sample.

This demonstration experiment was done under far from optimal conditions. The beam was intensified in flux (x-rays/sec/mm<sup>2</sup>) by only a factor of 50 over the incident beam. We have observed gains as high as 960 in other pipettes<sup>8</sup>.

A series of Laue diffraction experiments were also performed to show that microbeam diffraction could be achieved with these tiny beams and vanishingly small amounts of crystalline material. The wide-bandwidth Laue method was chosen over the monochromatic rotation method for its simplicity. The exposure time is 100 to 1000 times faster than for the monochromatic rotation method and no oscillation of the crystal is needed during expo-

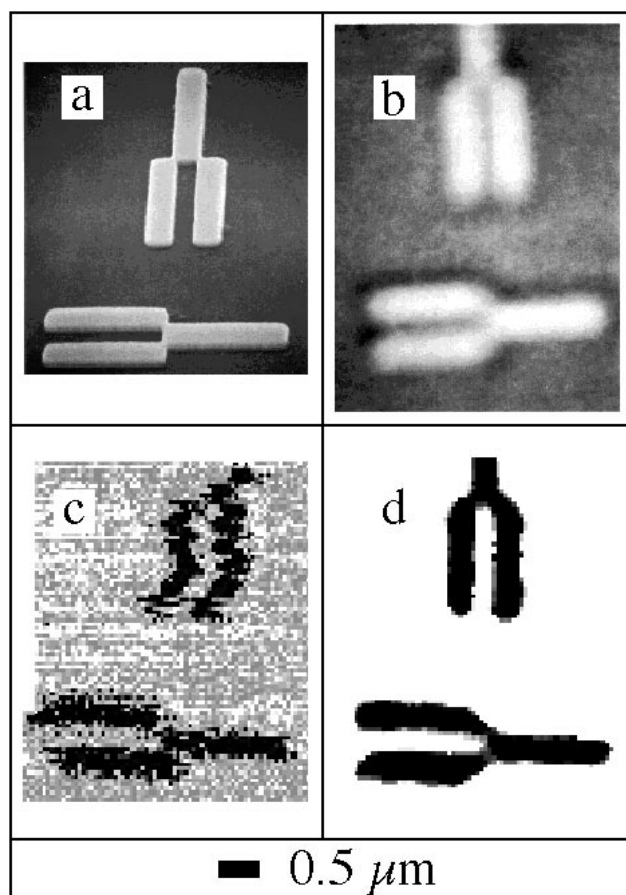


(Figure 2) a) The line widths of the features are 300 nm wide in as seen in scanning electron micrograph. b) Optical image obtained with a visible-light microscope with a numerical aperture of 0.9. The image is fuzzy because the structure is below the resolving power of the light microscope. c) Unprocessed x-ray absorption image. The image was formed from a two-dimensional scan with piezoelectric crystals consisting of 50 nm by 50 nm pixels. d) X-ray image after processing. The data in each row were horizontally shifted to compensate for the effects of spatial drift (thermal, air currents, electronic, etc.). A median processor was then applied, which averages all pixel intensities located in a circle of radius of 2 pixels.

sure. Figure 3 shows a lysozyme diffraction image taken with a 5.6 micron diameter beam, about 1/20th the diameter (and 1/400th the area) of the 100 micron diameter collimators typically used for small protein single crystals. Obviously smaller diameter beams may be employed, but the lower bound in size will probably be determined by the x-ray radiation resistance of the sample and/or the unit cell size.

In a separate study, radiation insensitive single crystal films of silicon and gold were examined. We were able to observe Laue diffraction from a 50 nm thick gold single crystal with a 300 nm diameter beam. In contrast to the perfect round spot shapes observed with a perfect 2 micron thick silicon wafer with the same capillary, the gold Laue spots were radially streaked, consistent with a mosaic spread of a few degrees. The same streaking was observed with larger diameter beams up to 45 microns in size. We conclude that the dimensions of the mo-

saic crystal domains were less than our beam size of 300 nm.

In the future, we hope to fabricate optimally-figured tubes which should come closer to achieving the higher gains that are theoretically predicted. It is also possible, in principle, to make smaller beams, down to perhaps 2 to 10 nm size, at which size the skin depth of x-rays penetrating into the glass turns out to be the fundamentally limiting parameter.

The capillary technology described here has received an R&D 100 Award from *R&D Magazine* for one of the year's most significant products in 1993. The individuals involved in this effort are Donald Bilderback; Stephen Hoffman, and Daniel Thiel of Cornell University; Aaron Lewis of Hebrew University, Jerusalem; and Edward Stern of the University of Washington. The lithography work was performed at the National Nanofabrication Facility at Cornell University. The work was supported by the National Science

Foundation and the National Institutes of Health.

### Call for Support of Microscience X-ray Station at CHESS.

The microscience group at Cornell is interested in new applications of microbeams to science. For instance, we plan to look at fibers of a few microns in diameter in the near future using wide angle x-ray scattering to determine the structural differences between the skin and core of composite fibers. We also plan to map the strain, microstructure, and composition of tiny polycrystalline crystals using high spatial resolution with microdiffraction and microfluorescence measurements. Many biological experiments are also in the conceptual stage.

We are in the process of raising funding for specific equipment to outfit a CHESS beamline for these kinds of investigations. A limited amount of work is being supported from the CHESS and MacCHESS organizations, but we need to generate additional support in the Material Science community. We are seeking funding to build a specialized beamline over a several year period of time, including a person to help construct and oversee collaborative experiments (miniature monochromators, translation stages, fluorescence detectors, tiny 2-D CCD detectors, etc.). We need to raise about \$200,000 to \$400,000 to adequately fund these efforts. Additionally, we would like to attract visiting scientists to come and join us in these efforts for some period of time. If you are interested in contributing in time, effort, or even funding for these activities, please contact Don Bilderback by phone at 607-255-0916 or via Internet at [dhb2@cornell.edu](mailto:dhb2@cornell.edu).

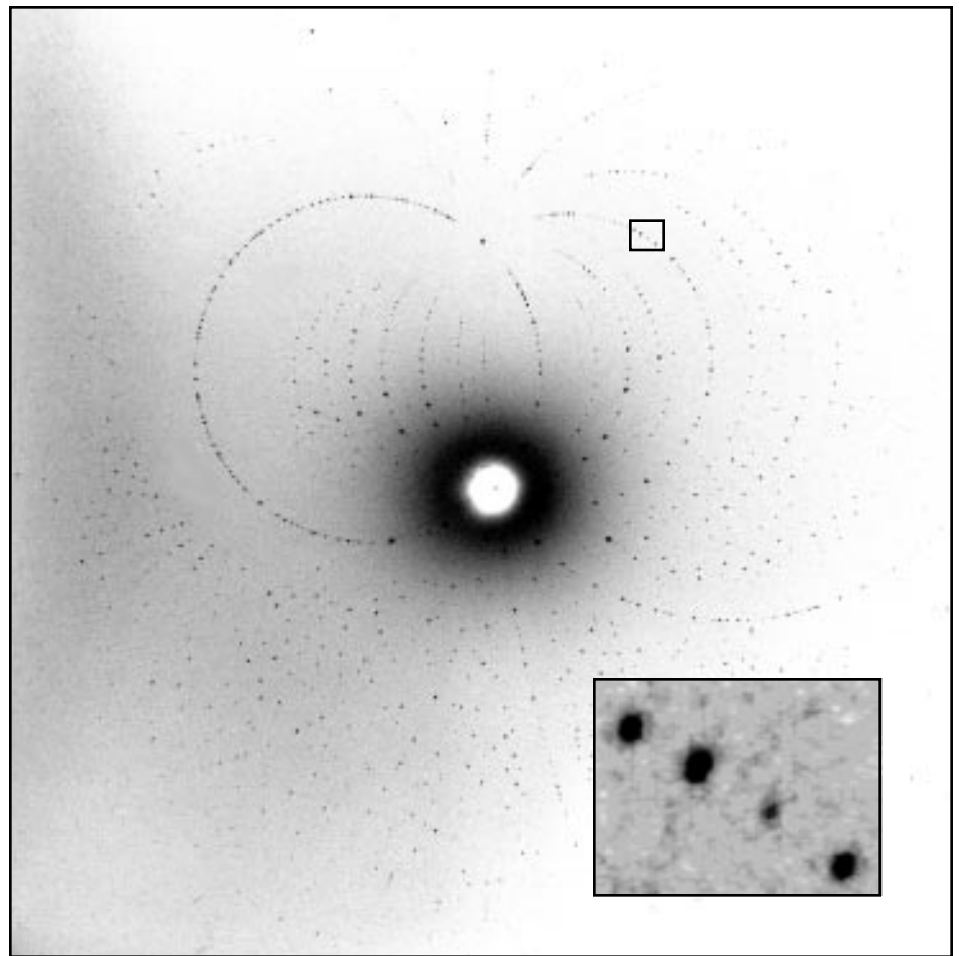


(Figure 3) Laue diffraction from a lysozyme crystal taken with a 5.6 micron diameter x-ray beam on Kodak DEF film with a spectrum extending from 5 to 25 keV. The room temperature sample was translated 3 microns every 24 seconds during the 300 second total exposure to minimize the radiation damage to the sample. The crystal diffracted to 2.2 Å resolution. The divergence of the microbeam was 2.6 mrad as determined by the spot size measured on the x-ray film. This experiment shows the possibility of using tapered capillaries in the study of biological materials that do not form the large (of order 100 micron) size needed for conventional x-ray crystallography.

\* Presently at Northwestern University

1. D. H. Bilderback, S. A. Hoffman, D. J. Thiel, *Science* **263**, 201 (1994).
2. E. A. Stern, Z. Kalman, A. Lewis, K. Lieberman, *Appl. Opt.* **27**, 5135 (1988).
3. P. Engström *et al.*, *Nucl. Instrum. Meth.* **A302**, 547 (1991).
4. D. J. Thiel, D. H. Bilderback, A. Lewis, E. A. Stern, *Nucl. Instrum. Meth.* **A317**, 597 (1992).
5. W. B. Yun *et al.*, *Proc. SPIE* **1740**, 117 (1993).
6. A 0.8 micron beam at 15 keV (submitted) has been made at the ESRF, Grenoble from a Bragg Fresnel lens designed by A. Snigirv and

V. Aristov, private communication from C. Riekell, 1993.

7. LBL-28001 UC-411, *Center For X-ray Optics - 1989,4-15*(1990).
8. Applications of Single Tapered Glass Capillaries: Submicron X-ray Imaging and Laue Diffraction, S. A. Hoffman, D. J. Thiel, and D. H. Bilderback, *Optical Engineering* **33**, 303 (1994).

NOTE: A version of this article will be published in *Synchrotron Radiation News*, May/June 1994.

# CHES gives researchers a nondestructive look at calcium stores in swallows

Reinhard Pahl\* and David Winkler\*\*

\*Humboldt Fellow, CHES

\*\*Section of Ecology and Systematics, Div. of Biological Sciences, Cornell University

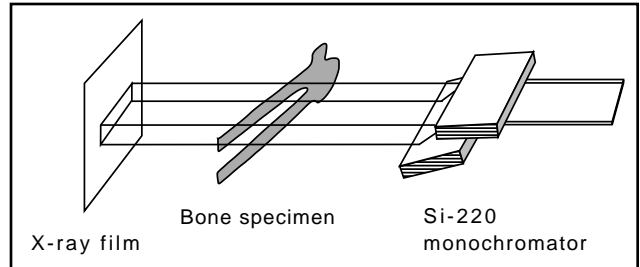
Every spring, when millions of small songbirds are returning from their southern wintering grounds to begin breeding, these birds are struggling to garner as many resources as possible to allow the earliest and most prolific reproduction they can manage. Of all the resources that a laying female has at her disposal, there are three that are likely to limit egg-laying: protein, fat and calcium. An ongoing research program has been designed to study the importance of fat and protein stores to reproduction in tree swallows, a small insectivorous bird that occupies nest-boxes in open areas throughout the U.S. Although we have methods for assessing the protein and fat stores of swallows on living specimens, we have not previously been able to assess the calcium stores without sacrificing the bird.

Calcium is likely to be important, because it is one of the principal constituents of egg shells. The amount of calcium that must be shunted through the laying females' system and deposited in shells every day is far in excess of the amount that she could obtain from the environment. All birds must rely on stores of calcium that can be built up before the breeding season and rapidly depleted during laying. Previous research on pigeons and chickens has indicated that the principal site for calcium storage is in the hollow interiors of their leg bones.

In a recent series of experiments on legs from collected swallows, one of us (RP) has recorded X-ray images that indicate the potential for quanti-

fying calcium stores in live birds without harming them. The leg bones of these birds are tiny (about 1.5 mm in diameter), and the challenge has been to visualize the interiors of the bones with sufficient acuity to measure the differential development of calcium deposits within them.

The experiments have been carried out at CHES beamline D1 using X-rays at 12 keV. Utilizing an asymmetric-cut Si-220 monochromator, a beam with a large cross section and an energy resolution of  $\Delta E/E=10^{-5}$  was obtained. Radiographs of the bone samples were stored on Kodak high-resolution X-ray film. Analysis is being done after digitizing the recorded information. The spatial resolution obtained is about 15  $\mu\text{m}$ . For future experiments a CCD system will be used, which will allow not only a much faster data acquisition but also 3-dimensional tomography

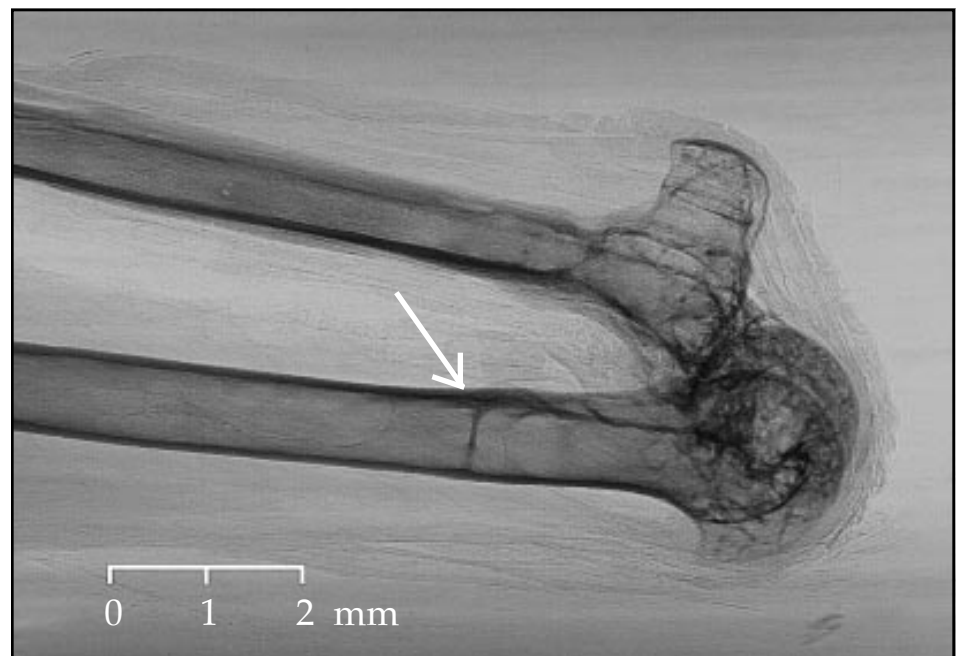


*Schematic experimental arrangement for radiography measurements at D-line.*

of the samples.

The use of the synchrotron radiation at CHES offers several advantages over other sources. The collinearity and the monochromatization of the light eliminates distortions present in images made with conventional X-ray sources. Most importantly, the high intensity of the beam (appr.  $10^9$  photons/sec) allows short exposure times (<0.4 seconds) that can be used with living birds.

A pilot test to discriminate differences among birds that are reflected in the size, thickness and number of eggshells the females lay is being planned for spring 1994.



*Lateral view of the tibiotarsal-tibiometatarsal joint from tree swallow collected during fall migration. Note that the bones are hollow in the long parallel-walled portions away from the joint. The arrow indicates small growths of material which appear to be associated with the storage of calcium for egg-laying.*

# Bombarding the AIDS virus Reverse Transcriptase with synchrotron radiation at CHESS

Jianping Ding

Center for Advanced Biotechnology and Medicine (CABM) and Rutgers University, Department of Chemistry

When the research article "Crystal structure of human immunodeficiency virus type 1 reverse transcriptase complexed with double-stranded DNA at 3.0Å resolution shows bent DNA" was published in the *Proc. Natl. Acad. Sci. USA* 90 (1993), the entire research group working on RT at CABM and Rutgers University could no longer contain their excitement and joyfulness; not only because this article represented a major breakthrough in the understanding of the structure and function of a very important enzyme, but, also, it symbolized that their persistence and hard work over the past six years would finally be acknowledged.

For six years, the RT group led by Dr. Eddy Arnold, an Associate Professor of Chemistry at Rutgers, had worked very hard to visualize and solve the crystal structure of human immunodeficiency virus type 1 reverse transcriptase (HIV-1 RT). HIV-1 RT is the enzyme which is responsible for the catalytic transformation of the AIDS virus RNA genome into a double-stranded DNA which can be permanently integrated into host cell chromosomes and cause the deadly disease, acquired immunodeficiency syndrome (AIDS).

Looking back over the six years, every member in the group had countless sleepless nights; we had frustration and encouragement, pain and joy, we had failures and eventually successes. Not many of us can really tell the entire story. However, people can never forget the synchrotron trips to CHESS, in Ithaca, New York. Without the synchrotron facility at CHESS we could not have achieved these accomplishments. Also, every single day we spent at CHESS was colorful and full of different kinds of stories.

## The dark night in the winter

In 1987, after having worked in the laboratory of Dr. Michael Rossmann at Purdue University for five years to complete the structure determination and refinement of human rhinovirus 14, one of the common cold viruses, Dr. Eddy Arnold moved on to establish his own macromolecular crystallography laboratory at CABM and Rutgers University. Though it might have seemed to be too ambitious and risky for a young scientist, Dr. Arnold had no hesitation in choosing to investigate the molecular structure of HIV-1 RT as the first major project in his lab.

AIDS, caused by HIV, continues to be one of the world's most serious health problems, and current protocols are not adequate for either prevention or successful long-term treatment of the disease. HIV-1 RT is a potential therapeutic target of many inhibitors against AIDS. Indeed, nucleoside analog inhibitors of RT, such as AZT, ddI, and ddC, are clinically effective drugs for treating HIV-1 infection. However, their effectiveness is limited by toxicity, which may reflect inhibition of cellular polymerases and/or alteration of nucleoside pools, and the mechanism of RT inhibition by these compounds is also unknown. It is anticipated that the three-dimensional structure of HIV-1 RT will provide a structural basis for understanding the inhibition mechanism and the mechanism of antiviral resistance to RT, which may lead to the development of improved inhibitors for the treatment of AIDS.

In the first three years, our laboratory struggled to crystallize RT crystals that could diffract X-rays. More than two years efforts were in vain and we were frustrated. However, we did not give up and continually used a variety of approaches to

determine the proper crystallization conditions. Finally, after unprecedented efforts particularly by Dr. Alfredo Jacobo-Molina and Art Clark, our group emerged as the one of a few groups able to successfully crystallize RT crystals. We had succeeded in obtaining crystals in several morphological types with size of up to 1.0 mm × 1.0 mm × 0.5 mm. This was really a breakthrough in our work. Unfortunately, as we mounted the crystals on the Xuong-Hamlin Mark II area detector in our home X-ray laboratory, the crystals refused to diffract X-rays; there were no spots on the image at all.

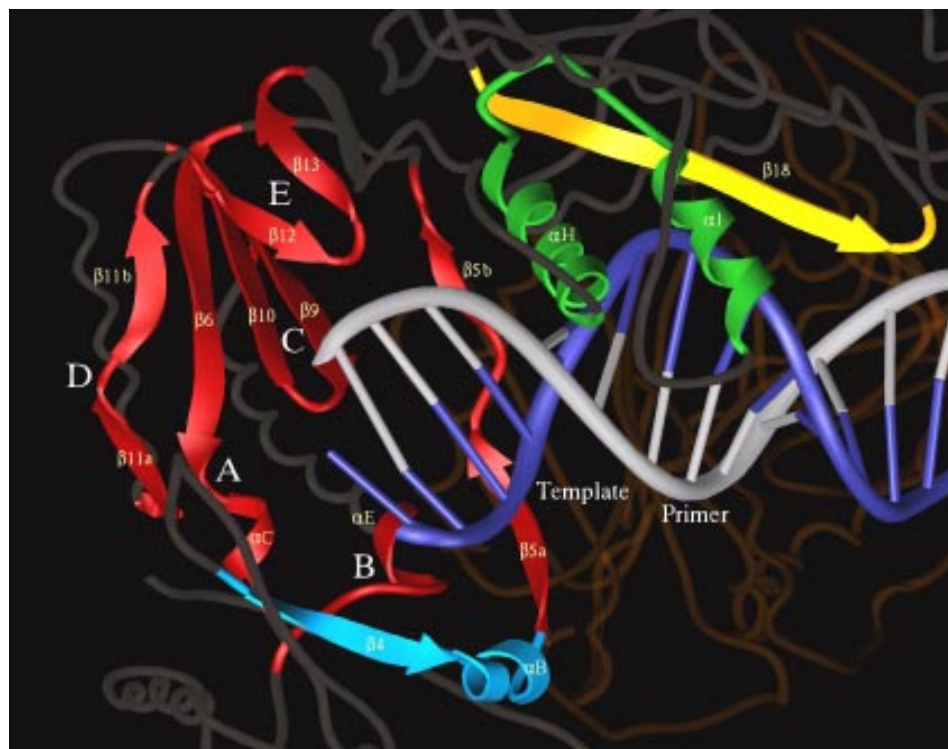
Our next hope was to bring the crystals to CHESS where the group was already collecting data successfully from virus crystals. CHESS is equipped with one of the most unique synchrotron facilities in the world; the synchrotron radiation there is extremely bright with short wavelengths which can extend crystal lifetime via reduced radiation damage. Even though the crystals of RT gave a no-spot diffraction pattern at the old A1 station with wavelength  $\lambda=1.55\text{\AA}$ , they did diffract X-rays to 6Å resolution at the F1 beam line with wavelength  $\lambda=0.91\text{\AA}$ . This success initiated more frequent synchrotron trips to CHESS for the purpose of RT data collection.

## A big event in the laboratory

Almost everyone in our lab has experience working in the synchrotron at CHESS. Synchrotron trips have become a big event in our entire lab, not only for the RT group. Usually months before a scheduled synchrotron trip, the preparations are in progress; crystallization, crystal searching to distinguish different kinds of crystal quality and size, heavy atom soaking, and ordering of

materials and equipment needed at CHESS. One member of the group whom we were always joking about because of his organizational tendencies was Dr. Raymond Nanni. He was such a careful and meticulous person that he prepared boxes with corresponding lists for each workstation at CHESS. No single item could be missing or be misplaced in the boxes. Of course, this effort proved to be very helpful and we are still benefiting from following his lists after he left this lab. Nevertheless, mistakes are still unavoidable. On a trip during winter, the synchrotron team drove a van full of boxes and equipment to Ithaca. As they prepared to shoot the crystal, they realized that they had brought everything they needed *except* the crystals. They had to call back to the lab and ask someone to drive overnight to Ithaca with the crystals.

In order to make our task at CHESS as painless as possible, we organized our team personnel into workstation subgroups; camera (taking photographic diffraction data), cold-room (mounting crystals), dark-room (developing photographic films), and scanner (scanning phosphor image plates). For best use of the precious beam time allocated for synchrotron data collection, the whole team is divided into two shifts and we work around the clock. For refreshment, the lounge room and the refrigerator were full of food, fruits, and drinks purchased from the local supermarket. Although everybody complained about these arrangements, no one wanted to spend an hour at a restaurant to have a good meal because people realized that sleeping is more crucial than eating. Especially for the night-shift people, after dancing with the RT crystals for more than twelve hours, they could simply fall asleep sitting on a chair in the early morning during the CESR injection. However, in celebrating the collection of a number of new datasets after five days and nights of work, everyone still looked very energetic and enthusiastic.



### Hope sprouts in the spring

As long as we saw the diffraction spots on the diffracting image of RT crystals, even if only to about 5 Å resolution at F1 station, we knew that a bright future was ahead. The winter was over, spring was just ahead. The low resolution diffraction of RT crystals greatly inspired us and fueled our enthusiasm. We tried various approaches to further improve and optimize the crystallization of HIV-1 RT. These included protein engineering aimed at changing specific amino acids on the surface, making complexes with antibody fragments, making complexes with synthetic nucleic acids that mimic template-primer substrates, and soaking the crystals in different conditions. Through these efforts, the quality of the crystals was significantly improved and especially for the crystals of the ternary complex of RT/dsDNA/Fab28, they diffracted X-rays increasingly better.

With these crystals, we were able to collect entire diffraction datasets to about 6 Å resolution with a single crystal using the Xuong-Hamlin Mark II area detector system at our home X-ray laboratory. Although the analyses of these results

*Structural elements near the HIV-1 RT polymerase active site that make potential contacts with the DNA; those corresponding to conserved motifs are shown and the secondary structural units are labeled.*

greatly facilitated the interpretation of heavy atom derivatives and initial structure determination of RT at 7 Å resolution, the resolution limit of the diffraction data could not permit us to solve the structure of RT in atomic detail. At the same time, the experiments carried out at CHESS made great progress: the diffraction of ternary complex RT/dsDNA/Fab28 crystals advanced from 5 Å to 4 Å, 3.5 Å, 3 Å, and finally to 2.8 Å resolution at -15°C using the beam at the F1 station of CHESS. Using the same crystallization and soaking conditions, we have been able to routinely collect a more complete native dataset to 2.8 Å resolution, more than twelve heavy atom derivative datasets in the resolution range of 3.0-4.0 Å for the RT/dsDNA/Fab28 crystals, and a number of datasets with comparable resolution for other RT complexes. This represented the beginning of a new era in the structure determination.

### Summer makes people crazy

In the spring of 1992, after bring-

CONTINUED ON PAGE 17

# Silver/sodium ion exchange in optical glasses: an XAFS study

S. N. Houde-Walter and J. M. Inman  
The Institute of Optics  
University of Rochester

Ion exchange is widely used to alter the optical properties of glass for application in emerging optical and photonics technologies (e.g., gradient-index imaging systems, optical waveguides, micro-optic lens arrays). The resultant dopant profile determines focal lengths, optical aberrations, and coupling efficiencies with optical fibers.<sup>1</sup> Several aspects of the ion exchange (i.e. concentration dependent diffusion and presence of certain oxides in the glass compositions) are critical in determining the quality of a given optical component and are thought to be somehow related to glass structure. However, the structural chemistry of this process is far from understood.

In recent years X-ray Absorption Fine Structure (XAFS) has become a pivotal technique in determining local environments in multicomponent glasses. Early XAFS results lead to the notion that in simple sodium silicate glasses, alkali ions form clusters or channels that are interlaced

throughout the silicate former matrix.<sup>2</sup> Ion exchange is expected to occur primarily through such channels and the measured atomic environments of alkali and network forming cations have recently been used to predict alkali ion transport properties in binary silicate glasses.<sup>3</sup>

We recently conducted a study on Ag/Na ion exchange in aluminosilicate glasses in collaboration with G. N. Greaves. The glass compositions and Ag/Na ion exchange pair are representative of those used in the fabrication of commercial optical waveguides and gradient-index optical components. We single out aluminosilicate glasses because alumina ( $\text{Al}_2\text{O}_3$ ) has a profound effect on glass properties. For example, the diffusivities of mobile cations improve as  $\text{Al}_2\text{O}_3$  is added to the alkali silicate glasses, reaching maximum values when the relative concentration  $R = [\text{mol}\% \text{Al}_2\text{O}_3]/[\text{mol}\% \text{Na}_2\text{O}]$  is unity. Good chemical durability and suppression of metallic colloid during

ion exchange with silver also result from the addition of alumina in silicate glass melts. As diffusion rates, chemical durability and colloid formation are all fundamentally linked to the behavior of modifier cations, one can expect to observe underlying structural changes in the cation environments as the alumina content of the glass is varied.

We obtained direct structural information on both the constituent ( $\text{Na}^+$ ) and the dopant ( $\text{Ag}^+$ ) cation sites in a variety of silicate and aluminosilicate glasses (compositions listed in Table 1 below) using XAFS on Na and Ag K-edges. We acquired silver K-edge (25.514 keV) transmission data on station A-2 at CHESS shortly before the new wiggler was installed on the A-line. We used the total electron yield technique<sup>4</sup> to collect data on the sodium K-edge (1.071 KeV) on station 3.4 at the Daresbury Synchrotron Radiation Source (SRS).<sup>5</sup> Analysis consisted of least-squares fitting of the structure-related parameters to the normalized fine structure using the Daresbury EXCURV90 program,<sup>6</sup> which is based on curved-wave theory. Procedural details and results can be found in a recent article in the Journal of Physical Chemistry.<sup>7</sup> First shell determinations are given in Table 2 with an estimated variation in fitted coordination number of  $\pm 0.5$  atom, in interatomic distance of  $\pm 0.02\text{\AA}$  and in variance of  $\pm 0.005\text{\AA}^2$ . While overlap exists in the values of  $N$  and  $2\sigma^2$ , it can be seen in Figure 2 that the sodium and silver

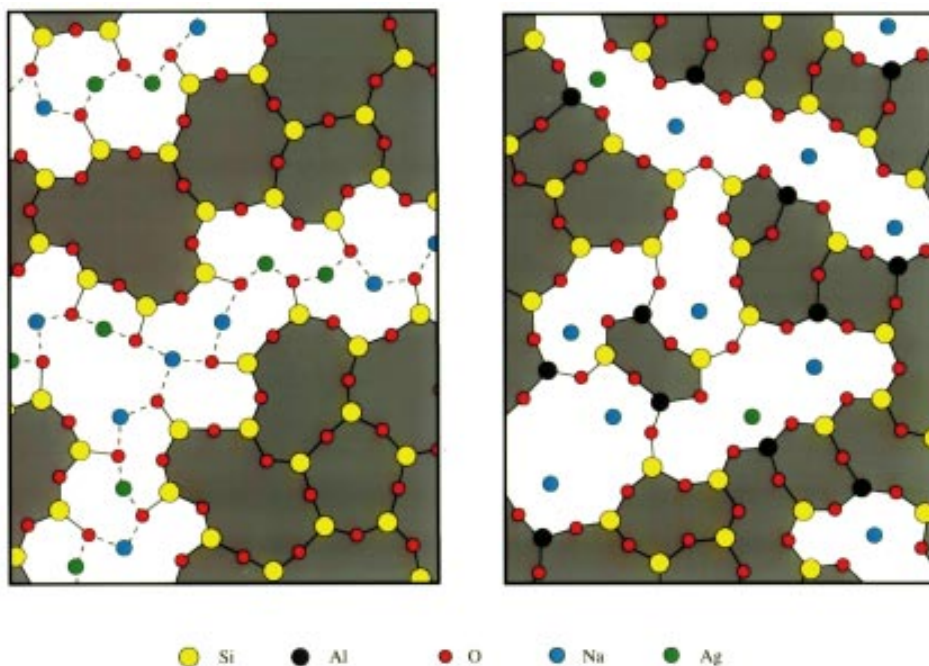


(Figure 1) Cartoon of ion-exchanged glass structure: an alkali silicate glass (left) and an alkali aluminosilicate glass (right). Silicon, aluminum and alkali are all 3-fold coordinated in this 2-D representation. The simple alkali silicate glass on the left includes bridging (2-fold) and non-bridging (3-fold) oxygen while the fully polymerized aluminosilicate shown on the right includes only bridging oxygen.

(Table 1) Glass Compositions and XAFS Edges; ( $R = [\text{mol}\% \text{Al}_2\text{O}_3] / [\text{mol}\% \text{Na}_2\text{O}]$ ).

<u>Composition</u>	<u>R</u>	<u>Comments</u>	<u>K-edges</u>	
$\text{Na}_2\text{Si}_4\text{O}_9$	0.00	tetrasilicate	Na	Ag
$\text{Na}_{0.17}\text{Al}_{0.03}\text{Si}_{0.23}\text{O}_{0.58}$	0.17	$\text{Al}_2\text{O}_3$ -poor; $R = 0.17$ NAS	Na	Ag
$\text{Na}_{0.17}\text{Al}_{0.15}\text{B}_{0.04}\text{Si}_{0.09}\text{O}_{0.56}^{11}$	0.92	$\text{Al}_2\text{O}_3$ -rich; $R = 0.92$ NAS		Ag

environments are in fact distinct from one another. The figure gives a comparison of parameter correlation maps<sup>8</sup> of Debye-Waller factor,  $2\sigma^2$ , and coordination number, N, for first shell fits on the Na and Ag environments in the glasses listed in Table 1. In each case the first shell  $2\sigma^2$  and N were varied to find the region in which the least-squares fit index differed from its minimum by no more than 5%. The parameter range that corresponds to a 95% confidence limit is enclosed by a heavy oval contour. It is obvious that despite the usual uncertainty associated with fitting correlated parameters for a single spectrum, the Na and Ag environments are distinct in all cases.

#### Sodium environments in silicate and aluminosilicate glasses

Crystalline binary sodium silicates are comprised of sheets of covalently bound silica tetrahedra, separated by soda-rich layers which depolymerize the network. The distinction between the trisilicate and disilicate species lies primarily in the number of silica sheets between the soda-rich layers.<sup>9</sup> This also appears to be true for the glassy sodium binary silicates. We found that the local Na environments in sodium tetrasilicate ( $\text{Na}_2\text{Si}_4\text{O}_9$ ) glass are virtually indistinguishable from those previously found<sup>2</sup> in sodium disilicate ( $\text{Na}_2\text{Si}_2\text{O}_5$ ) glass. However, the addition of even small amounts of alumina changes the Na environments, as is seen in the  $R=0.17$  glass (Table 2). While the Na-O distance is essentially unchanged, the coordination drops from 4.3 to 2.8 and the static disorder increases significantly.

The change in Na environment can be understood by consideration of crystalline albite ( $\text{NaAlSi}_3\text{O}_8$ ). Albite is an open aluminosilicate net-

work in which both Si and Al are four fold coordinated by oxygen to form tetrahedra arranged as three-dimensionally interconnected cages. All oxygen in this crystalline structure "bridge" between either Si or Al cations through covalent bonds. The negative  $[\text{AlO}_4]^-$  groups are charge compensated by  $\text{Na}^+$  ions which occupy the oxygen-rich cages off-center. Similar features can be expected in aluminosilicate glasses.

In glasses with equal parts  $\text{Al}_2\text{O}_3$  and  $\text{Na}_2\text{O}$  ( $R=1$ ), the  $\text{Na}^+$  cations can be envisioned as "stuffing" the oxygen rich cavities of the fully-polymerized former network. On the other extreme, in binary glasses ( $R=0$ ), the  $\text{Na}^+$  cations are tethered to the silicate network through non-bridging oxygens (NBO's). The distinction is shown in the cartoons (Fig. 1) of two 2-dimensional ion exchanged glasses: a binary silicate for which  $R=0$  and an aluminosilicate for which  $R=1$ . The modifier cations are colored  $\text{Na}^+$  (blue) and  $\text{Ag}^+$  (green). Bridging and non-bridging oxygen (both yellow) are distinguished by their coordination to surrounding cations. Note that the binary silicate contains both types of oxygen, while the  $R=1$  glass contains only bridging oxygen. In the  $R=1$  glass, the clustering of alkalis that is present in the binary silicate is essentially absent. Further, the bridging oxygen cavities are such that the alkali sites generally fall off-center. The difference in the Al-O and Si-O distances (1.7Å and 1.6Å, respectively) and the extra disorder in the alkali sites that results is not obvious from the cartoon. In aluminosilicate glasses for which  $0 \leq R \leq 1$ , some combination of the two extreme structures can be expected. Evidence for this is seen in Table 2.

#### Silver environments in the same glasses after Ag/Na ion exchange

Ion exchange usually involves a one-for-one substitution of an alkali ion (e.g.,  $\text{Na}^+$ ) from the glass by a monovalent dopant cation (e.g.,  $\text{Ag}^+$ ). The common assumption is that the dopant makes an isostructural replacement of the constituent.<sup>10</sup> However, we found the Ag environment in the ion-exchanged tetrasilicate glass to be remarkably different than that of the Na which it replaces. In the tetrasilicate glass, the cation coordination number drops from 4.3 (Na-O) to 2.1 (Ag-O) on ion exchange, the distance shortens from 2.32 Å (Na-O) to 2.08 Å (Ag-O) and the Debye-Waller factor sharpens from a  $2\sigma^2$  value of 0.017 Å<sup>2</sup> (Na-O) to 0.012 Å<sup>2</sup> (Ag-O). The local Ag environment is very similar to our determination of the Ag environment in crystalline  $\text{Ag}_2\text{O}$ : two oxygen at 2.04 Å with  $2\sigma^2 = 0.008$  Å<sup>2</sup>. The differences are certainly not due to the presence of metallic colloid since the Ag-Ag distances in silver metal occur at 2.89 Å; these did not feature in the XAFS spectra. The change in oxygen surround can be interpreted in terms of the higher field strength of the silver, the increased covalency of the Ag-O bond and the relative ease with which the mostly ionic NBO/modifier cation bonds can bend. Similar results are obtained for the Ag environments in the low alumina glass in which NBO's predominate the modifier cation sites.

In the alumina-rich ( $R=0.92$ ) glass, virtually all modifier cation sites will be associated with bridging oxygen. The change in the silver environment (oxygen distances increase from 2.08 Å ( $R=0$ ) to 2.23 Å ( $R=0.92$ ), coordination numbers increase from 2.1 ( $R=0$ ) to 2.5 ( $R=0.92$ ) and Debye-Waller factors rise from

(Table 2) First Shell XAFS Fits

<i>Glass</i>	<i>Cation</i>	<i>Coordination Number, N</i>	<i>Shell Radius r [Å]</i>	<i>Debye-Waller Factor, 2σ<sup>2</sup> [Å<sup>2</sup>]</i>
sodium disilicate	Na	5	2.30	0.011
sodium tetrasilicate	Na	4.3	2.32	0.017
R = 0.17 NAS	Ag	2.1	2.08	0.012
	Na	2.8	2.30	0.024
R = 0.92 NAS	Ag	1.8	2.11	0.018
	Ag	2.5	2.23	0.036

0.012Å<sup>2</sup> to 0.036Å<sup>2</sup>) reflects the new constraints experienced by the silver in the stiff, fully-polymerized network. The bridging oxygen bonds are not so free to bend as are the NBO bonds in low alumina glasses, and the silver is unable to pull nearby oxygen into its preferred Ag<sub>2</sub>O-like configuration. Instead, the silver must conform to the available oxygen distances in the relatively rigid network and it therefore is accommodated in the network by a higher coordination number and greater local disorder. Incidentally, these fully polymerized aluminosilicate glasses are exactly the compositions used to inhibit formation of metallic silver colloid in ion exchanged glasses.

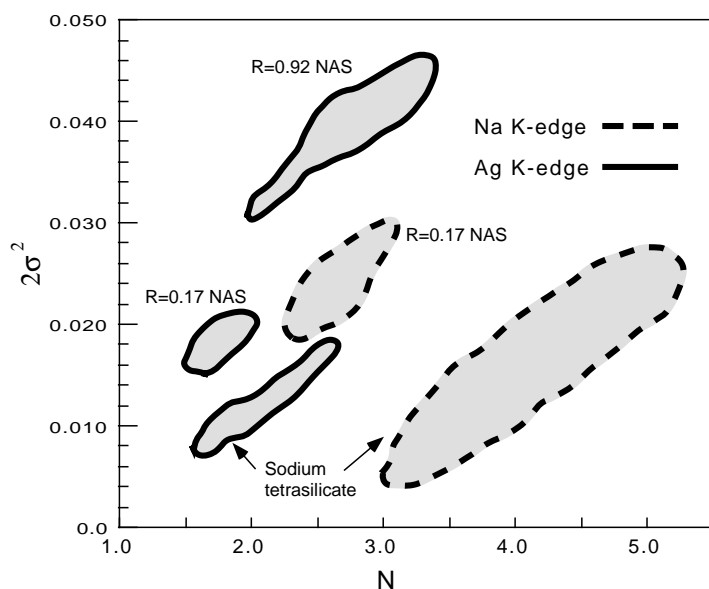
### Ionic Diffusion and Ion Exchange

The different environments of the dopant and constituent cations have important implications for ion exchange. For example, relative silver and sodium diffusion rates can be inferred from structural information in these glasses. The electrostatic binding energy  $E_b$  for an isolated alkali is given by

$$E_b = \frac{1}{4\pi\epsilon_0\epsilon_\infty} \frac{e^2}{r_{M-O}} \quad (1)$$

where  $\epsilon_\infty$  is the high frequency dielectric constant and  $r_{M-O}$  the alkali-oxygen distance which can be obtained from XAFS. Compared to the host sodium sites, the shorter Ag-O bonds and consequently larger Coulomb forces on the silver indicate that the binding energy,  $E_b$ , is larger for silver than for sodium, so slower diffusion rates can be expected. This is born out by experiment at all temperatures of interest. For example, the

(Figure 2) Superimposed correlation maps of Debye-Waller factor versus coordination number for first shell fitting to obtain the parameters for the glasses listed in Table 2: (1) sodium in sodium tetrasilicate, (2) sodium in the R = 0.17 aluminosilicate, (3) silver in ion-exchanged sodium tetrasilicate, (4) silver in the R = 0.17 aluminosilicate and (5) silver in the R = 0.92 aluminosilicate glass. The region of 95% confidence is given. The sodium environments group to the right and the silver environments to the left. Note the distinction between environments of the same cation in different glasses (e.g. R=0, 0.17, 0.92) and between different cations in the same glass.



silver diffusion coefficient is 4 times smaller than that of the sodium in the R = 0.17 glass at typical diffusion temperatures (T @ 500°C).<sup>11</sup> In terms of the hopping of isolated cations, we can express the diffusivity ratio,  $D_{Na}/D_{Ag}$ , at a given temperature as

$$\frac{D_{Na}}{D_{Ag}} = \frac{R_{Na}^2 v_0(Na)}{R_{Ag}^2 v_0(Ag)} \exp\left(\frac{E_b(Ag) - E_b(Na)}{kT}\right) \quad (2)$$

where  $R_{Na}$  and  $R_{Ag}$  are the respective hopping distances,  $v_0(Na)$  and  $v_0(Ag)$  the corresponding hopping attempt frequencies and the cation binding energies  $E_b(Na)$  and  $E_b(Ag)$  are given by eq. 1. Since the glass network is common to both cations, it reasonable to expect that  $v_0(Na) \cong v_0(Ag)$  and that the frequency dielectric constants,  $\epsilon_\infty(Na)$  and  $\epsilon_\infty(Ag)$ , are also approximately equal. If we assume further that the hopping distances  $R_{Na}$  and  $R_{Ag}$  scale with the respective nearest neighbor oxygen distances, then eq. 2 is simply a function of  $r_{Na-O}$  and  $r_{Ag-O}$ . Inserting the measured  $r_{M-O}$  values from Table 3 in eq. 1 gives a host to dopant diffusivity ratio  $D_{Na}/D_{Ag}$  of 3 - close to the observed value of 4.

The unequal mobilities of the host sodium and exchanged silver cations results in concentration-dependent interdiffusion coefficients, where

$$\frac{1}{\bar{D}} = \frac{N_{Na}}{D_{Ag}} + \frac{N_{Ag}}{D_{Na}} \quad (3)$$

and  $N_{Na}$  and  $N_{Ag}$  are the cation mole fractions.  $\bar{D}$  for ion-exchanged glass de-

depends on silver concentration in a manner completely analogous to the Mixed Alkali Effect.<sup>11,12</sup> This effect is manifest by low ionic conductivities in mixed alkali glasses compared to those in the single alkali counterparts. The increase in activation energies for ionic conduction have been attributed to alkali-alkali interactions at short distances.<sup>13</sup> Therefore, the fundamentally different structures of the NBO-rich silicates and the fully polymerized alumina-rich glasses should result in different levels of concentration dependence. For example, in binary silicates one would expect strong cation-cation interactions resulting from the coordination to NBO's on the modifier sublattice. In the fully polymerized glasses ( $R \approx 1$ ), the concentration dependence should be less pronounced.

We recently tested this hypothesis at the University of Rochester using energy-dispersive x-ray spectroscopic measurements of silver and sodium concentration profiles in ion

exchanged glasses. We find that alumina-rich glasses do indeed show less-pronounced concentration dependence than their NBO-rich counterparts. This is news to both the glass science and the photonics communities and has important implications for the development of new optical glasses. Examples in glass science in which structural knowledge (vs. empirical studies) is used to predict glass properties are rare. This is an encouraging turn of events in the search for better waveguide, micro-optic and gradient-index materials.

### Acknowledgments

This work was supported by the National Science Foundation, the Center for Optics Manufacturing and the NATO Collaborative Research Grant Fund. Many thanks are also due to the staff at both SRS Daresbury and CHESS.

(1) Houde-Walter, S.N. Gradient Index Optics and Miniature Optics, SPIE Proc. 935, 2. (1988).

- (2) (a) Greaves, G. N. *J. Non-Cryst. Solids* **71**, 203 (1981). (b) Greaves, G.N.; Fontaine, A.; Lagarde, P.; Raoux, D.; Gurman, S. J. *Nature* **293**, 611 (1981).
- (3) Vessal, B.; Greaves, G.N.; Marten, P.T.; Chadwick, A.V.; Mole, R.; Houde-Walter, S.N. *Nature* **356**, (1992) 504.
- (4) Elam, W.T.; Kirkland, J.P.; Neiser, R.A.; Wolf, P.D. *Phys. Rev. B* **38**, 26 (1989).
- (5) Synchrotron Radiation Source, Science and Engineering Research Council (SERC), Daresbury Laboratory, Warrington WA4 4AD, UK.
- (6) (a) Gurman, S.J.; Binsted, N.; Ross, I. *J. Phys. C: Solid State Physics* **17**, 143 (1984). (b) Gurman, S.J.; Binsted, N.; Ross, I. *J. Phys. C: Solid State Physics* **19**, 1845 (1984).
- (7) Houde-Walter, S.N.; Inman, J.M.; Dent, A.J.; Greaves, G.N. *J. Phys. C:chem.* **37**, 9330 (1993).
- (8) Joyner, R.W.; Martin, K.J.; Meehan, P. *J. Phys. C: Solid State Phys.* **20**, 4005 (1987).
- (9) Jamieson, P. B. *Nature* **214**, 794 (1967).
- (10) (a) Urnes, S. *Phys. Chem. Glasses* **1972**, 13, 77. (b) Guaker, R.; Urnes, S. *Phys. Chem. Glasses*, **14**, 21 (1973).
- (11) Houde-Walter, S.N., manuscript in preparation.
- (12) Day, D.E. *J. Non-Cryst. Solids* **21**, 343 (1976).
- (13) (a) Harder, H.; Bunde, A.; Dieterich, W. *J. Chem. Phys.* **85**, 4123 (1986). (b) Araujo, R. *J. Non-Cryst. Solids* **153**, 70 (1993). (c) Catlow, C.R.A. *Phys. Stat. Sol. (a)* **46**, 191 (1978).

CONTINUED FROM PAGE 13

ing back to our lab over a few thousand photographic films and a few hundred 8-mm magnetic tapes which recorded the digitized diffraction images the crystallographers in the group began to work more than 15 hours a day at the computer trying every effort possible to index and process every film and image plate using a modified version of the Purdue oscillation film processing package. With a few months of effort, the digitized images were transformed into a number of datasets. One typical dataset was usually merged together from more than sixty films and/or image plates with 0.7-1.0° oscillation collected from twenty to forty crystals. For RT/dsDNA/Fab28 complex, the native dataset was merged from 186 films and image plates exposed from 36 crystals and has 76,903 unique reflections ( $I > 3\sigma$ ) to 2.8 Å resolution with an  $R_{\text{merge}}$  (I) factor of 0.13 and completeness of 88%.

As the diffraction data were be-

ing processed, the initial phase problem was solved using the multiple isomorphous replacement method and solvent flattening techniques, and improved by successively incorporating more heavy atom derivatives information (in a total of twenty one derivatives used, eleven datasets came from CHESS). The MIR phased maps very clearly showed the polypeptide chains of the protein and the backbone of the bound DNA.

The people here went crazy, working fiercely day and night for many weeks to finish the backbone tracing along the whole course of polypeptide chains in the RT p66/p51 heterodimer, the antibody fragment Fab28, and bound 19/18 template-primer dsDNA. At this time, the structure of HIV-1 RT complexed with a small molecule, the non-nucleoside inhibitor nevirapine at 3.5 Å resolution, was reported by Dr. Thomas Steitz's laboratory in Science. The availability of the folding diagrams from the RT/nevirapine structure further facilitated the assign-

ment of some connection regions in our RT/dsDNA/Fab28 structure. Further phase improvement, by combining partial structure information with MIR phases and structure refinement, was carried out using the program XPLOR on the CRAY super-computer at NCI, NIH (another key facility that enabled us to solve the RT/dsDNA/Fab28 structure at high resolution). This significantly improved the quality and reliability of the structure of RT and permitted us to visualize three-dimensionally the pernicious enzyme in atomic detail.

### Autumn is the harvest season

Now the crystal structure of HIV-1 RT/dsDNA/Fab28 was unveiled some very important and intriguing results ensued. Though the two peptides of p66 and p51 subunits share the identical amino acid sequence in the N-terminal polymerase domain, the spatial arrangement of their secondary structural elements are dramatically different. As the first structure of a polymerase bound

CONTINUED ON PAGE 19

# Probing surface grating structures of 300 nm periods with 1 Å X-rays

Qun Shen

Periodic nanostructures of sizes 1 to 100 nm on semiconductor crystal surfaces have attracted great interests in recent years because of their unusual electronic band structures due to quantum confinements, and their potential applications in electronic and optoelectronic devices. The periodically structured grating surfaces also serve as model rough surfaces with a predominant spatial frequency for studying atomic kinetics involving surface diffusion and step arrangements. To date, optical diffraction using lasers and scanning electron microscopy have been the primary methods of characterizing surface grating structures. Compared to these methods x-ray scattering is a natural extension of optical diffraction for probing shorter wavelength gratings with higher spatial resolution.

In collaboration with Professor J.M. Blakely's group in the Department of Materials Science & Engineering here at Cornell, we have developed a program of using hard x-

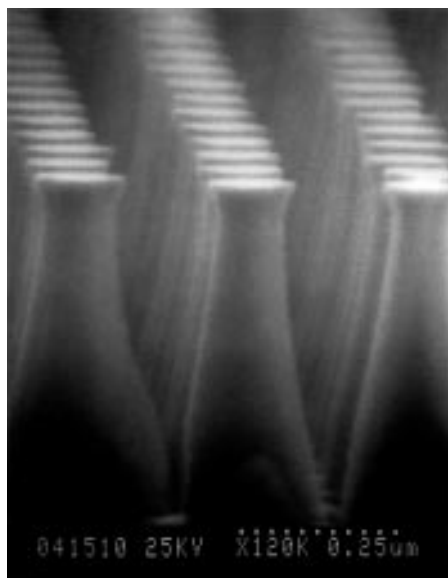


(Fig. 1) A scanning electron micrograph of a 2D grating structure on Si (001) surface.

ray diffraction to study surface grating nanostructures and their evolutions when being annealed or etched. Two-dimensional (2D) grating structures (Fig.1) on Si (001) surfaces are fabricated at the National Nanofabrication Laboratory at Cornell by e-

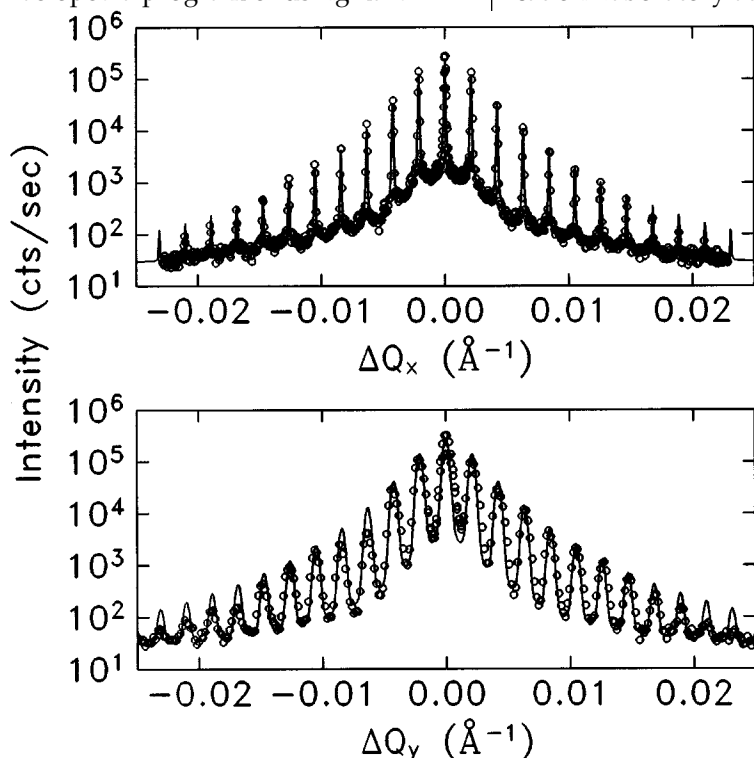


(Fig.2) High resolution diffraction pattern from a silicon (001) 2D-grating surface. The data (open circles) were collected around the (220) Bragg reflection in a glancing-angle diffraction geometry, along the [110] (bottom) and the [1  $\bar{1}$  0] (top) directions respectively. The solid curves are calculations using the kinematic theory of x-ray diffraction.

beam lithographic techniques, and the x-ray experiments are performed at the F3 and the B2 stations at CHESS. Because of the long coherence length available with synchrotron radiation and perfect crystal monochromators, extremely sharp diffraction satellite peaks are observed around each bulk Bragg reflection. An example of such a diffraction pattern is shown in Fig.2. These satellite peaks are the result of interference due to the extra grating periodicity on top of the existing crystal lattice. In the language of crystallography, these grating pillars constitute "super molecules" that form a super lattice on the surface. The data illustrate that a mesoscopic scale (~3000 Å) periodic structure can be investigated in a straightforward way by diffraction of 1 Å x-rays!

The x-ray diffraction pattern from crystal surface gratings can be analyzed in analogy with optical Fraunhofer diffraction from multiple slits [see Shen, Umbach, Weselak & Blakely, Phys. Rev. B **48**, 17967 (1993)]. The grating peak positions are determined by the grating wavelength and their intensities are modulated by the diffraction intensity from a single grating period. By analyzing these quantities various grating parameters can be deduced. The intensity variations along a grating rod normal to the substrate surface provide information on the height of the grating pillars and their side wall slopes and shape. By comparing the grating reciprocal lattice with the crystal lattice, the orientation of the grating lines and their atomic registry can be obtained with respect to the bulk crystal.

One of the unique abilities of x-ray diffraction is to measure lattice strain, defects, and disorder on an atomic scale, and unevenness in the size of the grating pillars. These crystal and grating imperfections are

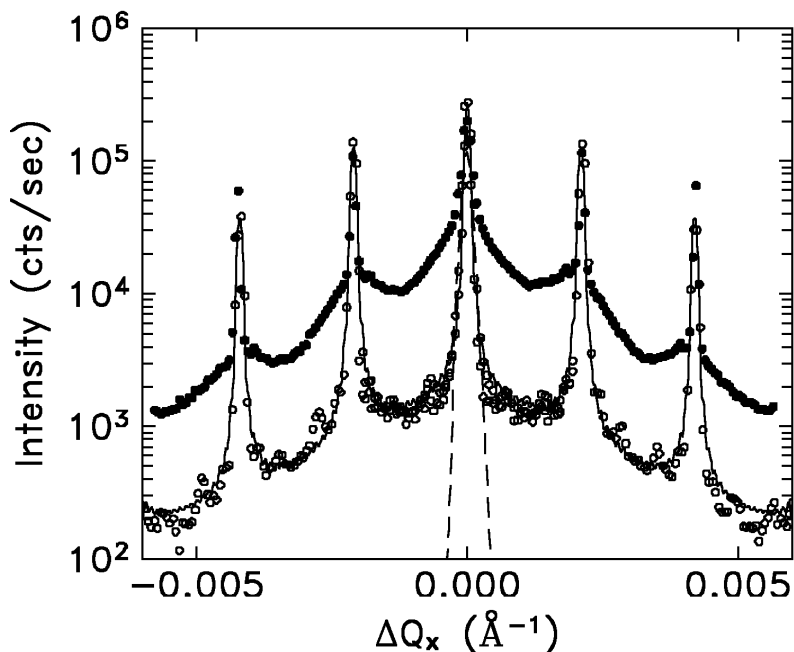
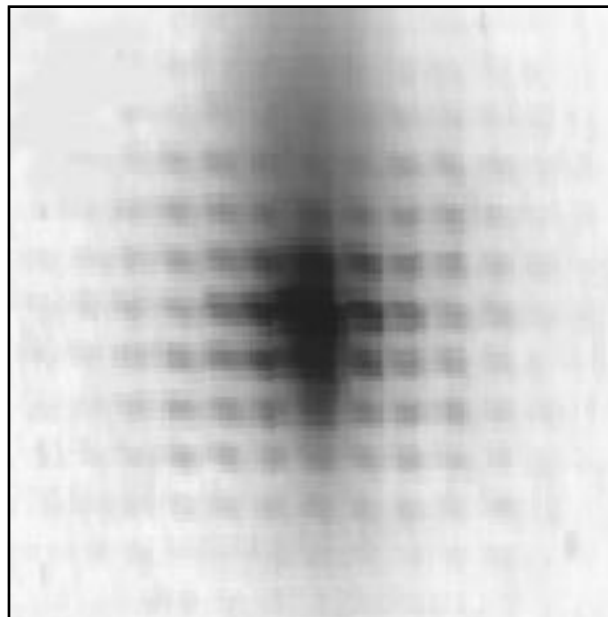


(Fig.3, left) Comparison of diffraction profiles from two different grating surface treatments. The data from a virgin sample are shown by open circles, which are part of Fig.2, and those from an oxidized-and-etched sample (needle-grating) are shown by filled circles. Note the line shape of the grating diffraction peaks, which contains information on the imperfections and the possible short-range-order in the grating pillar structures. The dashed line illustrates the experimental resolution, taken on a perfect crystal Si wafer.

(Fig.4, below) Laue diffraction image using white beam from a 2D Si (001) grating surface. The image is around the (004) Bragg reflection and is recorded on a Type 55 Polaroid film with a 3 min exposure time. The film to sample distance is 80 cm and the image border in the plot corresponds to roughly 5 mm × 5 mm in real scale.



important to the understanding of the physics in quantum confinements and to the growths of semiconductor overlayer structures. Figure 3 illustrates that these imperfections can produce interesting and distinct diffraction profiles (filled circles) on the grating reflections. In this study, the sample shown in Fig.1 was oxidized in a controlled fashion to grow SiO<sub>2</sub> on the pillar surfaces. The oxide was then removed by a subsequent HF etch. The treatment produced extremely sharp needle-like pillars, which may therefore contain some variation in their sizes, and some intrinsic lattice strain and short range order. An analysis of the x-ray diffraction data on the diffuse scattering

part will provide valuable information on these imperfections in the grating pillar structure.

The diffraction data from the surface grating structures can also be collected using a highly collimated polychromatic synchrotron beam, just like taking a Laue diffraction photograph. An example is shown in Fig.4, which is a magnified diffraction spot of the Si (004) Bragg reflection recorded on an x-ray film. With this technique a grating diffraction pattern of more than 100 peaks can be collected in just 2-200 seconds. We believe that the time

resolution can be further enhanced by using a CCD detector, and therefore Laue white beam diffraction is a promising technique for doing real time-resolved diffraction experiments on periodic surface grating structures.

CONTINUED FROM PAGE 17

with a nucleic acid in a mode that is relevant for nucleic acid synthesis, it demonstrated a novel hybrid assembling of A-form and B-form bound dsDNA. Based on the structure, we could postulate detailed mechanisms by which the RT enzyme copies the single-stranded viral RNA genome into double-stranded DNA. Furthermore, we have been able to map out the drug resistance mutations for both nucleoside and non-nucleoside inhibitors in a three-dimensional context. This knowledge provides a structural basis for understanding the inhibition mechanism and the

mechanism of antiviral resistance to RT.

Along with the publication of the structure of HIV-1 RT/dsDNA/Fab28 at 3.0 Å resolution, the coordinates of HIV-1 RT were deposited into the Brookhaven Protein Data Bank, making them immediately available to the scientific community. The accessibility of this information not only supplies the basis for three-dimensional interpretation of the results from genetic, biochemical, and antiviral analyses of HIV-1 RT, but also could result in a significant acceleration of rational design of improved and/or new drugs against

AIDS.

I would like to thank all the members of the RT group for their dedicated efforts in this work. This project is an ongoing collaboration with the laboratory of Dr. Stephen Hughes at the Frederick Cancer Research and Development Center. We are also grateful to the entire CHESS staff for their continuing development of MacCHESS and support of our work.

# Transient structure of a driven charge-density wave in NbSe<sub>3</sub>

E. Sweetland and J.D. Brock

School of Applied and Engineering Physics, Cornell University

The fundamental statistical physics describing systems which are so far out of thermal equilibrium that the notion of a partition function is not valid is currently not well understood. The goal of this experiment is to study the structural response of a very simple system as it is driven between two distinct steady state configurations which are described by different partition functions, paying close attention to the transition regions. We chose to study the charge-density waves (CDWs) found in quasi-one-dimensional metals because the equilibrium properties of these systems are well understood. Experimentally, the structure of the stationary and the sliding CDW states have both been measured at high resolution. Theory and experiment are in excellent agreement<sup>1</sup>. On the other hand, the dynamics of CDW systems are relatively poorly understood. Although a large number of electronic transport experiments have been performed, the results of these experiments are difficult to interpret in



terms of microscopic models and time-resolved structural data are very limited.

In an effort to address these issues, we used a time-resolved, high-resolution x-ray scattering technique to measure the evolution of the structure of the sliding Q<sub>1</sub> CDW in NbSe<sub>3</sub> as the direction of the driving electric field is reversed. In a full report of this work,<sup>2</sup> we interpret our data using an equation of motion for the phase of the CDW order parameter which pertains at low temperatures and at large applied fields.

Found primarily in one-dimensional metal crystals, the CDW state is characterized by a periodic density wave appearing in the conduction electron density and a concomitant periodic longitudinal lattice-distortion wave. The properties of CDW systems have been studied extensively during the past 15 years. A large fraction of this research has been devoted to studies of the nonlinear electronic transport exhibited by some CDW systems.<sup>3</sup> This nonlinearity can now be explained simply. The incommensurate periodicities of the lattice and the CDW imply that there is no preferred location of the CDW in the crystal. Since there is no energetically preferred location, there can be no elastic restoring forces acting on the CDW. Consequently, an arbitrarily small applied field is able to accelerate the CDW, causing it to slide rigidly through the crystal lattice, producing a collective current.<sup>4</sup>

In any experimental realization, electrical contacts are required to

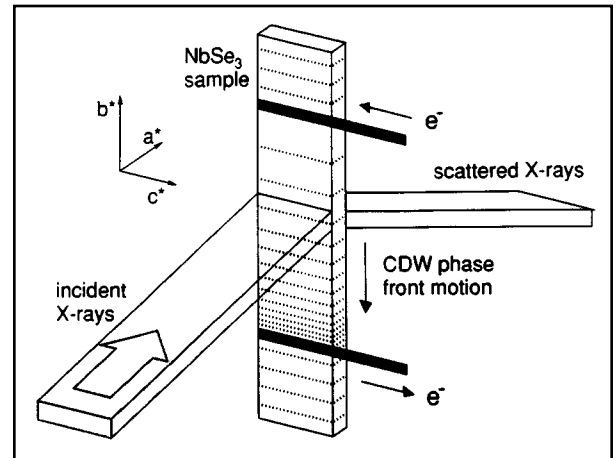


(Figure 1) Schematic illustration of the experimental configuration. Normal current is injected and extracted from the current electrodes. CDW or collective mode conduction takes place only in the region between the current electrodes.

produce the electric field which drives the CDW into the sliding state. The boundary conditions imposed on the CDW state at the electrical contacts play a crucial role in determining its sliding structure. The system is illustrated schematically in Fig. 1. The electric field is created inside the quasi-one-dimensional metal crystal by applying a voltage between two widely spaced electrodes. In the region between the electrodes, the applied voltage creates the electric field,  $E_{app} = V_{app}/L$ . In the regions of the sample which are outside of the two contacts, the electric field is zero. To achieve a steady-state collective current due to the CDW sliding, current must be injected at one electrode and extracted at the other. Equivalently, CDW phase fronts must be added at one electrode and removed at the other. In the figure above, the dashed lines indicate lines of constant phase of the CDW. In the region of the sample between the contacts, the CDW phase fronts are moving when the CDW is sliding. In the regions of the sample which are outside the electrical contacts, there is no collective

Joel D. Brock (left) and graduate student Emma Sweetland examine the tip of a refrigerator cylinder that is used to chill tiny metal samples for x-ray experiments. (Photo: Charles Harrington/Cornell University Photography)

current and the CDW phase fronts are stationary.

The mechanism which converts normal current to collective current at the electrodes is straightforward. Before the electric field is applied, the CDW is uniform. As the electric field is applied, phase fronts in between the electrodes try to move down, dilating the CDW near the electrode on the top. This strain can be relieved by nucleating a dislocation loop, which quickly grows to be the size of the sample, inserting a new phase front as it does so.<sup>5</sup>

A one-dimensional theory of the steady state current conversion process has been developed by Ramakrishna *et al.*<sup>6,7</sup> One of the specific predictions of this theory is that, as in the discussion above, the CDW should be strained in the region between the electrodes. Using synchrotron-based high resolution x-ray scattering techniques and the facilities at CHESS, DiCarlo *et al.*<sup>8</sup> have observed a position, temperature and electric field dependent strain of the sliding  $Q_1$  CDW in  $NbSe_3$  consistent with this prediction. The goal of the present experiments is to measure the time dependence of this strain field as the sign of the electric field is

reversed.

The x-ray scattering measurements were performed at the F2 experimental station. The storage ring was running at an energy of 5 GeV and the stored positron current typically decayed from 80 to 40 mA during a 50 minute fill cycle. For the purposes of comparing different data sets, we have normalized the data to counts per second at 100 mA ring current. A Si(111) double-bounce monochromator selected a wavelength of 1.5Å from the white x-ray beam produced by the 24-pole wiggler. A flat Au-coated mirror in the hutch suppressed harmonics of the fundamental wavelength passed by the monochromator. The sagittally-bent second monochromator crystal focused the x-ray beam in the out-of-scattering-plane direction at the sample position. Tantalum slits restricted the x-ray spot size at the sample to approximately 0.8 mm × 3 mm. The resulting x-ray beam contained  $4 \times 10^{10}$  x-rays/second/100mA of stored positron current. The scattered x-rays were analyzed by a triple-bounce channel cut Si(111) crystal and detected by a standard NaI(Tl) scintillator and photomultiplier tube.

To measure the transient structural response of the CDW, we utilized a stroboscopic detection system<sup>9</sup>. The CDW is subjected to a continuous square wave voltage wave form. The half period of the square wave is divided into time intervals of equal size. X-rays detected during a particular time interval are summed over a large number of square wave periods. Typical count rates at the

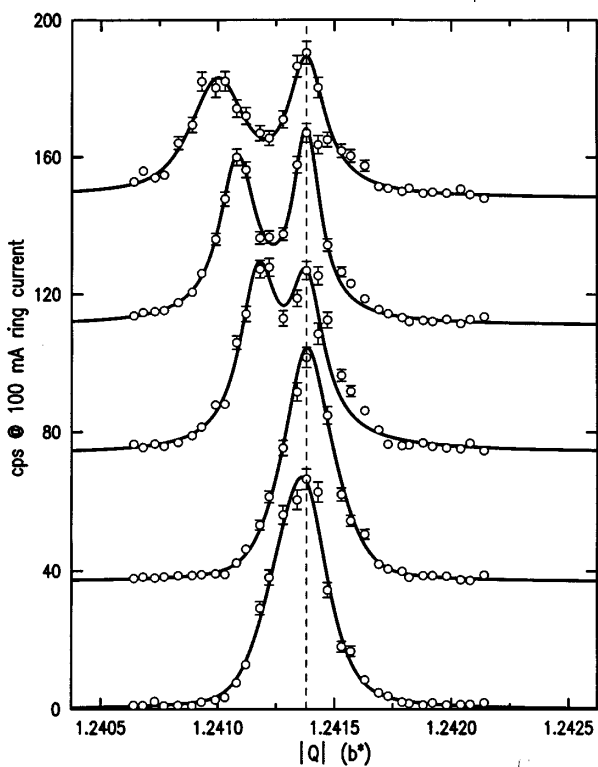


(Figure 2) A succession of  $(0 Q_1 0)$  reciprocal space scans taken from different time slices of a data set taken at 17 mA. The centers of the time bins, measured from the rising edge of the driving wave form, are 0.014, 0.030, 0.050, 0.062, and 0.078 seconds. Successive scans are displaced by 35 cps @ 100mA.

peak of the  $(0 1+Q_1 0)$  CDW satellite were on the order of 50 counts/second @ 100 mA of ring current. Therefore, in order to obtain reasonable counting statistics we sum over roughly 10,000 voltage wave form cycles.

All of the data we discuss here were taken at 70 K. The depinning current of this sample was determined by measuring the differential resistance as a function of current with a lock-in amplifier. The depinning current was  $20 \pm 3$  mA.

Close inspection of the data reveal that the CDW satellite peak does not have the same shape or width for the different current directions. This is most clearly seen at lower driving fields. For example, Figure 2 shows a series of longitudinal scans through the  $(0 1+Q_1 0)$  CDW satellite from different time intervals as the current direction is switched. These data were taken at 70 K and with a driving current of 17 mA. Each scan is offset by 35 cps @ 100 mA for clarity. The top and bottom scans represent the steady-state for the two current directions. The remaining scans show that the CDW satellite peak evolves from a single peak to a bimodal line shape. Data sets taken with higher driving current magnitudes exhibited the same systematic structure. In general, as the driving current magnitude was increased, the area under the stationary peak decreased. At 29 mA, the stationary peak is no longer measurable. The width of the moving peak is slightly broader in the transient regions.

A simple interpretation of this data is that near threshold the CDW shears into two or more independent domains. Some portion of the system remains pinned and does not slide. The CDW in these pinned portions of the sample does not exhibit the time-dependent strain of the sliding portions. Therefore, the CDW satellite peak due to these pinned regions remains fixed. Thus, the depinning current measured above using the lock-in amplifier cannot be interpreted simply as the current at which the CDW is depinned over the

entire crystal.

Figure 3 shows the difference in position of the sliding and pinned peaks as a function of time for one complete period of the driving current wave form. The particular data set shown was taken at a current of 29 mA but is representative of the data taken at all currents. To characterize the time scales of these transients, we fit these relative peak positions to the solution of the driven diffusion equation.<sup>2</sup> The solid line in Figure 3 is the best fit to that solution. For the data set shown, the time constant  $\tau_0$  obtained for the switch to larger values of  $Q$  was  $2.58 \pm 0.37$  msec and for the switch to smaller values of  $Q$  was  $4.71 \pm 0.74$  msec.

In summary, we have used a time-resolved high-resolution x-ray scattering technique to measure the transient structural response of a simple quasi-one-dimensional CDW system as it is driven between two distinct steady state configurations. We find that a simple Langevin equation of motion for the phase of the CDW, which is based on the notion of a background strain which is driving the nucleation of dislocation loops, accurately describes the re-

sponse of the CDW to a reversal in the direction of an applied electric field, well above the threshold to sliding. As the driving field approaches threshold from above, the line shape becomes bimodal and the fraction of the CDW which is stationary increases monotonically. This suggests that, in this sample, the CDW did not depin throughout the entire sample at one well defined voltage.

This work was supported by the Materials Science Center (NSF Grant No. DMR-88-1858-A02) and by the NSF (Grant No. DMR-92-57466). Additional support was provided by the AT&T Foundation.

- 1 D. DiCarlo, R.E. Thorne, E. Sweetland, M. Sutton, and J.D. Brock, (submitted to Physical Review B).
- 2 E. Sweetland, A.C. Finnefrock, W.J. Podulka, M. Sutton, J.D. Brock, D. DiCarlo, R.E. Thorne, Submitted to Physical Review B.
- 3 For comprehensive reviews of the electronic properties of CDW systems see P. Monceau, in *Electronic Properties of Quasi-One-Dimensional Materials* (Reidel, Dordrecht, 1985), Pt. II, p. 139; G. Grüner, Rev. Mod. Phys. **60**, 1129 (1988).
- 4 H. Fröhlich, Proc. R. Soc. London, Ser A **223**, 296 (1954).
- 5 For a comprehensive review of previous work on CDW phase slip, see F. Ya. Nad', in *Charge Density Waves in Solids*, edited by L.P. Gor'kov

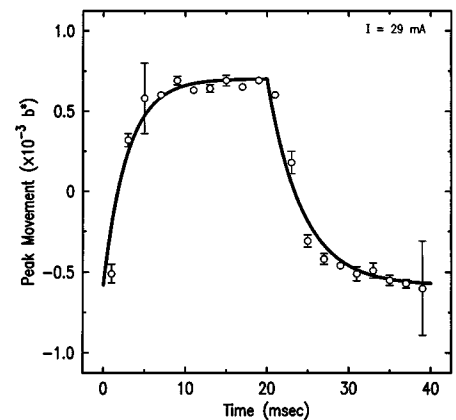


(Figure 3) Positions of the moving peak are shown for a data set taken at a current of 29 mA ( $I_T \approx 20$  mA). The solid lines are the best fit to a driven diffusion equation.

and G. Grüner (Elsevier, Amsterdam, 1989), p. 189.

- 6 S. Ramakrishna, M. P. Maher, V. Ambegaokar and U. Eckern, Phys. Rev. Lett. **68**, 2066 (1992). Note that the definition of  $z$  used in this paper differs from that used in the present one.
- 7 Satish Ramakrishna, Phys. Rev. B **48**, 5025 (1993). Note that the definition of  $z$  used in this paper differs from that used in the present one.
- 8 D. A. DiCarlo, E. Sweetland, M. Sutton, J. D. Brock and R. E. Thorne, Phys. Rev. Lett. **70**, 845 (1993). Note that the definition of  $z$  used in this paper differs from that used in the present one. Similarly, contrary to the present paper, this paper combines  $K_z$  and  $\Delta^2$  into one variable.
- 9 Similar techniques have been used to study  $K_{03}MoO_3$ . See, for example, T. Tamegai, K. Tsutsumi and S. Kagoshima, Synth. Metals **19**, 923 (1987) and references therein.

## MAD phasing on F2: crystallographic results and station developments

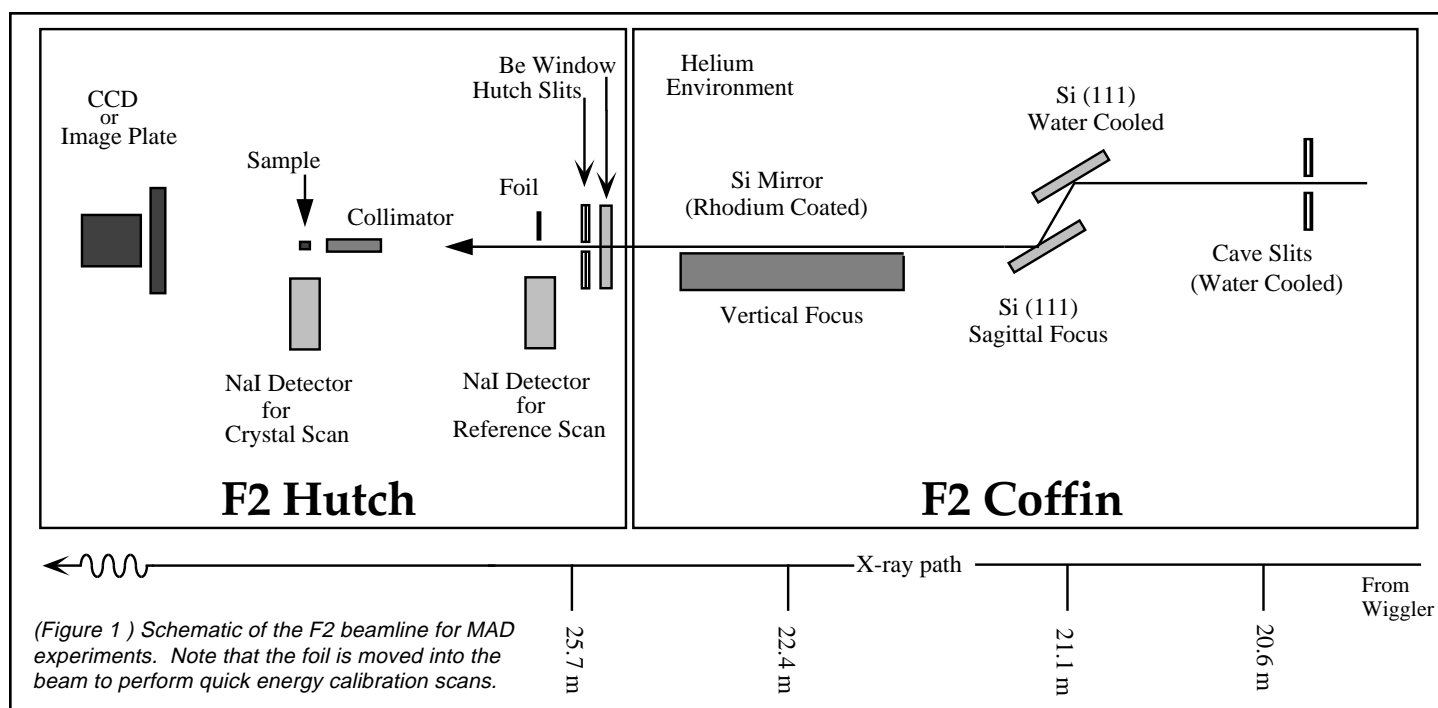
Dan Thiel, Park Doing, and Steve Ealick

Over the last few years, the crystallographic technique known as MAD, or multiwavelength anomalous diffraction, has emerged as one of the more powerful methodologies available to the macromolecular crystallographer.<sup>1</sup> Many structures have now been solved using this technique; however, along with the superior power of the method come extra instrumentation challenges facing the experimenter. At CHESS, the instrumentation for conducting MAD experiments is maturing to the point where outside users are now capable of carrying out MAD runs without relying on their own instrumental resources.

To carry out a MAD experiment, the researcher needs only one crystalline form of the sample - the use of heavy atom derivatives is eliminated. This crystal form must contain a low number of sites (typically between 3 to 10) of an elemental component with an atomic weight preferably in the range of  $Z=20$  to  $Z=40$  or  $Z=60$  to  $Z=92$ . With the one crystalline form, the phase problem can be solved with essentially no ambiguity. This is done by tuning the incident x-ray beam to appropriate energies relative to the absorption edge of this particular atomic element and recording the diffraction data using these various x-ray energies. In such a man-

ner, the positions of these few atoms can first be solved forming a reference point for solving the entire structure.

Obviously, a tunable beamline with the usual high flux and low divergence is necessary to carry out such an experiment. At CHESS, such a facility exists at the F2 doubly-focused wiggler beamline. A 24 pole, 1.2 Tesla permanent magnet wiggler installed in a straight section of the 5.3 GeV Cornell Electron Storage Ring (CESR) emits 6.4 kW of radiation into a 4 mrad horizontal opening at 100 mA of positron current. Station F2 accepts 2 mrad of this radiation which is monochromatized by a



fixed offset, sagittally-focussing monochromator. A schematic of the station optics is shown in Figure 1. A rhodium coated Si mirror located downstream of the monochromator is used to focus the beam vertically and to suppress unwanted harmonics. This doubly focussed wiggler beam has a focal size of 3.6 mm x 0.32 mm in the hutch. At 13 keV, the flux is  $10^{10}$  ph/s after a 0.3 mm collimator (at 100 mA).

Provisions have been built into the MAD setup which permit a rapid periodic check of the calibration of the monochromator to insure that the anomalous signal is being properly recorded. With one computer command, the experimenter rotates a reference foil into the beam at the upstream end of the hutch and initiates a quick scan of the monochromator through the edge energy. After the absorption spectrum is displayed on the terminal, the reference foil and the monochromator return to their starting positions. If the spectrum shows a shift in the calibration, the monochromator is set to the proper position. This process is typically carried out at the beginning and the end of each fill, consuming less than 1 minute of beamtime for each check. During a recent MAD experiment, a

series of reference scans done at the beginning of 4 fills over an 8 hour period showed an energy drift of less than one eV. While this degree of stability was often observed, variations of up to 4 eV have also been seen. Clearly, close monitoring of the calibration of the monochromator is still essential for a successful MAD experiment.

Using this facility, we have recently completed a MAD experiment in collaboration with Menachem Shoham of Case Western University studying the copper-containing protein rusticyanin. The data were collected using the CCD camera which has recently arrived at CHESS (see separate CCD article in this newsletter). Data processing is currently underway.

The results of some earlier MAD experiments demonstrate the effectiveness of the F2 beamline. In August 1992, Aneel Aggarwal's group from Columbia collected MAD data from the restriction endonuclease *bamHI* in which 5 methionine residues were replaced by seleno-methionines. A total of 5 crystals were shot at 3 wavelengths relative to the selenium absorption edge, corresponding to the edge, peak, and a remote wavelength above the edge.

The quality of the data was outstanding, with 97% of the intensities having  $I/\sigma$  greater than 3.0. This data resulted in a  $1.95\text{\AA}$  structure which refined to an R-factor of 19%. From this structure, the researchers have noted that the protein resembles EcoRI despite the lack of sequence similarity.

Finally, Tom Steitz' group from Yale carried out MAD experiments on F2 resulting in the solution of two crystal structures. The core fragment of the E. Coli *lac* repressor was solved using the  $L_{III}$  edge of the anomalous scatterer Hg (12.284 keV) in a non-isomorphous crystal form. Also, a Se edge (12.658 keV) experiment resulted in the structure of the phage T4 gene 32 single-stranded DNA binding protein.

These results highlight the MAD phasing work that has occurred on F2. In the future, we expect to see two of CHESS' strengths exploited in the MAD work - using higher x-ray energies to probe the edges of other anomalous scatterers and carrying out the measurements with the more sensitive CCD camera rather than image plates. Additional exciting results are sure to follow.

<sup>1</sup>For a review see Hendrickson, W. A., Science **254** pp. 51-58, 1991.

# Muscle diffraction at CHESS

Tom Irving

The modern concept of muscle contraction is based on structural, mechanical and biochemical studies, all indicating that relative sliding between the two filament types in the structural sarcomere unit depends upon cyclic ATPase-coupled interactions between so-called cross-bridges. These bridges join thick filaments, made up primarily of the protein myosin, to thin filaments consisting primarily of the protein actin. These filaments, 30 nm and 10 nm in diameter, respectively, form an interdigitating hexagonal lattice. The prevailing "swinging cross bridge model" envisions a 90 to 45 degree "power stroke" or rowing motion of the cross-bridges that translocates thin actin-containing filaments relative to thick myosin-containing filaments, leading to sarcomere shortening.

There have been a number of exciting results in recent years leading toward understanding the structural basis for this process, including *in-vitro* motility assays which have shown that isolated myosin S1 cross-bridges can move isolated actin filaments in fruit flies. But the exact nature of the force-generating myosin-

actin interaction, the ATP-driven power stroke, remains unclear.

There is no doubt that structural studies of *intact* muscle fibers are indispensable to unraveling these mechanisms, since actin or myosin in crystals cannot generate force. Fiber diffraction of muscle has a key role in such studies because of its ability to study muscle fibers under hydrated, physiological conditions, in fact even in the living state. Furthermore, it has the ability to detect global changes in sarcomere structure at the physiologically relevant millisecond and sub-millisecond time scale.

## Measuring the extensibility of muscle filaments

In the last CHESS Activity Report we described a small angle camera designed<sup>1</sup> to fit in the high flux F-1 station. We have used this setup to obtain very accurate spacing measurements of certain wide-angle meridional reflections from contracting muscles. The intent of these measurements was to test the assumption that the flexibility of the filaments is essentially negligible, and that there is no measurable change in spacing when the muscle goes from the relaxed state to isometrically contracting. This is the central assumption of many influential theories of muscle contraction based on mechanical experiments. This assumption turns out to be false.

To show this, we (H. E. Huxley, A. Stewart, H. Sosa and myself) studied the behavior of the first actin meridional reflection (at a spacing of approximately

2.73 nm), the second order of this reflection (1.365 nm) and the 15th order myosin meridional reflection at approximately 2.86 nm (Fig. 1) from living frog sartorius muscles either relaxed or electrically stimulated to contract. These reflections are very weak and require the high intensity available at the F-1 station to collect enough signal before the muscle fatigues.

These reflections also undergo significant changes in spacing which can be measured with great accuracy in an arrangement which allows patterns at different levels of tension during a single experimental series to be compared side by side on the same image plate (Fig. 1). We found that when the muscle changes from the relaxed state to that of isometric contraction, the actin 2.73 nm reflection increases in spacing by between 0.3 and 0.35 %. The force exerted on the filaments can be augmented or diminished by applying moderate speed length changes to a contracting muscle essentially allowing the compliance of the filaments to be measured.

Analysis of these data is still proceeding, but a preliminary look (Figure 2) shows an approximately linear relation of filament length change to the level of force exerted by the muscle. More sophisticated analysis of the paired data suggest some nonlinearity at low tension levels. Notice that the curve for thick filaments has a non-zero intercept. This corresponds to a spacing change associated with activation or "turning on" the muscle. The thin filaments do not appear to show such a change.

In the experiments described so far, we were looking at fairly long lived states (large fraction of a second), much longer than the time scale of the basic force producing process (~ ms). We were also able to show an actin spacing change of 0.25 - 0.3% during a 2 ms time frame immediately following a quick release,

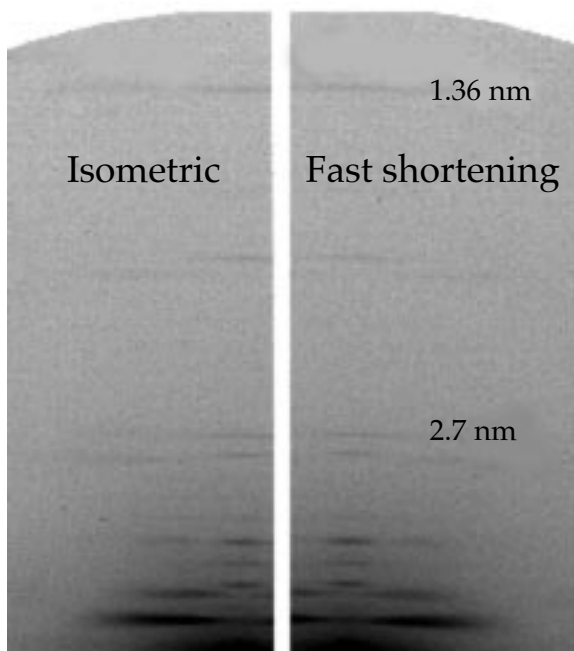


(Figure 1) A side-by-side comparison, on a single image plate, of diffraction from living frog sartorius muscles either relaxed (left) or electrically stimulated to contract. In the contracted state (right), the 1.36 and 2.7 nm layer lines are seen to move to higher angle.

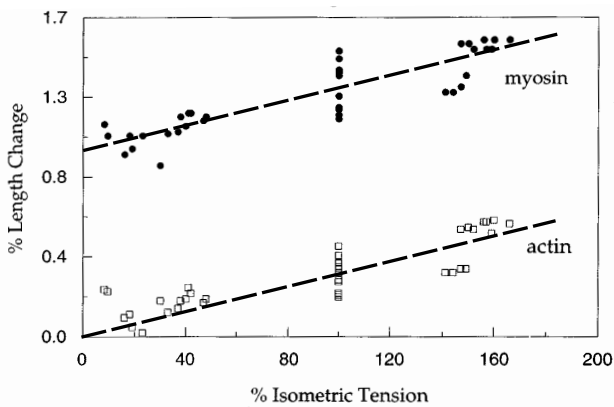


(Figure 2) Filament length as a function of force exerted by the muscle. Data were extracted from x-ray images like those in figure 1.

dulator source (which is also small to start with) can be very helpful for single fiber experiments, since for a given focus size one can deliver more flux to the sample than for a wiggler source delivering the same total flux. To get

showing that this elastic behavior is rapid and is relevant to the basic force producing event. These experiments<sup>2</sup> also show that very detailed X-ray diffraction patterns can be obtained to the required millisecond level time scale on the F-1 beam line. Until small angle facilities at third generation synchrotron sources such as the ESRF and APS become available, these kinds of experiments will be possible only at CHESS.

Single cells are a much better mechanical preparation than whole muscle; but because they are so much smaller, they give correspondingly less diffraction signal. They are also very labor intensive to prepare. Cecchi *et al.* have reported<sup>3</sup> time resolved x-ray diffraction studies of single muscle cells (fibers ~3mm x 200  $\mu$ m) during the rise of tetanic tension. This study used a one-dimensional wire counter with a sampling time of 10 ms to record equatorial x-ray intensity during tetanus rise, while simultaneously monitoring sarcomere length and tension. It would be very desirable to extend these studies to the millisecond or sub-millisecond time resolution which is the time scale of the mechanical events we are studying.

A truly international collaboration of Eric F. Eikenberry (Robert Wood Johnson Medical School), Fredrik Osterberg (Princeton University), G. Cecchi, M. A. Bagni, (Florence), C. C. Ashley, and P.J. Griffiths (Oxford) and myself collected time resolved, two-dimensional x-ray diffraction patterns during the CHESS undulator run last October. The low beam divergence of an un-

around the count rate limitations of delay-line type detectors we used a quantum-limited large format (1Kx1K) CCD detector operating as a streak camera, in which one dimension of the detector recorded time with a sampling interval of 1 ms, while the other dimension recorded distance along the equator in the conventional manner.

The CCD image in Figure 3 gives a direct visualization of the evolution with time of the equatorial x-ray pattern. The equatorial (10) and (11) reflection from single fibers of *Rana Temporaria tibialis anterior* muscle were recorded. During fixed-end tetanus rise, the previously reported

transient increase in equatorial spacing was clearly defined. The excellent spatial resolution of the CCD detector allowed following diffraction peak widths to the same time resolution, showing a marked transient increase in disorder (of the second kind) which gives information on the cooperative movement of groups of fibril components. The physiological significance of this effect is being investigated.

The CCD detector used in this study is the same as that used to record crystallographic data with exceptionally high precision ( $R_{\text{sym}} = 2\%$ ) (see CCD article on page 36). Only a software selection was required to switch between the streak camera and conventional modes of operation. Thus this kind of detector shows great promise for investigating transient phenomena at the very high flux beam lines that are becoming available.

[1] Camera designed by H.E Huxley, Brandeis; J. Bordas, Daresbury, and T. Irving, CHESS. See a descriptive article in "Synchrotron Radiation and Biophysics," Irving, T, and Huxley, H. E., (Oxford University Press) 1994.

[2] These observations of filament extensibility complement and extend studies done by Dr K. Wakabayashi (Osaka) and colleagues at the Photon Factory who studied the changes in spacing upon contraction as a function of muscle length. The two groups will submit their results together in the near future.

[3] Cecchi, *et al.*, *Biophys. J.* **59**, 1273-1283 (1991)

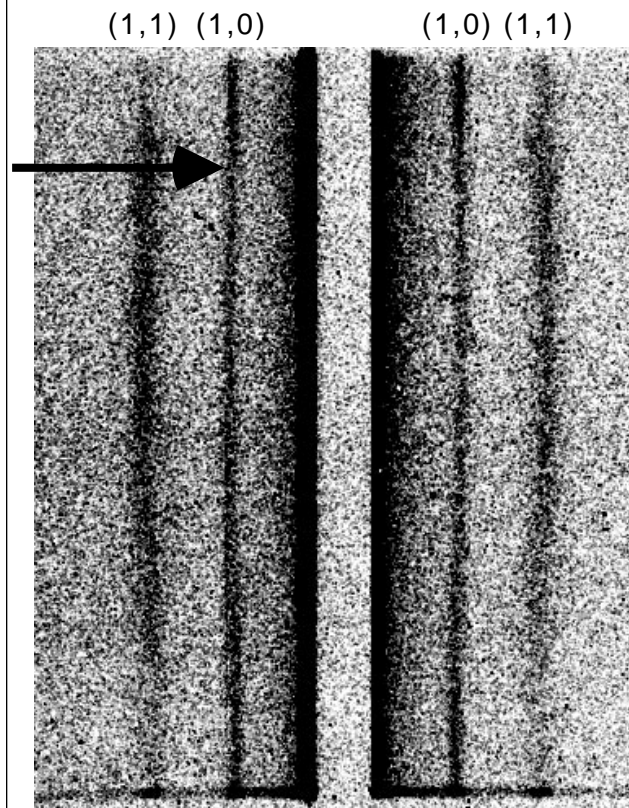


(Figure 3) CCD streak camera image of x-rays diffracted from single fibers of *Rana Temporaria* muscle during fixed-end tetanus rise. Each horizontal row is a one-dimensional pattern recorded during 1 millisecond. The arrow shows the onset of a transient increase in lattice spacing. The (10) and (11) hexagonal lattice reflections are as indicated. Note the varying width of the (11) reflection.

# Circular magnetic X-ray dichroism in crystalline and amorphous GdFe<sub>2</sub>

J.C. Lang<sup>\*s</sup>

Ames Lab - USDOE and Department of Physics and Astronomy,  
Iowa State University, Ames, Iowa 50011

With the advent of intense synchrotron radiation sources there has been renewed interest in utilizing x-rays to examine the magnetic properties of a variety of materials. One technique which has recently attracted great interest is Circular Magnetic X-ray Dichroism (CMXD).<sup>1</sup> CMXD is defined as the difference,  $\mu_c = \mu^+ - \mu^-$ , between the absorption of left and right circularly polarized x-rays by a magnetized sample, with  $\mu^+$  ( $\mu^-$ ) representing the absorption coefficient for x-rays with the wave vector parallel (antiparallel) to the local magnetic moment of the absorbing atom. Since x-ray absorption involves transitions from well understood core levels with well defined angular momenta, observed structure in the dichroic spectra can yield information about the ground state spin polarization and spin-orbit coupling of final states.<sup>2</sup> Further, the information obtained is element and orbital specific since the technique requires scanning through a specific absorption edge. This technique can provide unique information since most magnetic measurements provide information about the total bulk moment. In the case of rare earth L<sub>2</sub> and L<sub>3</sub> edges the final states correspond to empty levels within the 5d bands which are primarily responsible for mediating the ordering among the 4f local moments.

To become a useful tool for probing electronic and magnetic structures CMXD spectra should also be material specific, i.e., sensitive to the changes in the band structure produced by different local environments. In this study, we compare the CMXD spectra of amorphous GdFe<sub>2</sub> with its crystalline counterpart and with a first principles theoretical calculation of the dichroic spectra for crystalline GdFe<sub>2</sub>. Changes in coordination and nearest neighbor distances in amorphous GdFe<sub>2</sub> should produce sufficient changes in the electronic structure to be detectable by CMXD measurements. Amorphous rare earth-transition metal materials are of considerable interest because of their many unique magnetic and magneto-optical properties.<sup>3</sup> For a better understanding of these effects, knowledge of the spin-polarization and spin-orbit coupling of individual orbitals is necessary.

CMXD analysis is, in principle, well suited to providing such information. Quantitative measurements of the degree of spin-orbit coupling are possible by employing recently derived sum rules, which relate the integrated intensity of the dichroic  $\mu_c$  and normal  $\mu_0$  absorption to the ground state values of the orbital<sup>4</sup>  $\langle L_z \rangle$  and spin<sup>2</sup>  $\langle S_z \rangle$  parts of the magnetic moment. Until now, a separate determination of the spin and orbital magnetic moments has been possible only by non-resonant magnetic x-ray scattering.<sup>5</sup> Owing to the small size of the magnetic cross section, however, this technique has been limited to samples with large magnetic moments (i.e. Gd  $\mu(4f) = 10\mu_B$ ; where  $\mu_B$  is the Bohr moment).<sup>6</sup> Further, this technique is not orbital specific and requires measurement of several magnetic diffraction peaks with different q values. CMXD, on the other hand, can give the values of moments on the order of  $0.01\mu_B$  with measurements at just the L<sub>2</sub> and L<sub>3</sub> absorption edges.

The CMXD measurements were made at the Cornell High-Energy Synchrotron Source bending magnet D line making use of elliptical polarization ( $P_c \approx 0.66 \pm 0.10$ ) of the synchrotron beam 0.11 mrad above the electron orbital plane. The beam was diffracted by a double crystal Si(220)

monochromator yielding an energy resolution of  $\sim 1.5$  eV in the vicinity of the Gd L edges. In order to eliminate harmonic contamination of the incident beam, the x-rays were reflected from a flat quartz mirror placed after the monochromator. The magnetization of the sample was reversed by a 3.5 kG electromagnet, with the magnetic field oriented at 30° to the beam direction.

The polarization of the field was flipped every 2s at each step in an energy scan through the edges, thus producing two absorption spectra.  $I^+$  is the transmitted intensity when the magnetic moment of the sample and photon wave vector are in the same direction and  $I^-$  the transmitted intensity when the two are in opposite directions. We relate these to the dichroic signal by

$$\mu_c d = \frac{1}{M' P_c \cos\theta} \left( \ln \left( \frac{I_0^+}{I^+} \right) - \ln \left( \frac{I_0^-}{I^-} \right) \right) \quad (1)$$

where  $I_0^\pm$  are the incident intensities and  $d$  the effective sample thickness. In order to account for different experimental conditions and sample characteristics, the data were normalized by  $M'$ , the fraction of the T=0K saturation magnetization attained at room temperature with the field employed  $P_c$  the degree of circular polarization of the incident beam, and  $\cos\theta$ , where  $\theta$  is the angle between the photon beam direction and the magnetic field direction.

The experimental spectra,  $\mu_0$  and  $\mu_c$  taken in 0.5 eV steps at the Gd L<sub>2</sub> and L<sub>3</sub> edges along with theoretical curves for crystalline GdFe<sub>2</sub> are shown in figs. 1a and 1b. A large enhancement of the amorphous dichroic spectra over the crystalline spectra is observed. This difference is believed to be due to a decreased spin-polarization of the 5d band in the amorphous material compared to the

(Figure 1) Top: Absorption of crystalline and amorphous samples. Middle: Dichroism signal  $\mu_c$  of crystalline and amorphous samples. Bottom: Theoretical curve for crystalline  $GdFe_2$ . a) Dichroism at the  $Gd L_3$  edge. b) Dichroism at the  $Gd L_2$  edge.

crystalline caused by a smaller Gd-Fe coordination. The Fe coordination around each Gd atom is  $6.5 \pm 0.6$  in amorphous  $GdFe_2$  as compared to 12 for the crystalline compound while the nearest neighbor distances remain roughly the same.<sup>7</sup> This smaller coordination number reduces the 5d(Gd)-3d(Fe) exchange thus diminishing the spin polarization of the 5d(Gd) band. This smaller degree of exchange reduces both the 5d and 3d moments, but since they are oppositely oriented their sum remains essentially constant. This results in a greater number of unoccupied holmium spin up states above the Fermi energy producing the observed enhanced signal. It should be kept in mind that CMXD is a measure of the empty state polarization. Thus, in this case, a smaller net 5d spin moment corresponds to a larger CMXD signal.

At the rare earth  $L_{2,3}$  edges, with initial p ( $l=1$ ) states, final d ( $l=2$ ) states, and 5d electron occupancy  $n \approx 1.8$  (from the band theory), the sum rules for the orbital  $\langle L_z \rangle$  and spin  $\langle S_z \rangle$  moments reduce to the following simple expressions,

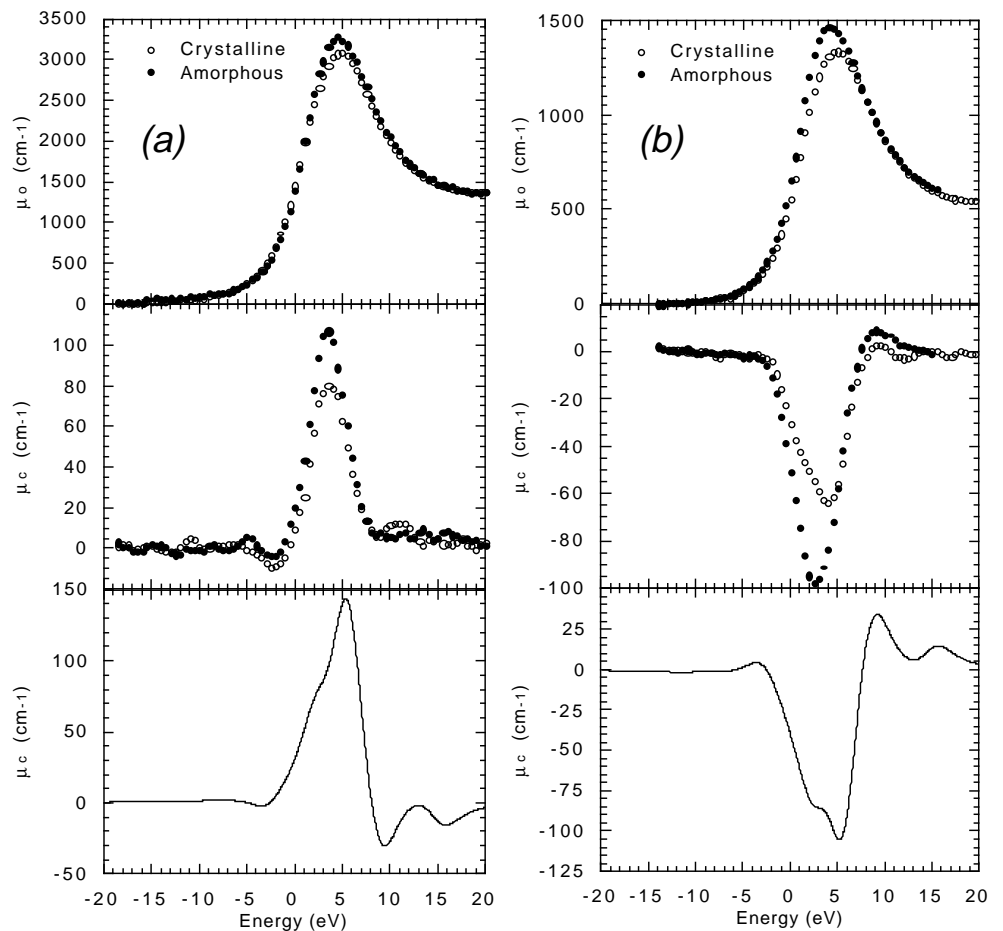
$$\int_{L_2+L_3} d\omega \mu_c \bigg/ \int_{L_2+L_3} d\omega 3\mu_0 = 16.4 \langle L_z \rangle, \quad (2)$$

and,

$$\left( \int_{L_3} d\omega \mu_c - 2 \int_{L_2} d\omega \mu_c \right) \bigg/ \int_{L_2+L_3} d\omega 3\mu_0 = 12.3 \left( \langle S_z \rangle + \frac{7}{2} \langle T_z \rangle \right), \quad (3)$$

with  $3\mu_0 \approx \mu^+ + \mu^- + \mu_0$ . In the expression above  $\langle T_z \rangle$  is the spatial average of the magnetic dipole operator<sup>2</sup> which is generally not  $\langle S_z \rangle$  in the expression for rare earth  $L_{2,3}$  edges. Thus, for the rare earth 5d states a quantitative value of only the orbital moment can be obtained.

Using these expressions, orbital moment values of  $0.018 \pm 0.005 \mu_B$  and  $0.005 \pm 0.003 \mu_B$  were obtained for the crystalline and amorphous samples respectively. The uncertainty in the size of the moments arises primarily from the uncertainty in the degree of circular polarization. Since both the amorphous and crystalline data are scaled by this value, the error in relative difference between the amorphous and crystalline samples is  $\sim 15\%$  less. The smaller value of the 5d band spin polarization in the amorphous sample is also responsible, in part, for the substantially smaller  $\langle L_z \rangle$  as compared to the crystalline sample, since a smaller net 5d moment implies a smaller orbital moment. The domi-



nant mechanism responsible for the quenching of the orbital moment, however, is believed to be the more random crystal field symmetry present in the amorphous sample. The average crystal field at a particular Gd site should be substantially more asymmetric in the amorphous compound as compared to the crystalline sample leading to decreased effectiveness of the spin-orbit coupling to produce an orbital polarization of the 5d conduction bands.

The theoretical dichroic spectra at the  $L_2$  and  $L_3$  edges reproduce the general features observed in the experimental spectra, however they possess more pronounced structure. It is believed that this is due to the neglect of core-hole effects. The inclusion of core hole effects would draw in, and narrow, the 5d band compressing the signal near the Fermi energy, as observed in experiment. The sum rules are not affected by the core hole, since they involve an integration over all states. The

value of the 5d orbital moment observed by experiment,  $.018 \pm .005 \mu_B$  for crystalline GdFe<sub>2</sub>, agrees well with the value obtained from theory,  $.014 \mu_B$ .

This study has demonstrated that the differences in the spin dependent band structure between amorphous and crystalline materials are easily observable by CMXD. Further, it has been shown that the differences can be quantified using the recently derived sum rules to obtain the size of the orbital moments. This information is unique since other methods provide information on the bulk moment and not that of individual orbit-

als and generally can not separate the orbital and spin contributions. This is important in materials such as rare earth transition metal compounds where changes in the 5d-3d spin polarization can cancel in a bulk measurement. This information should prove valuable in analyzing the magnetic and magneto-optical properties of amorphous rare earth-transition metal materials. It is expected that, with the advent of third generation synchrotron sources, CMXD should become an increasingly important tool to probe the magnetic properties of a variety of materials.

\* Present address, Advanced Photon Source, Bldg. 362, Argonne Natl. Lab., Argonne, IL 60439.

- § A full report is forthcoming in Phys. Rev. B.
- 1 G. Schütz, M. Knülle, R. Wienke, W. Wilhelm, W. Wagner, P. Kienle, and R. Frahm, *Z. Phys. B* **73**, 67 (1988).
  - 2 P. Carra, B.T. Thole, M. Altarelli, and X. Wang, *Phys. Rev. Lett.* **70**, 2307 (1993).
  - 3 K.H.J. Buschow in Handbook on the Physics and Chemistry of Rare Earths Vol. 7, Ch. 52, eds. K.A. Gschneidner Jr. and L. Eyring (North-Holland, Amsterdam, 1983).
  - 4 B.T. Thole, P. Carra, F. Sette, and G. van der Laan, *Phys. Rev. Lett.* **68**, 1943 (1992).
  - 5 M. Blume and D. Gibbs, *Phys. Rev. B* **37**, 1779 (1988).
  - 6 Doon Gibbs, D.R. Harshman, E.D. Isaacs, D.B. McWhan, D. Mills, and C. Vettier, *Phys. Rev. Lett.* **61**, 1241 (1988).
  - 7 G.S. Cargill III, *Solid State Phys.* **30**, 227 (1975).

## Energy dispersive XAS and diffraction

Ken Finkelstein

CHES will soon provide users the opportunity to perform Energy Dispersive X-ray Absorption Spectroscopy (EDXAS) and Diffraction (EDXD) experiments utilizing a focusing crystal polychromator and position sensitive diode array detector (PSD). A preliminary series of measurements with this type of system has resulted in two papers; one on Circular Magnetic X-ray Dichroism (CMXD)<sup>1</sup> and a second on EDXD<sup>2</sup>.

An energy dispersive optical system permits the simultaneous collection of data with good energy resolution over a wide energy range<sup>3</sup>. The data are collected using the geometry illustrated in Figure 1. A tightly bent silicon monochromator crystal collects and focuses a horizontal swath of bend magnet radiation. The focused beam has a broad energy width because of the asymmetric cut and large focal ratio. The sample is positioned at the focus and the beam

is either transmitted through, or diffracted from this point. The PSD is placed a sufficient distance from the sample to permit the beam to spread out and be collected with good spatial resolution. The perfect crystal monochromator combined with a small source and detector pixel size afford high energy resolution.

The monochromated intensity is the same as, for instance, a 2cm wide beam at C2 but the energy is spread out over a 100 - 1000 eV range. The PSD made by Princeton Instruments

uses a 1024 pixel (25  $\mu\text{m}$  pixel size) Redicon chip and 16-bit ADC where typically one count is one x-ray photon. It can be read out at a rate of 5 microseconds per pixel and has a minimum exposure time of 5  $\mu\text{s}$ . (or 10 mseconds between exposures). Thus the maximum count rate, about  $10^{10}$  photons/second, is well matched to the intensity from the mono. In a typical experiment one signal averages by accumulating several seconds or more of exposure; in a high count rate situation this means thousands

(Figure 1, right) Schematic layout of an energy dispersive optical system. The monochromator is a bent perfect crystal (top). The transmission geometry at left is used for x-ray absorption studies. At right is illustrated the arrangement for dispersion-matched diffraction from a sample single crystal.

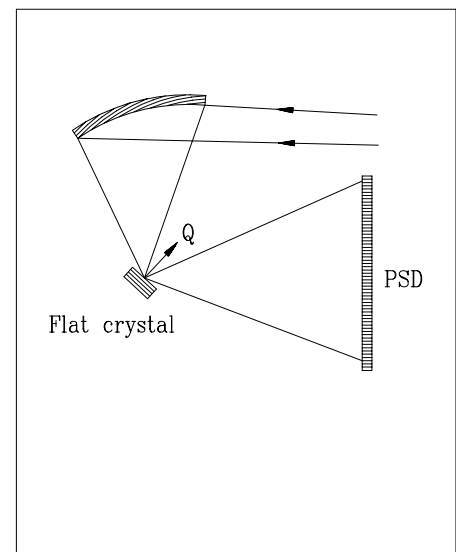
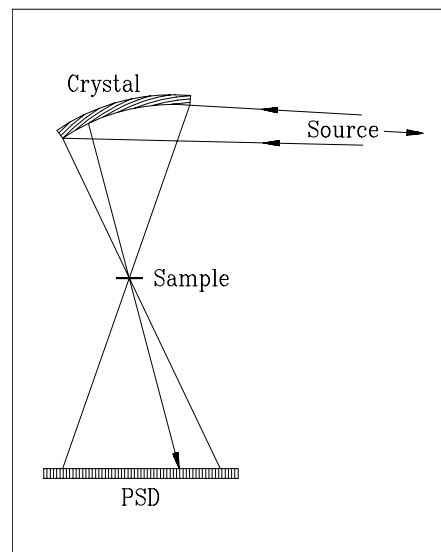
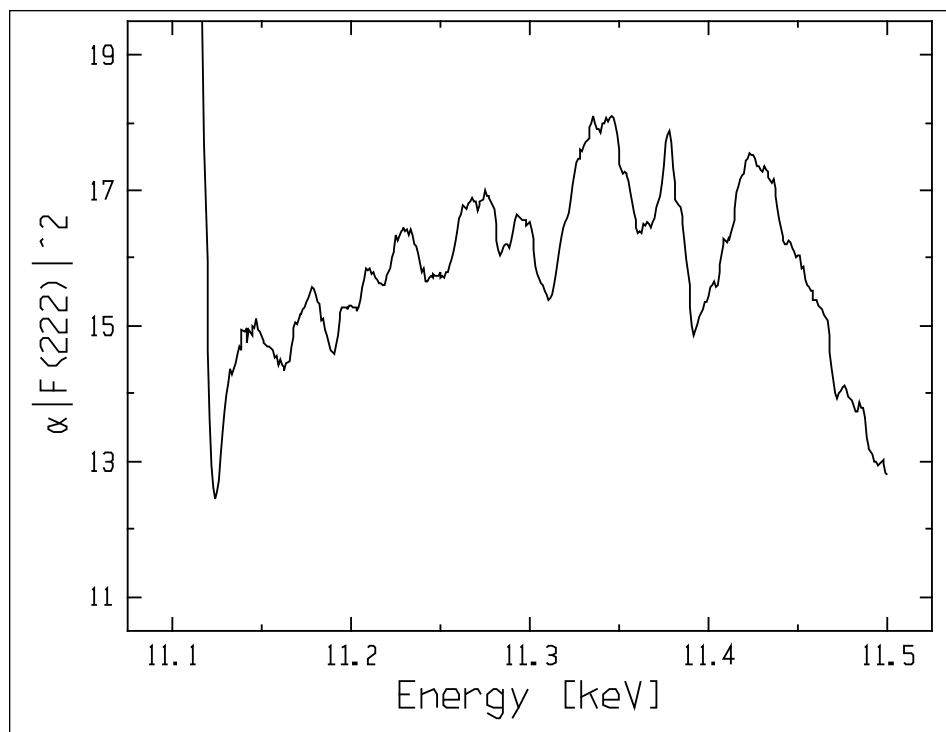


(Figure 2, right) The simultaneous collection of diffraction data from the (222) reflection in a germanium single crystal. A cusp at the K-edge (11.106KeV) and the so-called DAFS are visible in the diffracted intensity.

of exposure-readouts. Unlike the ion chambers we typically use for absorption spectroscopy, the PSD has readout noise (1-2 counts/readout) that will ultimately limit the maximum accumulated signal to noise ratio. This feature would most strongly affect experiments where a weak signal is to be measured in the presence of a large background intensity. It has not proven to be a significant deficiency. One strength of the arrangement is the possibility of time sampling the signal with a frequency range from 100 to 0.01Hz. For short time resolution processes, the best experiments are those for which the excitation can be repeated many times and the sequence of time slices averaged.

The scientific applications of this method can be illustrated by several examples. In the field of electrochemistry, EDXAS is used for the *in-situ* structural study of active sites on surface confined electrocatalysts. Standard electrochemistry has offered only indirect information on the structural nature of such sites. They are known to act as low energy pathways connecting reactants and products. The promise of this approach comes from combining element specificity with an ability to monitor in time (or as a function of electrode voltage) changes in short range order.

In a related area, workers at CHESS have used EXAFS to study the self-sustaining oscillatory oxidation of carbon monoxide over supported platinum catalysts<sup>4</sup>. The basic question is whether small metal clusters making up the catalyst display morphological change as their oxidation state changes. The most interesting part of this reaction is re-ignition which lasts less than one second. By repeated observation of the reaction cycle it should be possible to resolve this question using the sub-second time sensitivity available with dis-



persive optics.

An important application for which the energy dispersive CMXD offers significant advantage is the investigation of magnetic order using elliptically polarized x-rays. This spin dependent, near-edge absorption technique is sensitive to the electronic environment and magnetic state of the spin-polarized electrons in a solid. Measurements at CHESS have shown that compared to a double bounce arrangement, a single bounce side-diffracting monochromator can produce more intensity at a higher purity of circular polarization. Reference 1 will describe some results of dichroism studied as a function of angle using the energy dispersed beam.

Finally, a novel application for dispersive optics is being developed at CHESS. In the area of anomalous diffraction it is possible to simultaneously collect a diffraction pattern over a continuous energy range from a single set of Bragg planes in a crystal. This idea is illustrated in figure 2 which shows the integrated intensity of a germanium (222) reflection in a 400 eV range about the germanium K-edge. We have analyzed<sup>2</sup> these oscillations and obtained germanium

near-neighbor distances in good agreement with the known values. By eliminating monochromator movement as the energy is changed and by taking advantage of the small focal spot size, this new method should facilitate anomalous diffraction studies on small crystals. In addition, the wide energy bandpass is ideal for measurement of diffraction anomalous fine structure (DAFS) in single crystals.

Results from our first energy dispersive run are very encouraging as is the interest it has generated in the user community. Since that time, Matt Borthwick, a Cornell COOP (undergraduate) student, has been developing software that permits the PSD to interface with the SPEC software used for data collection at our stations. A second run is being planned for early Spring 1994. Please contact CHESS to discuss other possible uses for dispersive optics.

1 J.C. Lang *et al.*, Submitted to Phys Rev B (1994).

2 K.D. Finkelstein and Mark Sutton, Nuc Instr. Meth. (1994) in press.

3 A. Fontaine, *et al.*, Rev. Sci. Instrum. **63** (1), 960 (1992).

4 H.J. Robota and Di-Jai Liu, submitted to J. Phys. Chem. (1993).

# An atomic monolayer of Ag on the Si(111) surface

Gary Navrotsky

Materials Science and Engineering, Cornell University

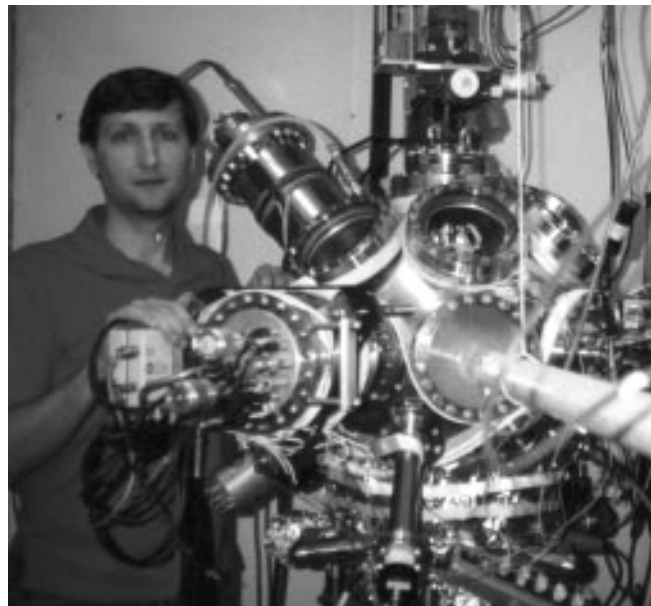
Probing an atomic monolayer of  $10^{13}$  atoms adsorbed on an ultra-clean,  $600^{\circ}\text{C}$ , semiconductor surface in ultra-high vacuum with 3.5 to 27 keV x-rays could be an experimentalist's nightmare — if it weren't for the facilities available at CHESS. The initiative to use synchrotron x-rays to study surface structure was launched at CHESS in the 1980's by Professors Bob Batterman, CHESS, and Jack Blakely, Materials Science, with funding provided through Cornell's Materials Science Center. Recently, interesting studies of submonolayers of Ag (adsorbate) on the Si(111) surface have been completed using the X-ray Standing Wave (XSW) and polarization dependent Surface EXAFS (SEXAFS) techniques.

## Why Ag? An Enigmatic 2D Phase System.

In 1967, K. Spiegel<sup>1</sup> was probably pragmatically motivated to put silver atoms on a silicon surface. There was a lot to understand about the nature of ohmic and Schottky interfaces at that time. A simple *model system* was needed where atomic structure was known so that electronic structure

could be calculated. There is only one d-metal/silicon system without a complicating silicide structure; only one combination that bulk studies had unambiguously shown not to intermix — that was the Ag on Si system. Spiegel conducted the first Low Energy Electron Diffraction (LEED) studies and showed that it took 1/3 of a monolayer (1 Ag atom for every 3 Si atoms in the surface unit cell) to cover the surface before subsequent Ag deposits produced crystalline Ag islands on top of this adlayer. The Ag/Si(111) interface was thus modeled as Ag atoms sitting in hollows formed by three Si surface atoms and making a centered-hexagonal network on the surface (see figure 1).

Today, 27 years later, this *simple*, non-silicide forming, non-intermixing system of silver atoms on a Si(111) surface has been repeatedly tested, by *every* available surface science technique. The result — not confirmation or refinement of the original findings — but total chaos! Over 125 different papers from almost as many research groups battle over which of at least fourteen surface structural models their results support. There is no consensus as to how many Ag atoms per Si surface unit cell constitutes a single monolayer and no consensus even as to wheth-



Gary Navrotsky with UHV chamber at D-line.

er the Ag atom sits on the Si surface or embeds itself in the top surface layer!

The most famous example of this confusion came in a 1987 *Physical Review Letters*. Two groups, working independently and using the newly developed Scanning Tunneling Microscope (STM) studied the Ag/Si(111) surface. Both groups were members of IBM's research laboratory system; Wilson<sup>2</sup> at IBM Almaden in California and Van Loenen<sup>3</sup> at IBM Watson Research Center in New York. The Almaden group determined that the Ag atoms sat in a honeycomb structure on the Si(111) surface — the Watson group concluded that the Ag atoms were embedded under a Si surface layer.

Today, the theoretical interest in Ag/Si(111) as a model system has long been forgotten. The applied interest in understanding Ag/Si as a Schottky barrier has been supplanted by experience. To surface scientists, Ag on Si(111) has just become an **enigma**. With the solution of its structure, we can, hopefully, begin to understand the interaction between

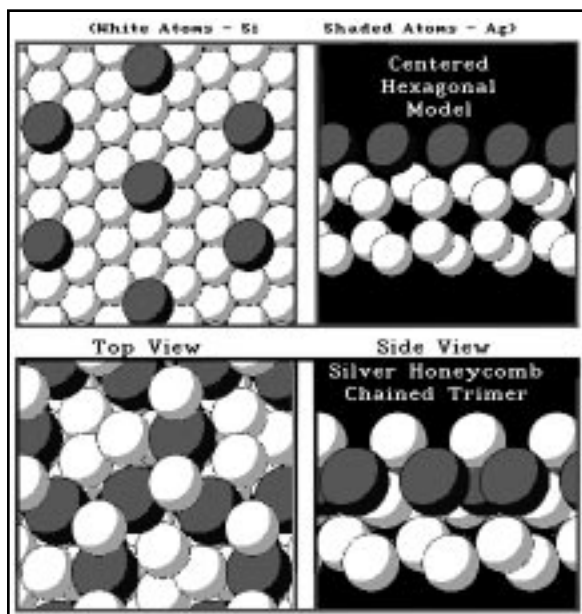


(Figure 1) Two of fourteen competing models for Ag/Si: (top) Spiegel's original CH model<sup>1</sup>, (bottom) recent SHCT model.

the crystallographic, electronic and chemical structures producing metal induced semiconductor surface states.

The research described here attempts to answer the basic question, "How can so many good researchers from so many good labs come to such fundamentally different conclusions about the surface structure of such a simple system!". XSW and SEXAFS have been done on the surface concurrently with LEED and other surface techniques, providing information that takes account of any surface contraction effects. Additionally, we have studied the rare  $3 \times 1$  to  $\sqrt{3} \times \sqrt{3} R30^\circ$  phase transition in order to gain insight into the Ag surface placement.

### Experiments at D-line.

The XSW technique provides a measurement of atomic position relative to bulk diffraction planes and SEXAFS provides bond-length information. To study silver and silicon without the interfering effects of other atomic species, experiments must be done under ultra-high vacuum conditions. At base pressures of  $8 \times 10^{-11}$  torr ( $1 \times 10^{-9}$  Pa.) and elevated temperatures of 400 to 600°C, there was a useful 18 to 24 hours experimental window before surface contamination became detectable.

A UHV beamline end-chamber was designed for use at CHESS station D-1 (see photo). Numerous pumping stages help this chamber to

reach a demonstrated  $5 \times 10^{-11}$  torr ( $0.67 \times 10^{-9}$  Pa.) base pressure. (For comparison, the Wake Shield Facility recently flown on NASA's February '94 Shuttle mission achieved a vacuum of about  $5 \times 10^{-9}$  torr while flying outside of the orbiter.) Instrumentation on the end-chamber includes LEED, a CMA for electron analysis, a Knudsen effusion/deposition source, sample furnaces and thermometry, a movable Si(Li) fluorescence detector port, a sample load-lock mechanism, 8" diameter Be windows for entrance and exit x-ray beams, viewports, an RGA system and internal quartz IR bake-out heaters.

Experiments were conducted at CHESS' D-1 bend magnet station. Specially designed Si(111) and Si(220) four-bounce crystal sets were used to provide the wide energy range needed for Ag K (25.5 keV) SEXAFS and lower energy XSW experiments. The four bounce designed provides for detuning the two-bounce pairs to reduce the monochromator energy band-pass and allow an accurate sampling of

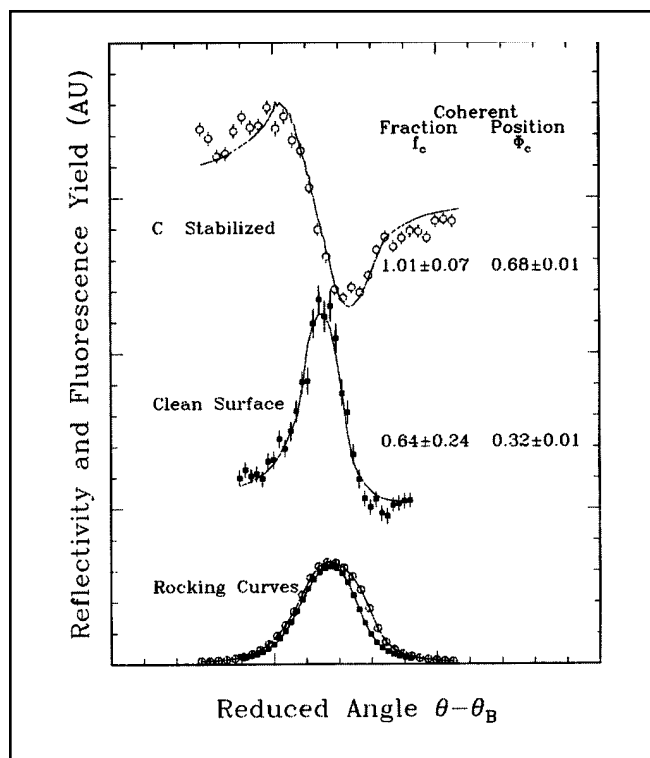


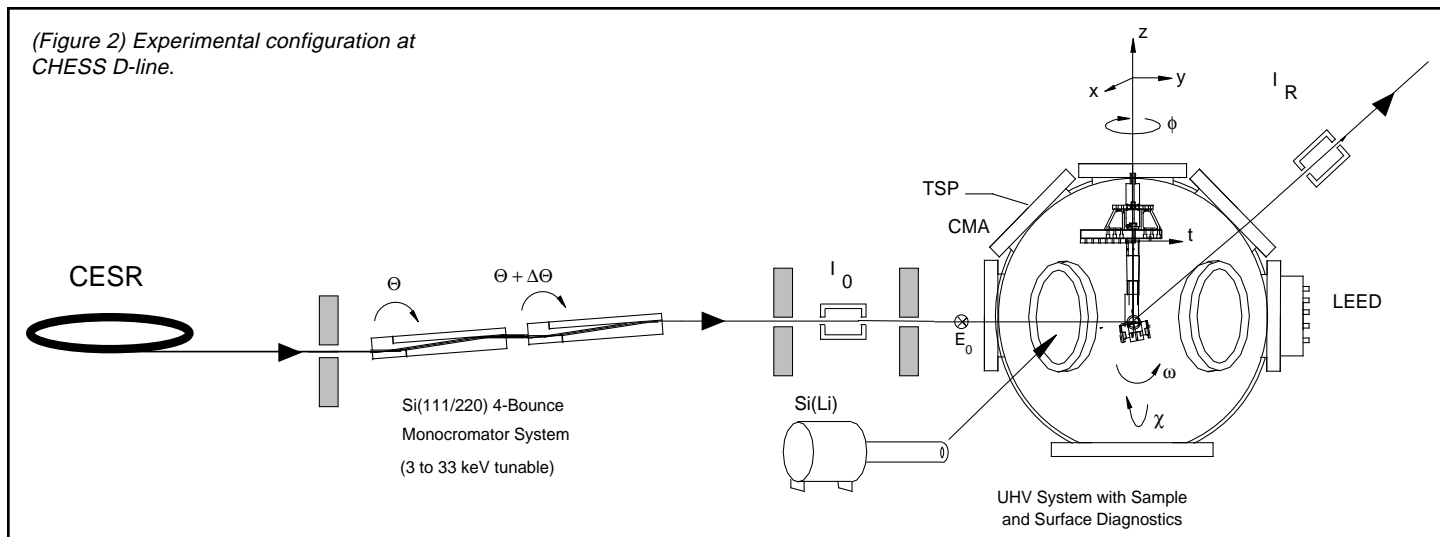
(Figure 3) XSW results for 0.2 monolayers at 400C: (top curve) well-ordered Ag on surface with slight carbon contamination, (middle curve) carbon free surface. The different coherent fractions and atomic positions indicate different Ag structures in the two cases.

the sample's Darwin reflection curve. (These monochromator sets are available for use at CHESS' D-1 and B-2 stations.)

### Results? Don't Just Expect the Unexpected — Count on it!

Two dominant factors were serendipitously found to control the surface structure. The first is carbon contamination; even slight amounts

(Figure 2) Experimental configuration at CHESS D-line.



will inhibit the formation of the  $3 \times 1$  phase. Unexpectedly, we found that the structure is path dependent, that is, the method used to get to a point on the surface phase diagram can dramatically affect the resultant structure.

A few of the interesting XSW experimental results are shown in figure 3. Curves are both from surfaces with about 0.2 monolayers of Ag on Si(111) at 400°C. LEED patterns from both surfaces show a strong  $\sqrt{3} \times \sqrt{3} R30^\circ$  structure; both data sets are taken from the same sample, prepared and cleaned in the same way. The difference is that one surface has trace amounts of carbon contamination which suppresses the  $3 \times 1$  phase and stabilizes

the  $\sqrt{3} \times \sqrt{3} R30^\circ$  Ag phase. The Fourier Transform (FT) SEXAFS spectrum,  $\sigma$ -polarization, also shows that Ag in the C stabilized surfaces is mono-positional while the Ag on the clean surfaces is multi-positional in the  $3 \times 1$  and  $\sqrt{3} \times \sqrt{3} R30^\circ$  phases. Depending on the path taken through the surface phase diagram and surface cleanliness, one can get a single nearest-neighbor bond length to dominate or, at other times, a three peaked structure to appear where there is bulk-like Ag behavior and multiple, but close, nearest neighbor distances.

Does this help explain the disparity in results of the last 27 years? Certainly! Normally reported in the literature is the final coverage and

temperature conditions of a test, but rarely the path taken to get to that endpoint. Once a method is found to reach that endpoint, the same path to that endpoint is typically taken, reducing the number of variations introduced in the procedure. Each experiment becomes self-consistent.

It may be possible that many experiments, different as they are, may be correct! We may not be closer to understanding the Ag-Si interaction but these recent results suggest areas in which greater care must be exercised in the future.

<sup>1</sup> K. Spiegel, *Surf.Sci.* **7** (1967) 125.

<sup>2</sup> R.J. Wilson and S. Chiang, *Phys.Rev.Lett.* **58** (1987) 369.

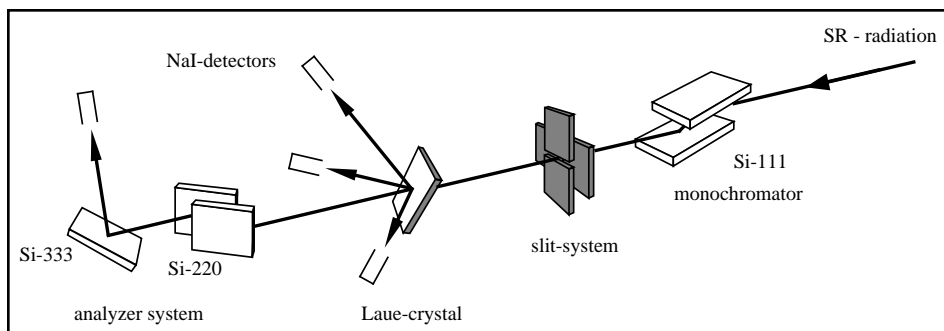
<sup>3</sup> E.J. van Loenen, J.E. Demuth, R.M. Tromp and R.J. Hamers, *Phys.Rev.Lett.* **58** (1987) 373.

## X-ray collimation by multiple beam diffraction

Reinhard Pahl  
Humboldt Fellow, CHESS

A unique method for the collimation of X-rays has been tested at CHESS. Employing multiple beam diffraction in thick Laue-crystals, a very narrow angular divergence in the forward diffracted beam has been obtained.

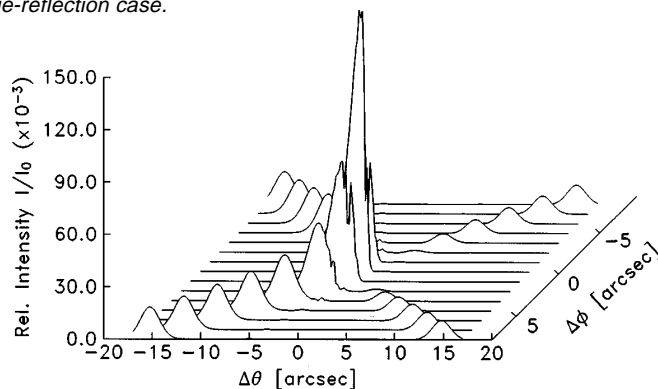
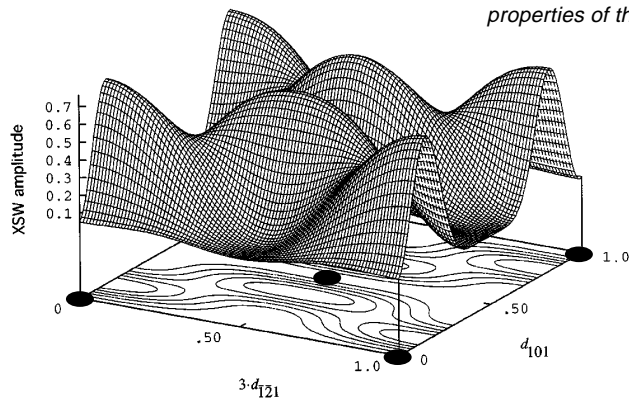
Simultaneous reflections from different sets of reciprocal lattice planes are a very well known diffraction process.<sup>1,2</sup> In Bragg geometry, this is commonly used for solving the so-called phase problem. In Laue geometry, the multi-beam reflection in some cases yields an enhanced trans-



(Above) Experimental setup at CHESS beamline D1.

(Below, left) Calculated amplitude for the x-ray standing wavefield in the (111)-plane of the Si lattice at the exact setting of the six-beam Laue diffraction case. Note that the wavefield has nodes at the locations of the Si atoms (black ovals), so that the attenuation is greatly diminished.

(Below, right) Calculated intensity distribution of the 0-beam for the  $Si-044, 2\bar{2}0, 20\bar{2}, 2\bar{4}2, \bar{2}24$  reflection. The narrow angular spread in both directions  $\Delta\theta$  and  $\Delta\phi$  shows the excellent collimation properties of this Laue-reflection case.



mitted or reflected intensity compared to the normal two-beam diffraction. This enhanced Borrmann effect is caused by a minimized absorption when interference of the wavefields inside the crystal results in a reduced amplitude in the vicinity of the lattice-atoms as shown in the figure. As the enhancement is limited to a narrow angular range the transmitted beam shows very good collimation in any direction normal to the propagation vector.

A computational analysis of multi-beam diffraction in Laue and Bragg geometries based on the dynamical theory of X-rays was carried out to study these effects for several crystal orientations. Significant effects were found for a germanium four-beam and a silicon six-beam Laue-reflection. In both cases the forward diffracted beam is expected to have a significantly higher transmission than in the two-beam cases combined with a very narrow angular width. The absorption coefficients at 8 keV have been calculated to be  $\mu_{\text{Ge}} = 21 \text{ cm}^{-1}$  and  $\mu_{\text{Si}} = 3.9 \text{ cm}^{-1}$  compared to  $\mu_{\text{Ge-400}} = 32.5 \text{ cm}^{-1}$  and  $\mu_{\text{Si-044}} = 21.5 \text{ cm}^{-1}$  for the corresponding 2-beam values of the main reflections respectively.

The experiments were performed at the CHESS beamline D1 using ger-

manium and silicon Laue-crystals with monochromatic X-rays at 8 keV. The angular intensity distribution  $I(\theta, \phi)$  of the 0-beam, i.e. the forward diffracted beam, was analyzed by a high resolution double-crystal system. For both multi-beam cases the observed divergence of the anomalous transmission is less than  $1.6 \times 10^{-5}$  rad. In particular, the Si-044, 220, 202, 242, 224 diffraction resulted in point-like collimation: the FWHM was measured to be approx. 9 mrad parallel and vertical to the main diffraction plane (see photo). The experimental data are in good agreement with theory.

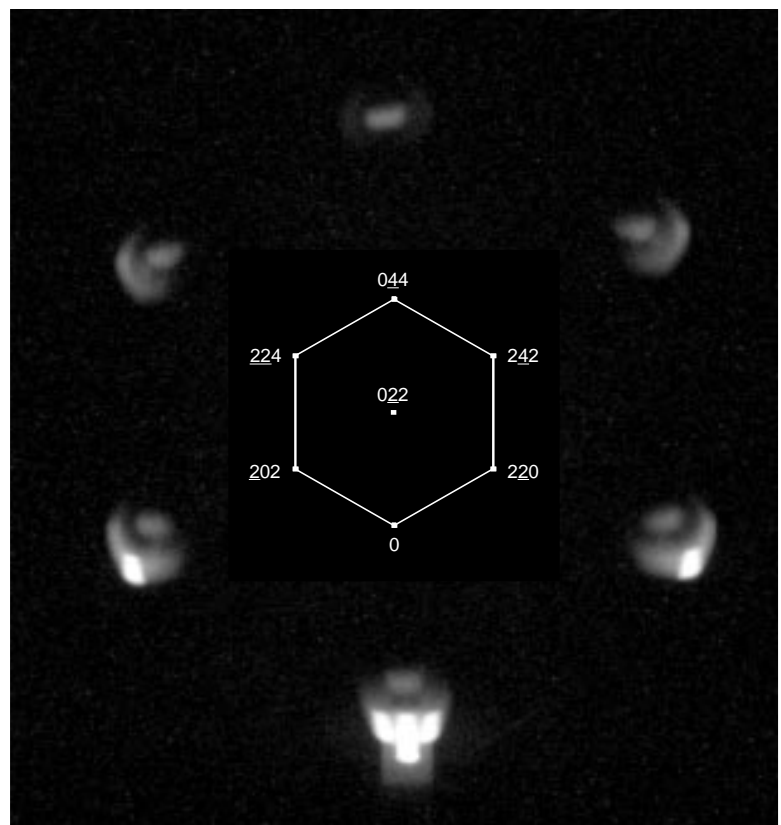
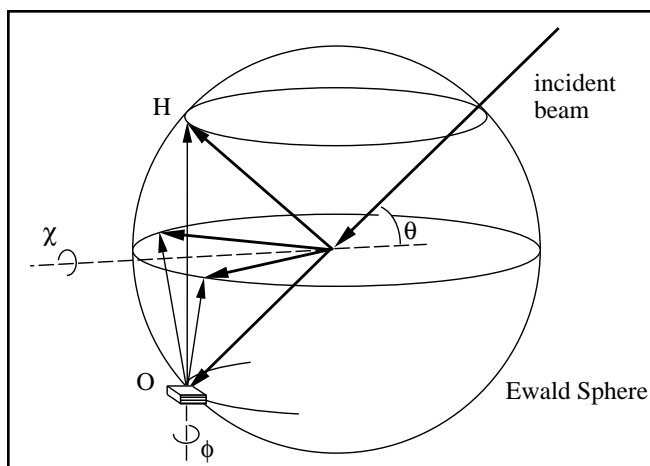
The point-like collimation is of particular interest in small-angle scattering at high scattering vectors  $q$ . Because the enhanced Borrmann effect reduces the absorption coefficient drastically, the transmitted beam still has sufficient intensity. A crystal-camera featuring two consecutive multi-beam diffractions has been designed and is currently under development.<sup>3</sup> Besides its very high angular resolution, this design is also characterized by an excellent monochromaticity. With these characteristics, the necessity of

desmearing recorded data can be avoided.

- [1] Borrmann, G. and Hartwig, W., *Z. Krist.* 121, 401-409 (1965).
- [2] Colella, R., *Acta Cryst.* A30, 413-423 (1974).
- [3] Pahl, R., Presented at the 8th Nat. Conf. Synchr. Rad. Instrum., August 23-27 (1993).

(Below) A schematic of the 4-beam diffraction process. All diffraction vectors that intersect the Ewald Sphere will be simultaneously excited.

(Right) A film record of the 6-beam Laue diffraction from a Si(111) crystal. The indices of the corresponding diffraction spots are shown.



# Elliptically polarized x-rays from a standard undulator

S. D. Shastri

School of Applied and Engineering Physics, Cornell University

Under suitable conditions, some samples, such as magnetic materials, scatter or absorb x-rays in a manner that can be quite rich in polarization dependence. Magnetic, nuclear resonance, and even electronic (nonmagnetic) resonance scattering can exhibit polarization-mixing phenomena where an incident linear polarization in (or out of) the diffraction plane is not conserved in the scattering process<sup>1</sup>. Circular dichroism is the occurrence of different absorption coefficients for left and right circularly polarized radiation<sup>2</sup> (see article by J. C. Lang on page 26).

All this has resulted in an interest in the generation of elliptically polarized x-rays, particularly circularly polarized x-rays where the handedness (i.e. helicity) can be "flipped". In addition to the use of off-orbital-plane bend magnet radiation, researchers have pursued this end on two fronts: the building of special (helical or asymmetric) insertion devices<sup>3</sup> and the development of x-ray "phase-plates" based on perfect crystal optics<sup>4</sup>.

A scheme of the latter approach

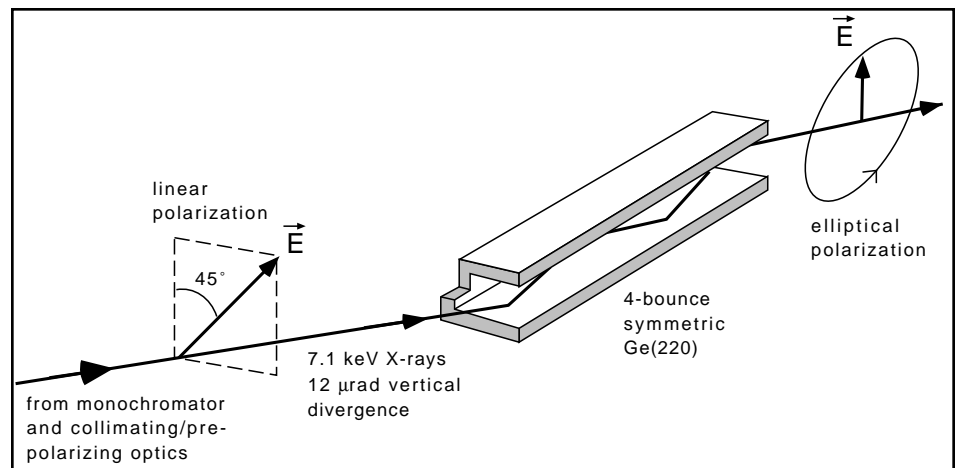


(Figure 1) The phase-shifting Ge(220) channel-cut crystal.

was tested by us<sup>5</sup> under the high-brightness conditions of a standard undulator. In this method<sup>6</sup> polarization selection is achieved by precise control of the incident angle of a collimated, 45-degree linearly polarized beam of x-rays entering a multiple-bounce Bragg reflection channel-cut Ge(220) crystal (figure 1). In addition to the efficiency of the device, the full polarization state of the output beam including the purity of circular polarization  $P_c$  (figure 2) was measured directly using the multi-beam Bragg re-

flection technique with a GaAs crystal polarimeter (see article p. 38). The reversibility of the circular helicity by changing the incident angle and the ability to scan the optics in energy was demonstrated at the vicinity of the Fe K-edge at 7.1 keV.

- [1] M. Blume and D. Gibbs, Phys. Rev. B. **37**, 1779 (1988); D. Mills, *ibid.* **36**, 6178 (1987); D. P. Siddons, J. B. Hastings, G. Faigel, L. E. Berman, P. E. Hausteijn, and J. R. Grover, Phys. Rev. Lett. **62**, 1384 (1989); K. D. Finkelstein, Qun Shen, and S. D. Shastri, Phys. Rev. Lett. **69**, 1612 (1992).
- [2] G. Schutz, W. Wagner, W. Wilhelm, P. Kienle, R. Zeller, R. Frahm, and G. Materlik, Phys. Rev. Lett. **58**, 737 (1987).
- [3] H. Kitamura, Synchrotron Rad. News, Vol. 5 No. 1, 14 (1992).
- [4] M. Hart, Philos. Mag. B **38**, 41 (1978); D. Mills, Nucl. Instrum. Methods A **266**, 531 (1988); J. A. Golovchenko, B. M. Kincaid, R. A. Lovesque, A. E. Meixner, and D. R. Kaplan, Phys. Rev. Lett. **57**, 202 (1986); K. Hirano, K. Izumi, T. Ishikawa, S. Annaka, and S. Kikuta, Jpn. J. Appl. Phys. **30**, 407 (1991).
- [5] S. D. Shastri, K. D. Finkelstein, Qun Shen, B. W. Batterman, and D. Walko, (to be published).
- [6] B. W. Batterman, Phys. Rev. B. **45**, 12677 (1992).

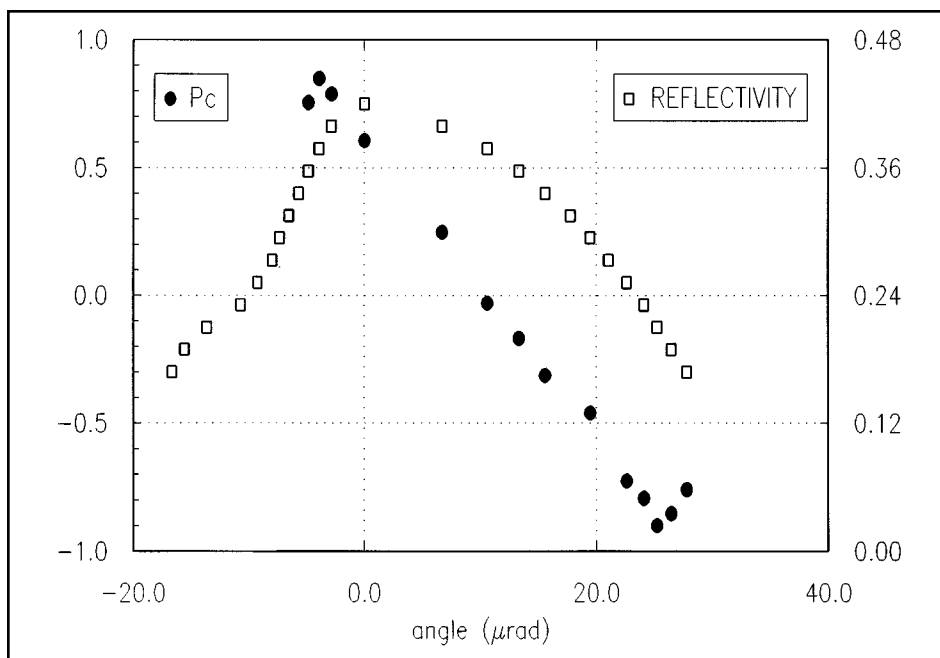
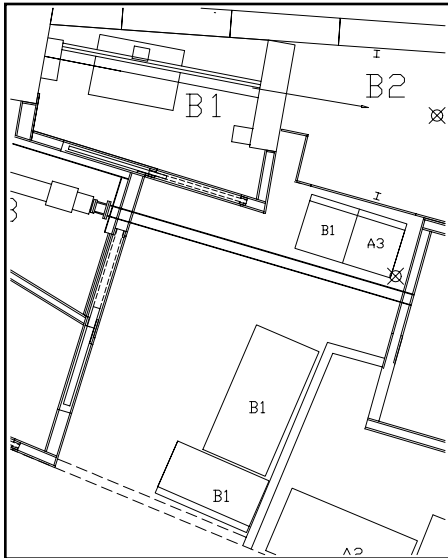


(Figure 2) The measured purity of circular polarization  $P_c$  as a function of incident angle at 7.07 keV. The reflectivity rocking curve of the 4-bounce Ge(220) channel-cut is also shown. Pure right or left circular radiation would be characterized by  $P_c = 1$  or  $-1$  respectively.  $P_c = 0$  reflects equal amounts of right and left, as would occur when a beam is purely linear or completely unpolarized.

# High pressure facility report

Keith Brister

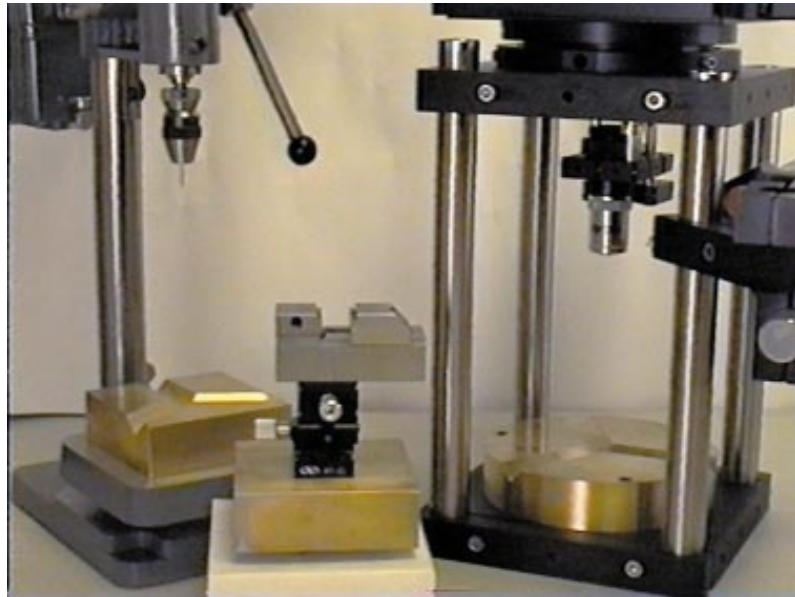
The past year has seen several advances in the instrumentation at the high pressure facility. The most obvious is the new space for the computer and equipment racks between the A3 and A2 hutches just outside the B1 door. This is a great improvement over the old arrangement near the R.F. area. Although the amount of table space is not greatly changed, the microscope now has its' own table and there are shelves to keep the clutter down.



Floor plan of user space around the B1 hutch.

Another practical change is the addition of a micro-drill press with an alignment microscope for drilling gasket holes (see photo). A pre-indentated gasket is clamped in a precision vise and centered in a special microscope. The vise, which is attached to a kinematic mount, is then placed on the drill press where the

(Right) Schematic of multichannel analyzer electronics modified for taking data from a sample with fluctuating temperature. Light from the PIN diode is amplified by the current to voltage amplifier. This signal is digitized by a flash ADC in the Temperature Grouping Unit and used to control the upper bits of the ADC. The user may choose what mapping to used between the digitized PIN signal and the bits manipulated. The system operates at 100 kHz, a value which is only limited by the rise time of the current to voltage amplifier.

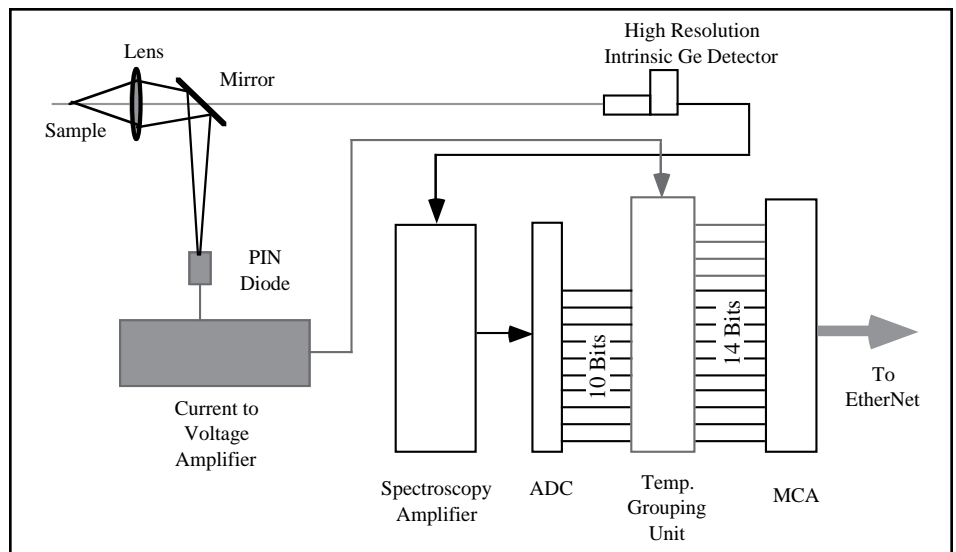


(Left) The micro-drill press (left), a vise mounted on an x-y stage (center), and the alignment microscope (right). The kinematic mounts on both stages assure that the specimen hole is drilled in the exact center of the diamond anvil cell gasket.

sample chamber is drilled. The total time spent drilling gasket holes is minimized since the most time consuming part, centering the gasket in the drill press, is done under the microscope while looking straight into the indentation made by the diamonds.

The laser heating system is now equipped with instrumentation to allow spectra (x-ray and optical) to be collected while the temperature of the sample is fluctuating. Incandescent light from the heated sample is focused on both a PIN diode as well

as the entrance slit of a spectrometer equipped with a diode array detector (see below). The current from the PIN diode is digitized and used to control the upper bits of the output from the ADC feeding the x-ray multichannel analyzer. The effect is to have up to 64 multichannel analyzer (MCA) groups each of which are at a different temperature. A trigger signal is also sent to the diode array gate for pyrometry measurements to calibrate the temperature of each MCA group. (See page 47 for an example of the MCA interface.)



# New CCD detector for macromolecular diffraction data

Rick Walter

Section of Biochemistry, Molecular and Cell Biology, Cornell University

Higher intensity beamlines at synchrotron sources have driven the development of new x-ray sensitive detectors with enhanced performance capabilities for the collection of macromolecular diffraction data. Desired characteristics include improved sensitivity, dynamic range, count rate, and efficiency of data collection. To address this, a new integrating detector based upon a silicon chip charge-coupled device, or CCD, has been developed and successfully applied to the collection of macromolecular diffraction data at CHESS.

This detector is currently being made available to the macromolecular crystallographic user community as part of the upgraded data collection capabilities of the newly recommissioned A1 line. Dan Thiel and I have helped users collect their first data on the detector. In its early applications, the detector has proven exceptional for the collection of macromolecular diffraction data.

The CCD detector has been developed as a collaboration between Don Bilderback of CHESS, the laboratory of Dr. Steven Ealick at Cornell, the group of Dr. Sol Gruner of Princeton University (including Sandor L. Barna, Michael E. Wall) and Dr. Eric Eikenberry of the Robert Wood Johnson Medical Center and Dr. John Lowrance of Princeton Scientific Instruments. Both a schematic and a photograph of the detector are shown.

Operationally, x-ray photons are converted to visible photons by a  $Gd_2O_2S:Tb$  phosphor. The pixel size at the phosphor end is  $50\ \mu m \times 50\ \mu m$ . This signal is transferred from the phosphor by a 2.6:1 fiber optic taper to a  $1024 \times 1024$  pixel CCD chip ( $\sim 20$  mm on an edge). Signal is stored in the chip by the generation of about 11 electrons per 13.6 keV x-ray absorbed, which is then maintained by an imposed voltage until readout. At

readout, charge stored in a pixel row is sequentially shifted horizontally to the single readout amplifier. Subsequently, the charge in each row of pixels above is shifted downward and read out in like manner. In this way, a stationary controller converts the horizontal and vertical position of each pixel and its stored charge to a digitized x,y coordinate on the detector face and a raw intensity. These data are then written to some sort of storage device (currently a magnetic disk or tape) and displayed on a monitor for inspection and limited manipulation.

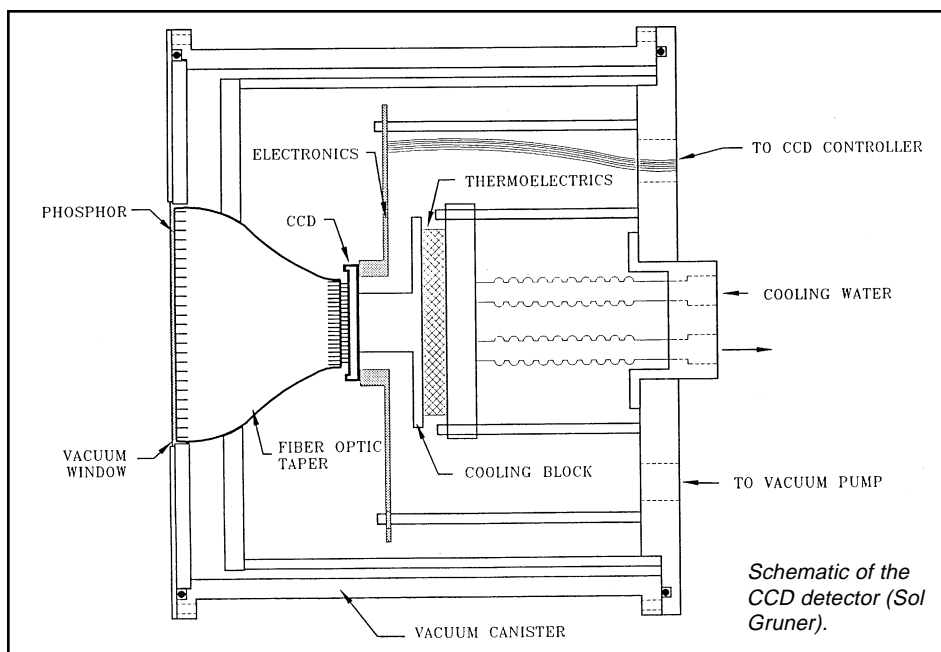
In practice, this detector has provided several advantages for the collection of macromolecular diffraction data. To begin, the CCD chip pixel size is  $19.46\ \mu m$  which translates roughly into  $50\ \mu m$  square pixels at the detector face. With a bloomed point spread function at full width half maximum of  $80\ \mu m$ , the detector truly gives a spatial resolution limited by the pixel size. Further, detector sensitivity at wavelengths from 8 keV to 14 keV, as measured by fraction of x-rays stopped, ranges from 99% to 70% efficiency, respectively. Finally, the readout dynamic range of the detector is 36,000 x-rays. In its current configuration, a 20 second CCD readout time is used. While this is comparatively slow for a chip of this size, it was chosen as a compromise between minimizing readout noise from the single amplifier and decreasing the duty cycle for each macromolecular diffraction image. (This time will be reduced in future detectors.) In addition to such



Photograph of the CCD detector in place at the CHESS A1 station. A protective metal screen (shown open at left) protects the phosphor when not collecting data.

performance capabilities, each image is immediately available for inspection and limited manipulation which includes image zoom and spot intensity integrating and profiling capabilities, among others. While the active area of the detector is rather small, its spatial resolution allows crystal to detector distances as close as 35 mm to be used (giving  $1.4\ \text{\AA}$  data on an edge with  $0.91\ \text{\AA}$  wavelength x-rays in a symmetric configuration). For medium to slightly larger unit cell dimensions (high resolution data for cells with axes up to  $180\ \text{\AA}$  have been successfully collected), the detector can be offset and pulled back to give more reasonable overlap while still recording high resolution data ( $< 2.0\ \text{\AA}$ )

Relative to crystallographic results, an example of a diffraction im-

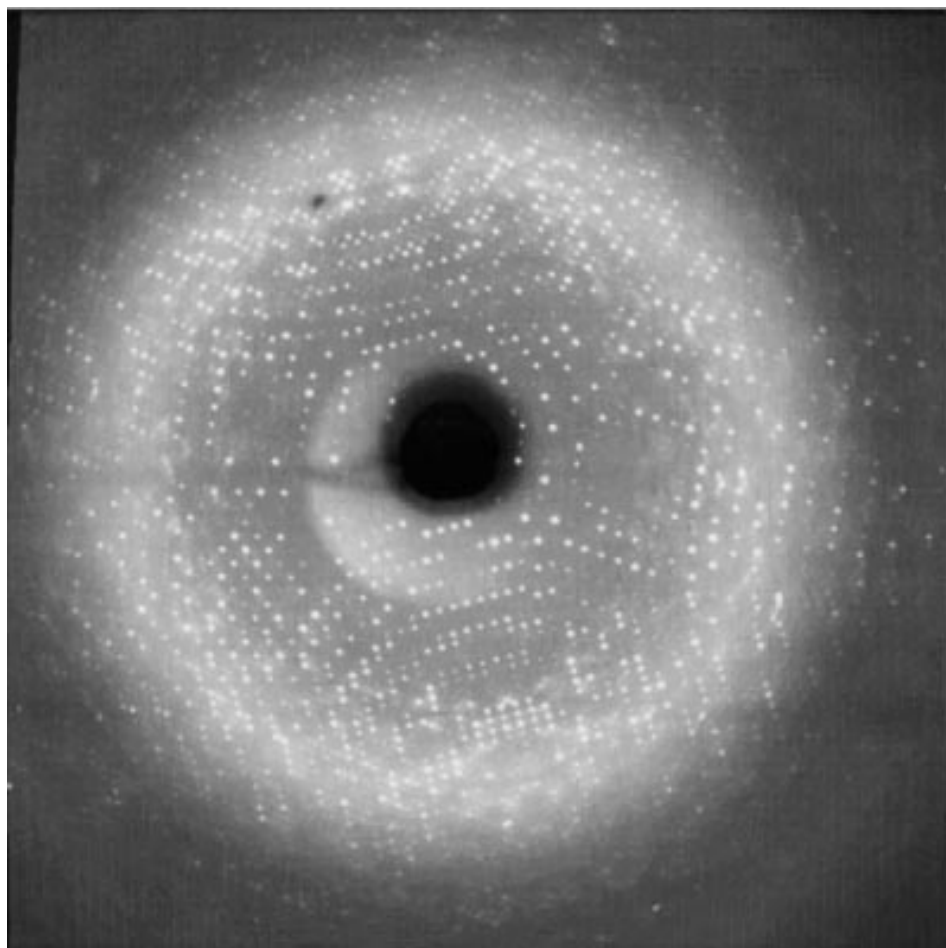


age from data collected using this detector on A1 is shown at right. During a three day experimental run in September, seventeen complete data sets were collected for five different protein crystallography projects. The diffraction image is from a frozen crystal of a complex between the enzyme nucleoside deoxyribosyl transferase and a substrate, deoxyuridine (cubic, I2,3 crystals with unit cell axes of 148.2Å). The  $R_{\text{sym}}$  for all data was 5.0% to 2.3Å, and it is currently being used for high resolution refinement and active site analysis. Because of detector sensitivity and speed and flash freezing of the crystals (see page 44), a complete (97%), high quality, high resolution data set was possible from a single crystal. This was previously impossible with these extremely radiation sensitive crystals.

A second example produced an electron density difference for the active site of the enzyme bovine purine nucleoside phosphorylase in complex with a non-cleavable substrate

*(Right) Diffraction image from a crystal of a complex between the enzyme nucleoside deoxyribosyl transferase and deoxyuridine, a substrate. Data was usable to 2.3Å in this data set. The image is a 20 second, 0.75° oscillation with a crystal to detector distance of 60 mm (this detector configuration allowed 2.2Å data on the edges and 1.7Å data in the corners of the detector).*

analogue, 9-deazainosine (cubic, P2<sub>1</sub>3 crystals with unit cell axes of 93.3Å). Again, high quality, high resolution data with an  $R_{\text{sym}}$  of 5.2% for all data to 1.7Å (94% complete) were obtained using the CCD detector in



conjunction with flash freezing. These data are currently being used to investigate the mechanism of the enzyme. Such results were typical of the data collected during this run. Since then, the detector has been used to collect thousands of images during a month and a half long MAD phasing run on the F2 beamline and is currently being applied to the collection of macromolecular data for outside users on A1.

At CHESS, the development of beamlines and improved x-ray detectors, such as the CCD, is going hand in hand. Plans for continued improvement in detector development are already in place. These include doubling the active area and decreasing the readout time to five seconds in the current design and a planned mosaic detector design. The CCD detector and planned improvements to it will play a role in keeping CHESS at the forefront of macromolecular crystallography for the foreseeable future.

# A multipurpose polarimeter for x-ray studies

K.D. Finkelstein, C. Staffa, Qun Shen

The controlled production, characterization, and use of x-ray polarization has become a significant area of interest in the synchrotron radiation community<sup>1</sup>. A polarimeter can be used to preferentially select and/or characterize the polarization components in an x-ray beam, much as a Polaroid sheet and phase plate are used in the visible spectrum<sup>2</sup>. The first x-ray polarimeter, used by Barkla<sup>3</sup> to produce polarized radiation, consisted of a block of graphite viewed at a 90 degree scattering angle. In this geometry radiation polarized normal to the plane of scattering is selected from an initially unpolarized beam. An informative review of the subsequent progress on the measurement and production of polarized beams by use of crystal optics has been given by Hart<sup>4</sup>.

This paper describes a general purpose polarimeter<sup>5</sup> which is designed for performing a full characterization of the polarization of an x-ray beam and in addition it may be used to select and pass a linearly polarized component over a continuous range of orientations. The former measurement has proven particularly useful for determining the polarization of a beam incident on an experiment, while the latter is useful in analyzing the state of a beam after in-

teraction with the sample. The device is compact and light enough to be mounted on the detector arm of a 4-circle diffractometer. It contains 4 axes of rotation (theta, two-theta, phi, and chi) but differs from a standard 4-circle in that the scattering plane can be rotated about the incident beam.

## Polarimeter Design

An overview of the polarimeter is shown in Figure 1. An aluminum box is suspended and attached to a c-shaped yoke by two large bearings that define the axis (chi) along which an x-ray beam passes. The yoke is bolted to an arm and dovetail rail to permit mounting on the detector arm of a 4-circle or to a base plate. The two-theta angle is manually adjusted and the arm mounted on the far side of the box. Inside the box are two motorized rotation axes: the theta axis sets the analyzer crystal Bragg angle and the phi axis typically rotates the crystal about the surface normal. The theta and detector axes are concentric; thus a theta rotation moves the crystal reflection vector in a scattering plane determined by the chi orientation. An analyzer crystal positioned 50mm above a standard goniometer stud on the phi stage will be centered on all four axes.

## Experimental Results

The polarization state of an x-ray beam can be described by the Poincare vector<sup>6</sup> with components  $(P_1, P_2, P_3)$  giving respectively, the fraction of beam intensity linearly polarized along orthogonal axes (usually horizontal and vertical), along another set at 45 degrees to the first, and the fraction which is circularly polarized. The fraction of unpolarized intensity  $P_0$  is obtained from  $P_0 = 1 - (P_1^2 + P_2^2 + P_3^2)^{1/2}$ . The components  $P_1$  and  $P_2$  are measured using a crystal and reflection that will diffract the beam with scattering angle near 90 degrees<sup>7</sup>. Four intensity measurements, integrated over theta, are made at chi separations of 45 degrees.  $P_1$  and  $P_2$  are obtained by taking the difference over sum of the results for orthogonal pairs of these integrated intensities.

Diffraction by a non-centrosymmetric crystal can determine  $P_3$ . This is done using multiple-beam diffraction (MBD<sup>5,7</sup>) where the incident beam amplitude is coherently split by diffraction that can occur in non-coplanar scattering planes. The splitting of incident beam amplitude in these two planes when combined with the non-centrosymmetric (i.e complex) structure factors associated with each reflection can produce a difference in phase along the two routes. As described in references 5 and 7, the crystal is oriented to diffract the beam in one (the primary scattering) plane and then rotated about that reflection vector through the second (multi-beam) reflection. When the incident beam possesses complex (elliptical) polarization the

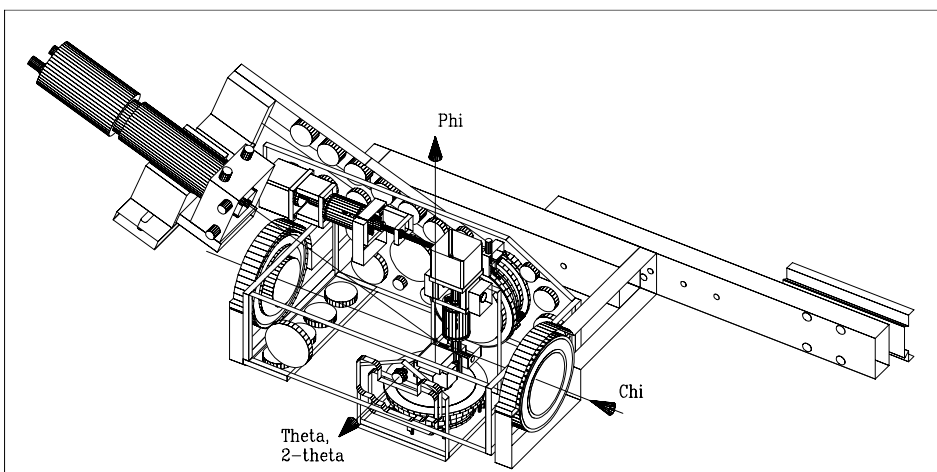


(Figure 1, left) The multipurpose polarimeter is shown in a perspective view. The four rotation axes permit a complete characterization of the x-ray polarization. The light weight design permits mounting on the detector arm of a 4-circle spectrometer. Mounting and detector hardware are also visible.

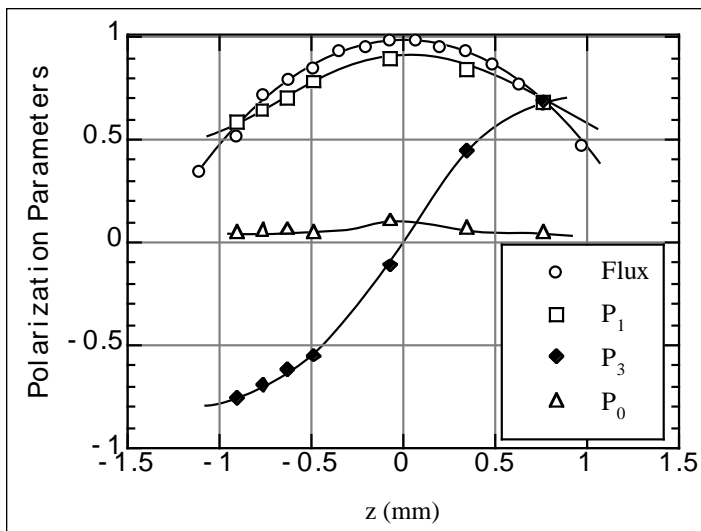


Figure 2. At CHESSE F3 bend magnet station, the polarimeter is used to determine polarization properties of a monochromatic beam at 7.1keV. The linear, circular and unpolarized components  $P_1$ ,  $P_3$ , and  $P_0$  are defined in the text. The horizontal axis gives the position of a slit 15 meters from the source which defines the angle of radiation off the synchrotron orbital plane. The flux, displayed on a relative scale, indicates the center of the radiation distribution.

result can be a well defined asymmetry in the primary diffraction intensity in passing through the multi-beam condition. One can fit this asymmetry to a calculation using known structure factors and extract the fraction of circular polarization in the incident beam.

The results of polarization measurements<sup>7</sup> using the gallium arsenide (222) reflection for linear analysis and the (222/311) combination for MBD are shown in Figure 2. The Poincare components are given as a function of position when a 0.25 mm vertical defining slit, upstream of the mono, is moved from below to above the synchrotron orbital plane. The behavior of  $P_1$  and  $P_3$  agree with expectation when the vertically diffracting silicon (111) double-bounce monochromator (which is detuned to 70% reflectivity at 7.1keV) is accounted for.  $P_2$  is zero within measurement error and  $P_0$ , the unpolarized component of radiation, is also reasonable.

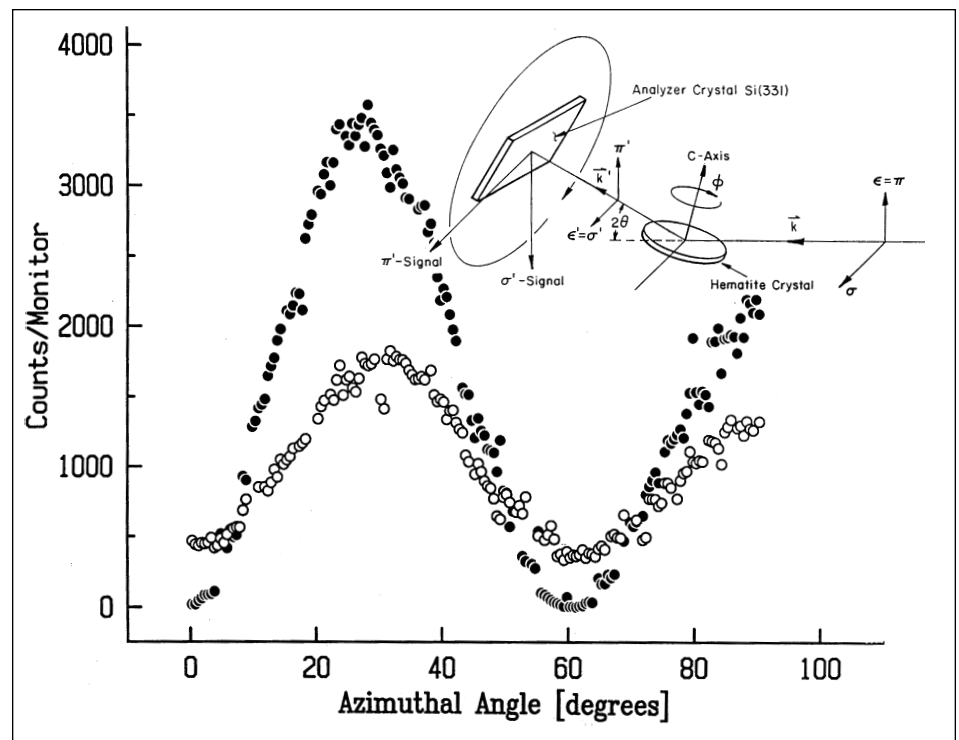
A second application of the pola-

Figure 3. Results of a linear polarization analysis on the beam diffracted from a hematite crystal 9eV below the iron K-edge. This reflection is usually forbidden but can be resonantly excited. The polarimeter permits resolving the rotated polarization state generated by and characteristic of this process. Open (solid) circles are the horizontal (vertical) polarization scattered by the resonance.

rimeter is shown in Figure 3. A Si(331) crystal was used to analyze the orthogonal components of linear polarization diffracted at the hexagonal (00.3) reflection in a sample of hematite 9eV below the iron K-edge<sup>8</sup>. This reflection is forbidden by space group rules, but occurs because the iron atom is in a crystal field which splits the half-filled 3d level allowing electronic-quadrupole transitions to be observed. The sample is kept on

the Bragg reflection as it is rotated about the reflection vector; this produces a six-fold intensity oscillation related to the crystal field symmetry. The polarization analysis permitted a definitive interpretation of these data and knowledge of the incident beam polarization was useful in understanding the relative size of the two diffraction signals.

1. Production and Analysis of Polarized X-rays, D.P. Siddons, editor, Proc. SPIE 1548 (1991).
2. M. Born and E. Wolf, *Principles of Optics*, 6th ed. (Pergamon, New York, 1983).
3. C.G. Barkla, Proc. Roy. Soc., London, **77**, 247 (1906).
4. M. Hart in *Proceedings of the ICAS Conference*, Aug. 17-21, 1992, Malente/Hamburg, Germany, ed. by K. Fischer, G. Materlik, C.J. Sparks (Elsevier Science Publishers B.V., New York, 1993).
5. Qun Shen and K.D. Finkelstein, Phys. Rev. B **45**, 5075 (1992).
6. M. Blume and D. Gibbs, Phys. Rev. B **37**, 1779 (1988).
7. Qun Shen and K.D. Finkelstein, submitted to Rev. Sci. Instr. (1993). In this paper we show that accuracy in the determination of  $P_1$  and  $P_2$  does not depend on a scattering angle of 90 degrees.
8. K.D. Finkelstein, Qun Shen, S Shastri, Phys. Rev. Lett. **69**, 1612 (1992).



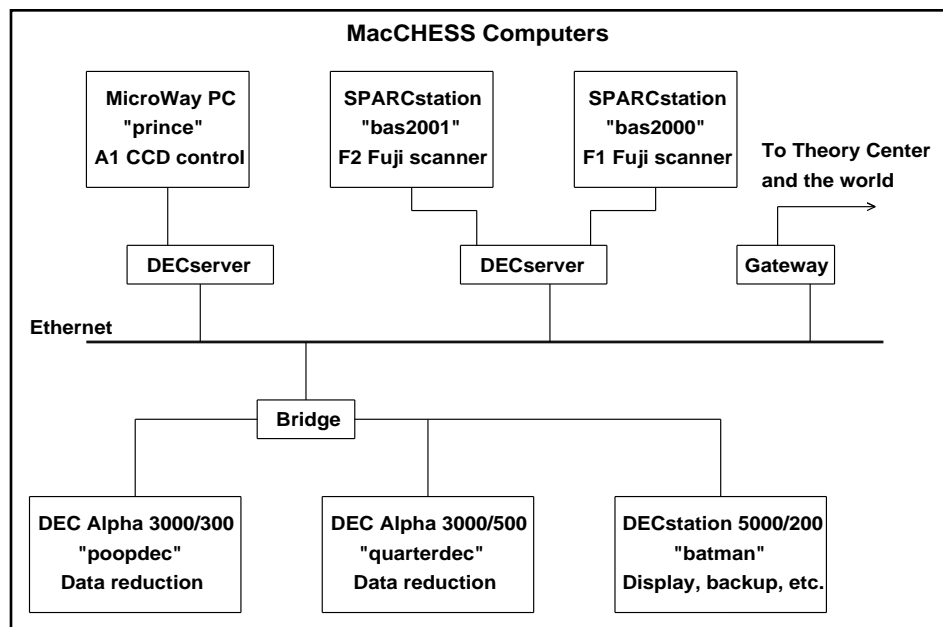
# MacCHESS data reduction capability

Marian Szebenyi

Early crystallographic users of CHESS collected precession, oscillation, or Laue data on film and took the films home to process; there were no facilities here for data reduction. The 20 minute time required to digitize a film made it completely impractical to process data as fast as they were collected. With the installation of a Kodak storage phosphor data collection system in 1988, the time to digitize an image was reduced to 5 minutes, and then MacCHESS director Keith Moffat set the goal of having users reduce data on-site and go home with h, k, l, F, sigma(F)'s instead of reams of raw images. Today we are well on the way to achieving this goal.

The first figure shows the components of the MacCHESS data collection and processing system. Most data are now collected on Fuji image plates and scanned on one of the two Fuji BAS-2000 scanners. These scanners have disk storage space for about 100 images each. Using the Network File System facility, the processing computers have direct access to the raw data files. Image files from the recently installed CCD detector are currently transferred for processing via ftp or 8-mm tape, but the planned installation of NFS software on the CCD control computer will allow images to be written directly to a remote disk.

Data processing is done on two DEC Alpha workstations, one Model 3000/500 (called quarterdec) and one Model 3000/300 (poopdec). These workstations were obtained under a grant from Digital Equipment Corporation to Steve Ealick. In addition, a DECstation 2000/500 (batman) is available for operations not requiring the great speed of the Alphas. For display and processing of oscillation images, the principal software is the HKL system, created by Zbyszek Otwinowski and Wladek Minor. It incorporates the display program XDISPLAYF (also called IPVIEW)



and the data processing programs DENZO and SCALEPACK.

The single command "denview" starts up IPVIEW and DENZO. The user enters the name of the first image to process, and it appears on the display. The user can also enter the wavelength and crystal-detector distance and indicate the position on the image of the direct beam, after which IPVIEW will provide a running display of the resolution at the cursor position. Any region of the image can be enlarged in a "zoom window", to evaluate spot shape and spacing. Overloaded pixels can be marked. The display can be in false color or gray-scale; the scale is determined automatically but can be easily altered by the user.

To begin processing, the IPVIEW peak search routine is used to obtain a list of spot positions on the image; the list is written to a file which is then read by DENZO. Commands to DENZO are typed into a window which is created by "denview". Usually files of commands are set up ahead of time and read in by typing "@filename". Given the list of peaks from IPVIEW and a few basic parameters such as wavelength and crystal-detector distance, DENZO automati-

cally determines the crystal orientation and provides a list of cell parameters in all possible crystal systems. Cell parameters and space group may be input but are not required. If they are provided, DENZO will accept the space group but redetermine the cell parameters. After indexing, DENZO refines crystal, camera, and detector parameters. Almost all parameters can be refined at once. Sample input files are available giving a reasonable sequence of refinement steps. During refinement, the predicted spot positions can be displayed on the image (see figure), so that agreement with the observed positions can be directly evaluated. The second figure shows a DENZO run midway in the refinement process. After refinement, DENZO integrates the reflections on the image, writing the results to an ASCII file, along with the refined parameters. The program is then ready to process the next image in the series. Autoindexing need be performed only once per series, but some refinement is done for each image before it is integrated.

The program SCALEPACK is run after a series of images have been processed. It determines relative scale factors between the images, can

post-refine cell parameters, mosaicity, and crystal orientation, computes Rsym's, and merges the data into a single set of h, k, l, F<sup>2</sup>, and sigma.

In addition to HKL, programs available on the MacCHESS computers include:

- \* The alternative image display program M.DISPLAY, which is less convenient but more flexible than IP-VIEW.

- \* The alternative oscillation processing suite MOSCO, a part of the CCP4 package.

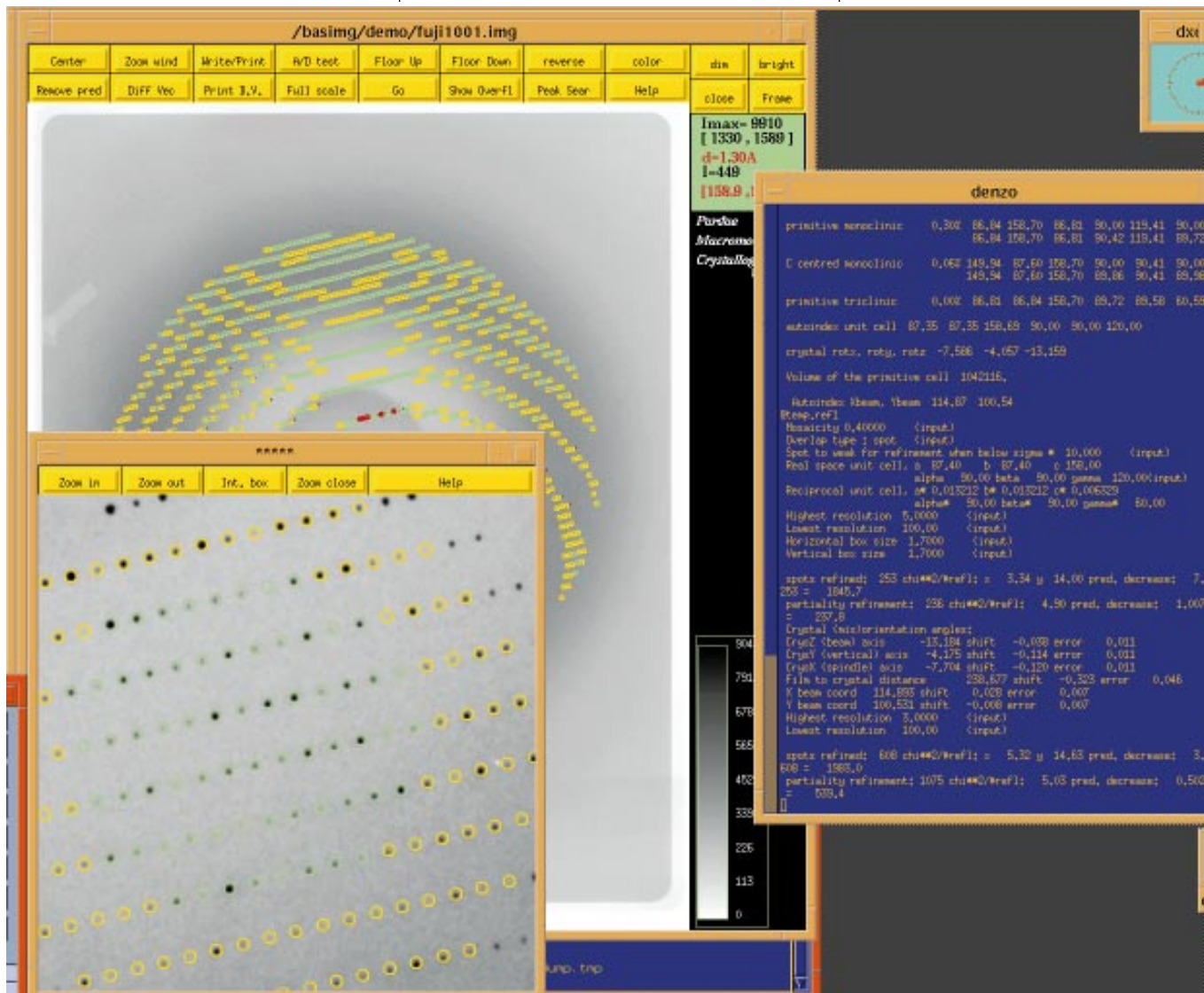
- \* The MacCHESS Laue processing package, consisting of the indexing program M.INDX, the refinement and integration program M.LAUE, and the scaling program M.SCALE.

- \* Miscellaneous ancillary routines.

Users are also welcome to temporarily install their favorite programs. The operating system is OSF/1 on the Alphas and Ultrix on the DECstation. Fortran, c, and X windows are available. The window management system is Motif on the Alphas and DECwindows on the DECstation.

One of MacCHESS's long-range goals is to have a true on-line data reduction system, in which data are processed as fast as they are collected. This is commonly done on laboratory area detector systems, but conditions at CHESS are more demanding. The Fuji scanners have a read-out time of about 90 seconds. The CCD detector betters this time by a factor of four. With typical exposure times of a few seconds, an on-line

system needs to be able to process an image in less than 30 seconds in order to keep up. The time to process an image on quarterdec is currently about two minutes, not including the time to index one image out of each series. Improvement in speed may be possible (aside from waiting for the next generation of computers) by adaptation of DENZO to the parallel-processing environment of the supercomputers at the Cornell Theory Center. Development of foolproof on-line data processing software will also require innovative programming to make the system run as automatically as possible and yet be able to detect when something has gone wrong and human help is needed. Efforts along these lines are being pursued.



Partial computer screen showing the predicted diffraction peak positions (yellow and green circles) overlaying the image data.

# An infrared thermometer for x-ray windows

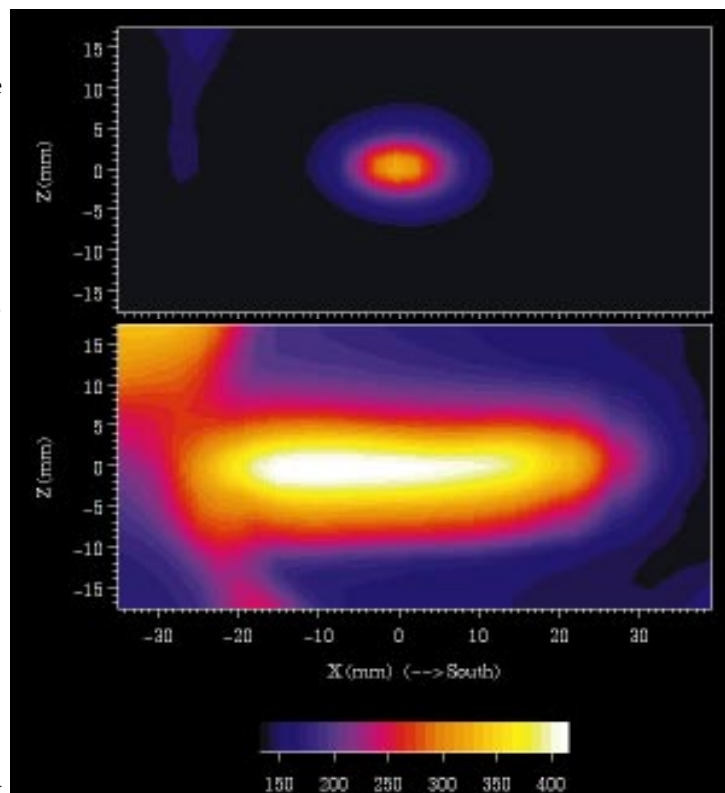
Ernie Fontes

Due to the high energy of the electrons and positrons in CESR (>5GeV), the CHESS 24-pole wigglers produce an enormous amount of total synchrotron light power. At 100 mA, nearly 7 kiloWatts is incident upon the x-ray windows that separate the A and F beamlines from the storage ring vacuum.

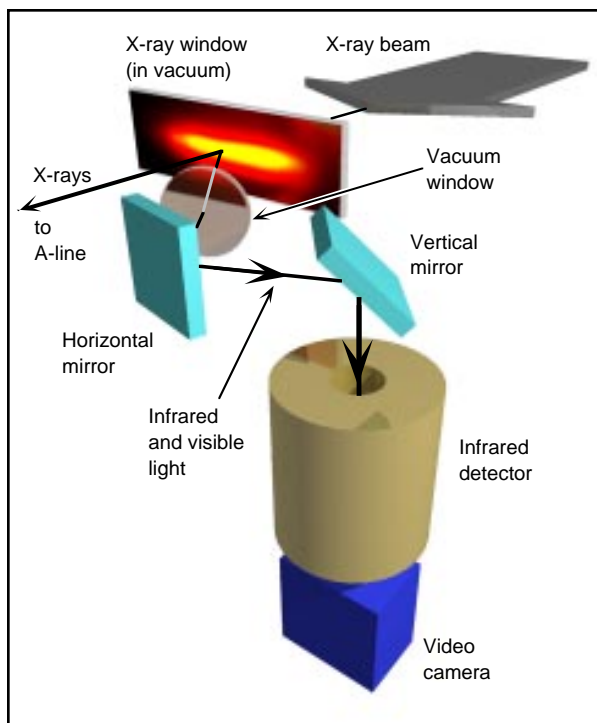
Measuring that temperature of the window requires a remote sensing Infrared (IR) detector. Since in most instances we need to monitor only the hottest spot on the window (where the beam intersects), a simple point-focussed IR detector is suitable for the task. The advantages of a point detector (versus an IR camera) are simplicity in construction and use, robustness in harsh radiation environments, virtually no need for maintenance, and low cost.

For the past two years we have used a "Modline Plus" Infrared Thermometer from Ircon, Inc. (Niles, Illinois). The figure below shows the geometry of a typical measurement. IR and visible light pass through a sapphire (or quartz) vacuum chamber viewport, located 30 degrees off

axis from the incident x-ray beam and looking at the downstream side of the X-ray window. This detector senses radiation in the 2-2.6 micron wavelength range, chosen to coincide with the range of transmission of the sapphire window, which is  $\approx 90\%$  transparent from 1-6.5 microns. Since CESR produces a great quantity of IR radiation, it is also important to choose a wavelength for which the X-ray window is opaque. Note that the choice of wavelength and the room temperature operation of the detector limit the measurement range from 120°C to 400°C.



Thermal images of the undulator (top) and wiggler (bottom) x-ray beams on a graphite filter (0.01 inch) on A-line. Temperatures in °C. The curved outer contours are due to the reflection of light from the inner walls of the vacuum chamber.



(Left) IR camera system monitoring the temperature of a window illuminated by the x-ray white beam.

The figure at left also shows the placement of two front-silvered mirrors that deflect the image of the X-ray window away from the beamline and below the synchrotron orbit. A coaxial view through the body of the IR detector provides access for a video camera view of the X-ray window. The IR detector has a reticle that indicates the 1 mm diameter active sensing area. Since the orientations of the two mirrors are controlled by a computer-DC stepping motor link, we can scan the entire X-ray window sur-

face, in effect pointing the IR camera at will. Linear scans in the vertical direction show the beam height and width, and two-dimensional mesh scans produce temperature profile images (see above).

Currently this detector serves two needs. First, the measured thermal profiles are compared to finite element analysis calculations (ANSYS) as an aid in designing new heat-load-capable windows. Second, since CESR has undertaken an aggressive program to increase the stored particle beam currents, we continually monitor window temperatures so as to avoid unexpected failures. This monitoring is a small part of a labwide program to design, fabricate and test new components that are able to withstand the enormous white-light power produced by high energy synchrotron sources.

# Crystal optics for 0.3 eV energy resolution

A.T. Macrander\*, V.I. Kushnir\*, R.C. Blasdel\*, E.D. Isaacs\*\*, and E. Fontes\*\*\*

\*Advanced Photon Source, Argonne National Laboratory, Argonne IL

\*\*AT&T Bell Laboratories, Murray Hill NJ

\*\*\*CHESS, Cornell University, Ithaca NY

A channel-cut silicon monochromator and bent germanium backscattering analyzer were tested using first harmonic radiation at 7.59 keV from the CHESS-ANL undulator.<sup>1</sup> A value of  $0.30 \pm 0.07$  eV was obtained for the FWHM of the elastic peak in the spectrum of radiation scattered from  $C_{60}$  crystals in powder form.

The optical arrangement of the experiment is shown schematically below. A Si(111) double-crystal monochromator with crystals cooled with liquid gallium was used to monochromate the white beam to a bandwidth of 1 eV. A channel-cut Si(620) monochromator was then inserted into the beam path to reduce the bandwidth. In order to obtain high efficiency, the acceptance angle of the channel-cut was matched to the vertical divergence from the undulator by cutting the crystal to have a  $13^\circ$  angle of incidence. We calculated

the bandwidth to be 0.15 eV.

The analyzer was constructed by waxing a 0.25-mm-thick (111) oriented germanium wafer to a spherically concave glass form having a radius of 1 meter. A focal spot size of 5 mm diameter for x-rays was measured for the central 50-mm diameter area of this optic. The bandwidth of the analyzer was calculated by applying x-ray dynamical diffraction theory to a spherically bent crystal,<sup>2</sup> and we obtained a value of 0.14 eV.

We used a silicon avalanche photodiode (APD) as a detector. This device had a 9 mm square active area and a time response sufficiently fast to permit discrimination of background counts based on a time-of-flight (TOF) analysis. That is, using the pulsed nature of the photons produced by CESR, we arranged to count only those photons with a TOF corresponding to the travel time

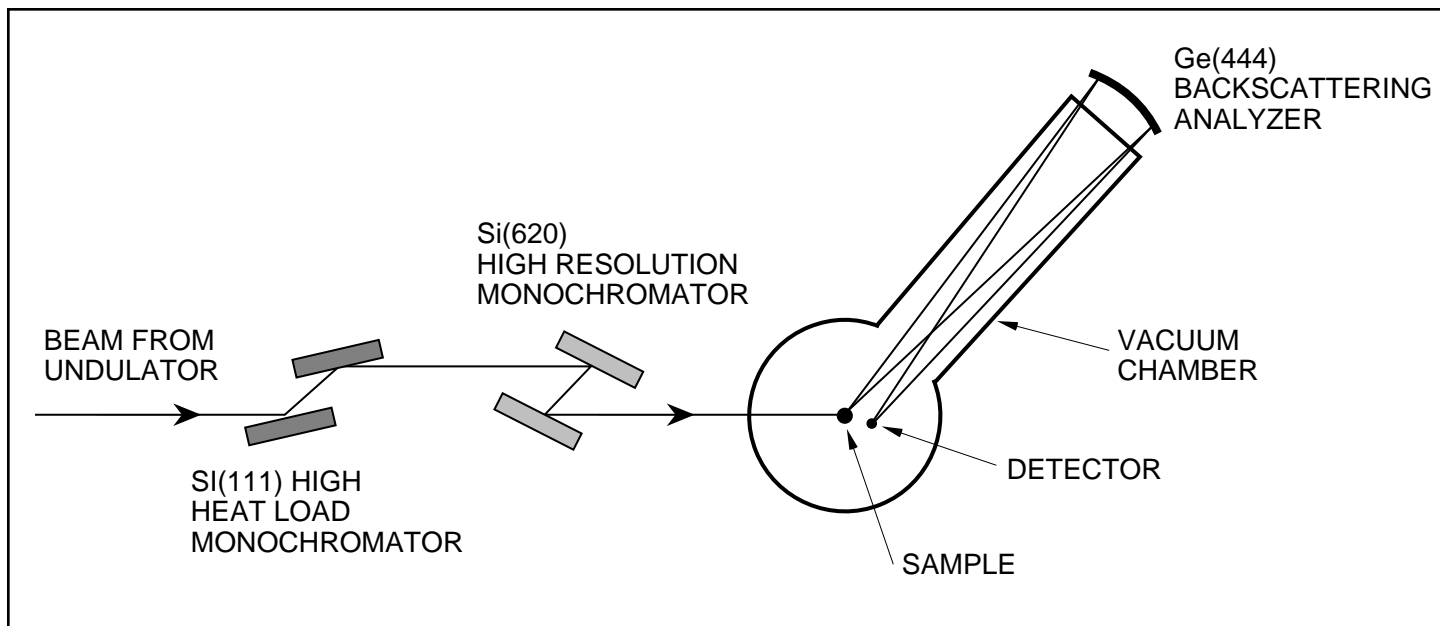
from the sample to the detector via the analyzer ( $\approx 6$  ns).

The measured value for the resolution,  $0.30 \pm 0.07$  eV, is to be compared with the quadrature addition of the calculated resolutions of the Si(620) monochromator and the Ge(444) analyzer, 0.20 eV.

We are grateful to E. Alp for the concept of using TOF for background discrimination, and to E. Alp, W. Sturman, and T. Toellner for assistance with the APD. We are grateful to D. E. Moncton, G. K. Shenoy, and D. M. Mills for support, and we are grateful to the entire CHESS staff for help and assistance.

[1] D.H. Bilderback, B. W. Batterman, M. J. Bedzyk, K. Finkelstein, C. Henderson, A. Merlini, W. Schildkamp, Q. Shen, J. White, E. B. Blum, P. J. Vicarro, D. M. Mills, S. Kim, G. K. Shenoy, K. E. Robinson, F. E. James, and J. M. Slater, *Rev. Sci. Instrum.* **60**, 1419 (1989).

[2] D. W. Berreman, *Phys. Rev. B* **14**, 4313 (1976).



# Shock freezing of macromolecular crystals at MacCHESS

Rick Walter and Joseph Navaie

The collection of macromolecular diffraction data has recently benefited from technique and equipment advances which have made low temperature data collection almost routine. The ability to freeze protein crystals at liquid nitrogen temperatures normally gives the level of radiation protection necessary to collect complete data sets from single crystals. The need to improve the radiation sensitivity of protein samples is an even more key issue at such intense x-ray sources as CHESS. To this end, MacCHESS has upgraded both its equipment and its capability to offer support to assure that visiting user groups can routinely collect low temperature data while at the synchrotron.

The collection of low temperature data on protein samples hinges around a loop mounting technique first developed here at Cornell by T.Y. Teng. In the original technique, crystals were mounted by lifting them in thin wire loops by surface tension from soaks of mother liquor containing some cryoprotecting molecule. These molecules were generally freezing point depressing solutes such as sucrose or low molecular weight alcohols such as glycerol, ethylene glycol, isopropanol, or methylpentanediol (MPD). In addition to such alcohols, lower molecular weight polyethylene glycols such as PEG 400 or 600 have been used successfully. Recently, the technique has been improved by replacing the wire loops with loops fashioned from glass wool, rayon, nylon, silk, or any other thin, non-diffracting fiber. Using such equipment, 360° of continuous rotation data can be collected from a single crystal without worrying about significant shadowing or increases in absorbance or scatter from the loop mounts. A schematic of a loop design currently used at CHESS and a photograph of an actual

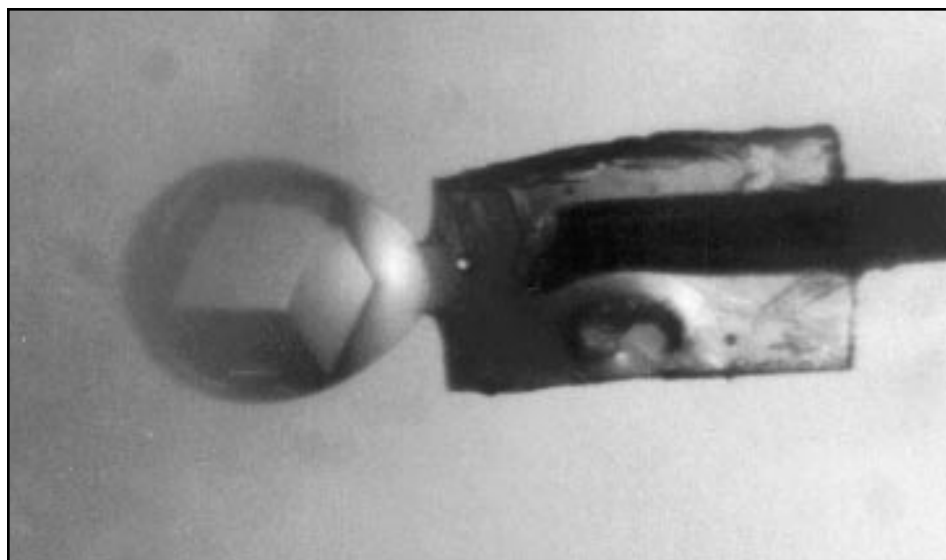
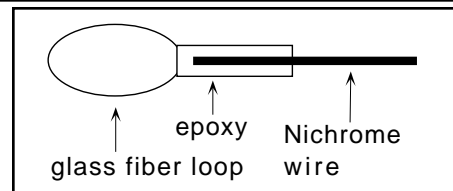


Figure 1. (Above) Freezing-loop-mounted crystal of nucleoside deoxyribosyl transferase (crystal dimensions are approximately 600 x 600 x 400 microns<sup>3</sup>) within a drop of cryoprotectant fluid. (Right) Schematic of the crystal mounting loop.



loop mounted crystal are shown in Figure 1.

The key to shock freezing crystals is maximizing the efficiency of the initial freezing rate, or the shock. Two methods are currently used to accomplish this. First, crystals can be frozen directly in the cold stream. In this method, a reliable cryostat capable of maintaining a laminar cold stream at -165°C to -175°C with a good flow rate is essential. Actual freezing involves temporarily deflecting the cold stream with something as simple as an index card while the crystal is quickly seated in the diffraction position (usually using a goniometer mounted magnet and a loop attached to a steel mounting cap). Then, the stream deflection is removed and the low temperature gas is used to flash freeze the crystal. In the second technique, loop mounted crystals are first immersed in some low temperature liquid such as liquid nitrogen, propane, or freon. Liquid propane freezing is the most

likely trend of the future as it provides the best thermal capabilities for heat conductance away from the immersed crystal. After immersion, the crystal is seated at the sample position still in the low temperature liquid, and the vessel containing the liquid is quickly removed. In this case, the liquid is used to cause the initial flash and the challenge is smoothly transferring the frozen crystal to the gaseous cold stream. Both techniques have been used successfully at CHESS by outside and local user groups.

As has been mentioned, equally important as technique to crystal freezing is the availability of good cryostats. There are two different cryostat systems available to shock freeze protein crystals at MacCHESS. The newest and most reliable units are the heat exchange MSC devices (Molecular Structure Corporation, The Woodlands, TX). Figure 2 shows a schematic of an MSC cryostat. A 160 liter Taylor-Wharton XL-45 liq-

uid/gas dewar (or more recently, a 240 liter Cryofab CLG-240-PB-C dewar) serves as the dry nitrogen gas supply. The gas pressure at the outlet is regulated to 25 PSI and fanned out to two gas lines, both equipped with flow meters and needle valves for fine control. One line is fed through a copper coil inside the 100 liter stainless steel wide mouth dewar which serves as the heat exchange reservoir. The gas reaches equilibrium temperatures near 77K in the coil and is transferred to the nozzle, placed within 1 cm of the sample position, by an evacuated stainless steel transfer tube. The second line is fed directly into an outer jacket around the nozzle and produces a collinear warm air outer stream which sheaths the inner stream from turbulence and prevents freezing of the nozzle. A heater and a thermocouple contained upstream of the nozzle give the ability to maintain and monitor any given temperature from +30°C to -190°C within ±1°C. Several transfer lines which provide the option of spindle collinear or perpendicular cold-streams are available at MacCHESS.

As an alternative, the older boil-off "MAX Cryostat" system developed at the Max-Planck Research Unit for Structural and Molecular Biology (Hamburg, Germany) is avail-

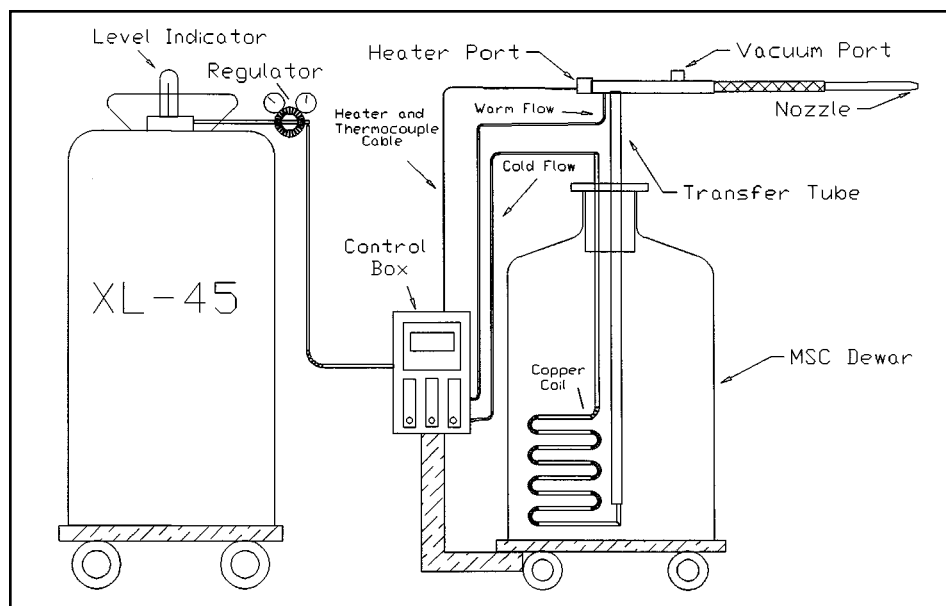


Figure 2. Schematic of Molecular Structure Corporation (MSC) cryostat and supply dewar.

able upon request and as an emergency backup. This system provides a stable temperature of better than -160°C at the sample, but suffers from a rather poor flow rate which can be problematic in difficult crystallographic problems if stream freezing is to be done. Low temperatures are achieved by using boiled off gaseous nitrogen supplied by the smaller evaporator dewar. A slight overpressure is produced inside the evaporator by an electrical resistor immersed in the liquid nitrogen. The

reservoir of nitrogen in a larger supply dewar is used to maintain a constant level of liquid nitrogen in the evaporator using an automatic level control device. When a platinum thermometer (PT100) inside the evaporator signals a low level, an electrical resistor at the bottom of the transfer dewar heats, boiling off nitrogen and forcing liquid nitrogen through a transfer line into the evaporator. While more fragile due to vacuum glass gas transfer lines, less reliable due to questionable electronics, and not capable of the high flow rate achievable with the MSC units, it does serve as a competent backup for emergency situations. Both systems provide the option of continuous refill allowing indefinitely long experiments with no fluctuation in sample position temperature.

Using the available equipment resources at CHESS, almost all protein data now collected are at low temperature. In fact, the beamline upgrades on the new A1 station have made it virtually impossible to collect anything but low temperature data without beam attenuation. In the unattenuated beam at A1, lysozyme crystals last for only 90-120 seconds of exposure at room temperature (previously, multiple data sets could be collected from single crystals), while even radiation sensitive

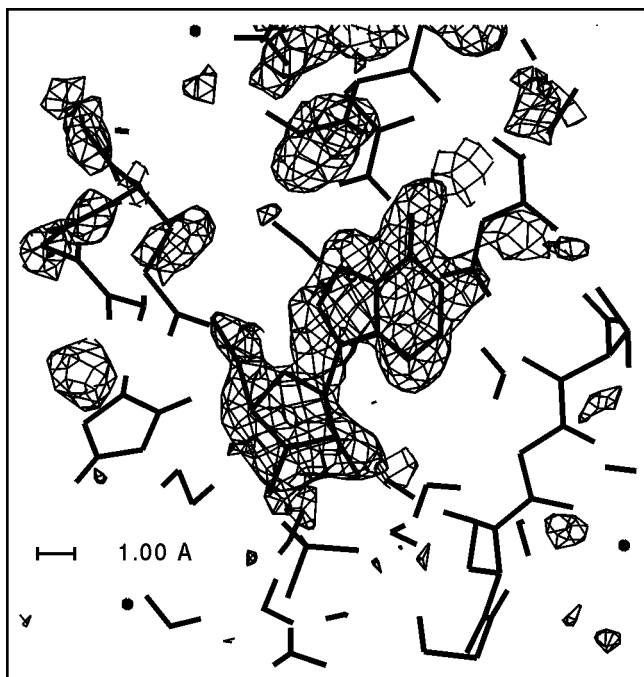


Figure 3. Section of a difference Fourier map of a complex between the enzyme bovine purine nucleoside phosphorylase and 9-deazainosine, a noncleavable substrate analogue. A refined model of the substrate analogue and the protein is shown fit to the difference density. All density not modelled by the substrate analogue is associated with a loop to helix conformational change in the protein induced by substrate binding. The map was calculated with the program PHASES using  $a_{\text{calc(native)}}$  and  $|F_{O(\text{complex})} - F_{O(\text{native})}|$  as coefficients.

samples can last almost indefinitely at low temperature. As evidence, a high resolution data set on a radiation sensitive crystal form in this lab (nucleoside deoxyribosyl transferase) which previously required 43 crystals at room temperature can now be done using a single crystal at low temperature. Similar successes have been achieved with almost every crystal attempted. High quality data at resolutions extending to 1.0Å have been collected on frozen crystals in the past months as shown by the 1.4Å data with an overall Rsym of ~3% collected on a single frozen crystal of lipoxigenase provided by Wladek Minor of Purdue University. Further, concerns of increased mosa-

icity and irreproducibility of unit cell constants from crystal to crystal have not been a problem in any project collected in the past six months.

As an example, figure 3 shows that good difference Fourier maps have been calculated using native and complex data collected at CHESS from frozen crystals of bovine and human purine nucleoside phosphorylase, showing a lack of crystal variation upon freezing. Thus, most concerns relating to low temperature data collection have been overcome and it is becoming almost a standard protocol in MacCHESS diffraction experiments.

In conclusion, MacCHESS now provides the resources necessary for

routine low temperature data collection on macromolecular samples. In addition to providing good, reliable, commercial cryostats, a level of expertise has been developed locally from interaction with visiting user groups at the forefront of development in this area. MacCHESS is currently planning a video loaning library in which the initial volume will discuss and demonstrate the techniques and theory of low temperature crystallography. In the interim, local support will gladly be provided at any level by contacting Rick Walter in the laboratory of Dr. Steven Ealick (email address: walter@vgx.tn.cornell.edu).

## 1993 publications from work done at CHESS

We expect that the following list is not complete. To keep our database current, we ask that users who have published data taken at CHESS, or written articles or student theses, please forward a complete reference to Lana Walsh at email address llw3@cornell.edu or FAX (607)255-9001.

- Agbandje, M., R. McKenna, M.G. Rossmann, M.L. Strassheim, C.R. Parrish, Structure Determination of Feline Panleukopenia Virus Empty Particles, *Proteins*, **16**, (1993), 155-171.
- Alp, E.E., T. M. Mooney, T. Toellner, W. Stuphahn, E. Witthoff, R. Rohlsberger, E. Gerda, H. Homme, and M. Kentjana, Time-resolved Nuclear Resonant Scattering from <sup>119</sup>Sr Nuclei Using Synchrotron Radiation, *Phys. Rev. Lett.* **70**, 3351 (1993).
- Bassett, W.A., M.S. Weathers, and T.C. Wu, Compressibility of Si C Up to 68.4 GPa, *J. of App. Phys.*, **74**, (1993), 3824-3826.
- Beutel, T., Z.Zhang, W.M.H. Sachtler and H. Knozinger, Temperature Dependence of Pd Cluster Formation in NaY and 5A Zeolites, *J. Phys. Chem.* **97**, (1993), 579-83.
- Blum, M.L., J. A. Down, A.M. Gurnett, M. Carrington, M.J. Turner and D.C. Wiley, A Structural Motif in the Variant Surface Glycoproteins of Trypanosoma brucei, *Nature*, **362**, (1993), 603-609.
- Brock, J.D., D.A. DiCarlo, W.J. Podulka, M. Sutton, E. Sweetland, and R.E. Thorne, Structure and Kinetics of the Sliding Q1 CDW in NbSe<sub>3</sub>, *Journal de Physique IV, Colloque C2*, **3**, (1993), 115.
- Brown, J.H., T.S. Jardetzky, J.C. Goprga, L.J. Stren, R.G. Urban, J.L. Strominger and D.C Wiley, The Three-Dimensional Structure of the Human Class II Histocompatibility Antigen HLA-DR1, *Nature* **364**, (1993), 33-39.
- Capehart, T.W., R. Mishra, F.E. Pinkerton, Determination of the Zirconium Site in Zirconium-Substituted Neodymium-Iron Boride, *J. App. Phys.* **73**, (1993), 6476.
- Capehart, T.W., R.K. Mishra, G.P. Meisner, C.D. Fuerst, and J. F. Herbst, Steric Variation of the Cerium Valence in Cerium-Iron-Boron and Related Compounds, *App. Phys. Lett.*, **63**, (1993), 3642.
- Chapman, M.S., K.H.Kyung, M.G. Rossmann, Structural Comparisons of Several Antiviral Agents Complexed with Human Rhinoviruses of Different Serotypes, *Internatl. Antiviral News*, **1**, (1993)53-54.
- Cheng, A.C., J.L. Hogan, and M. Caffrey, X-Rays Destroy the Lamellar Structure of Model Membranes, *J. Mol. Biol.*, **229**, (1993), 291-194.
- Chumakov, A. I., Smirnov, B. V., Baron, A. Q. R., Arthur, J., Brown, D. E., Ruby, S. L., Brown, G. S., and Salashchenko, N. N., Resonant Diffraction of Synchrotron Radiation by a Nuclear Multilayer, *Phys. Rev. Lett.* **71**, 2489 (1993).
- Coulthard, I., D.T. Jiang, J. W. Lorimer, and T.K. Sham, Reductive Deposition of Pd on Porous Silicon from Aqueous Solutions of PdCl<sub>2</sub>: An X-ray Study Absorption Fine Structure Study, *Langmuir*, **9**, (1993), 3441.

CONTINUED ON PAGE 48

# Customized data collection and handling at CHESS

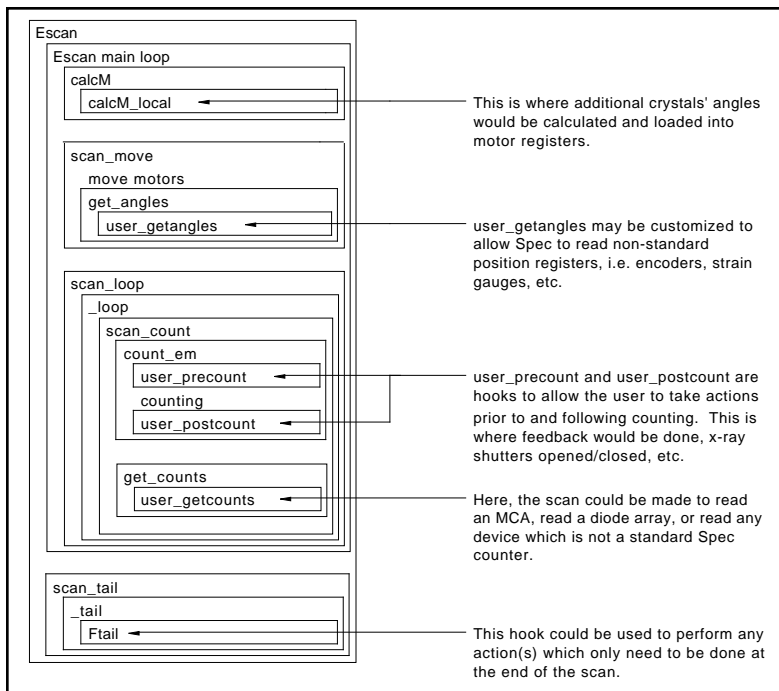
Jim Laluppa

During the last CHESS undulator run, nearly all of the experiments required customization of some of the standard Spec scans in order to collect the necessary data. For example, the circular polarization optics experiment (see page 34) required an energy scan to move three crystals in synchronization with the monochromator. In fact, we implemented a routine that not only moved the crystals, but optimized the x-ray throughput of each element after each move. Also, to switch the left-right polarization, one crystal had to be moved over its rocking curve width at each point in the scan.

The brute force approach to accomplishing this would have involved making the standard "Escan" non-standard, with the cost of having to recreate and debug a large portion of the Spec software package. Luckily, the version of Spec now used in the lab provides a more efficient cus-

tomization.

Shown schematically at right, each of the common scan macros makes a call to user-definable "hooks." A hook is a user-definable subroutine, normally having a null definition, but which can be made to take any action the user desires. This eliminates the need for duplicating entire scans, and allows the user to add only the

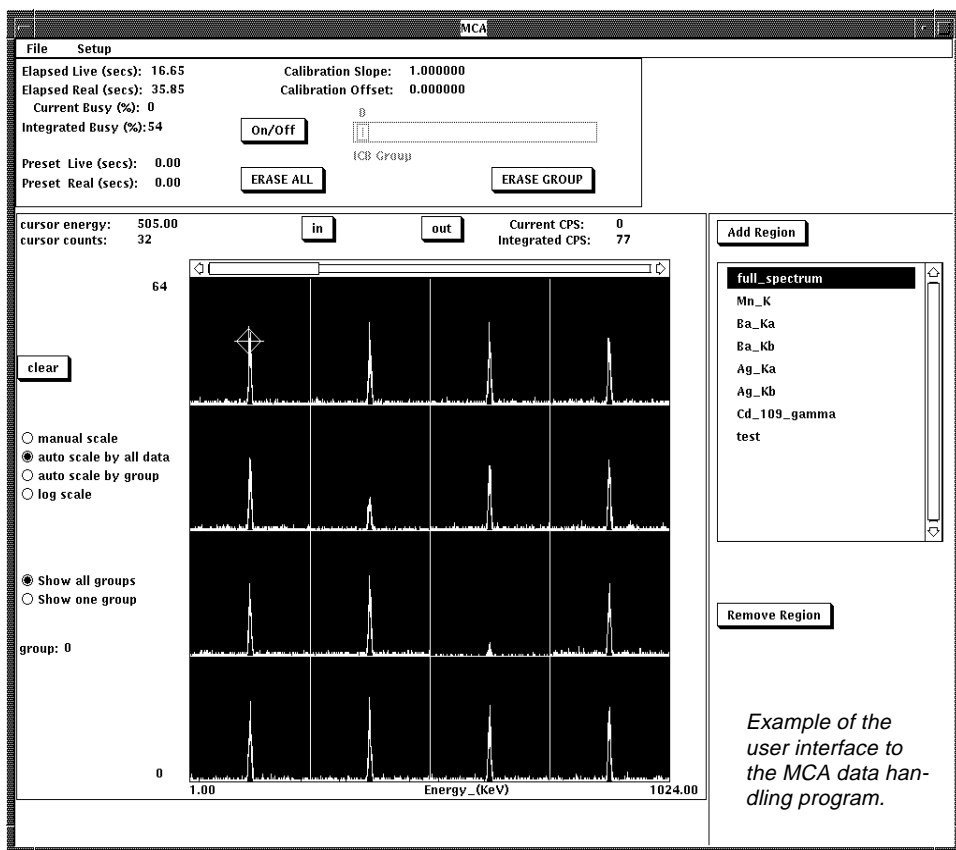


Outline of the standard Spec energy scan showing locations for user subroutines.

minimum code necessary to customize the scan. Moreover, this method makes the alterations universally applicable, so that all scans may utilize them.

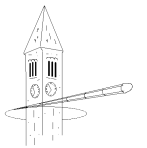
In another area of development, the MCA interface for the High-pressure facility has been vastly improved. The control panel now allows energy spectrum groups to be displayed simultaneously in individual "subwindows." This required the addition of new scaling options and increased software control. Another new feature provides a way to set which individual data group is monitored. And finally, the file output style was changed so that all groups could be written into a single data-file.

Documentation Helpscreens are now available at all the stations, encompassing most of the site-specific macros in general use at CHESS. Look in the CHESS help file for pointers to more information about specific macros.



- Denes, G., Y.H. Yu, T. Tyliczszak and A.P. Hitchcock, Sn-K and Pb-L3 EXAFS, X-ray Diffraction and 119 Sn Mossbauer Studies of Ordered B-PbSnF<sub>4</sub>, Disordered Pbl<sub>x</sub>Sn<sub>x</sub>F<sub>4</sub>(x=0.3, 0.4) Solid Solutions, and PbSn<sub>4</sub>F<sub>10</sub> High Performance Fluoride Ion conductors, *J. Solid State Chemistry*, **104**, (1993), 239-252.
- Desgreniers S. and R. Legault, High Density Crystalline Structures of Copper Oxides, *Proc of the 1993 Joint APS/AIRAPT XIII Conference, Colorado Springs, (1993)*.
- DiCarlo, D.A., E. Sweetland, M. Sutton, J.D. Brock, and R.E. Thorne, Field-Induced Charge-Density-Wave Deformations and Phase Slip in NbSe<sub>3</sub>, *Physical Rev. Letters*, **70**, (1993), 845.
- Finkelstein, K.D., and Mark Sutton, *Nucl. Instr. and Meth.* (1994).
- Finkelstein, K.D., C. Staffa, Qun Shen, *Nucl. Instr. and Meth.* (1994).
- Finkelstein, K.D., Michael Hamrick, and Qun Shen in *X-ray Resonant (Anomalous) Scattering: Theory and Experiment C*. Sparks and G. Materlik, eds. Elsevier Science Publishers (1994).
- Fontes, E., J. R. Patel, and F. Comin, Direct Measurement of the Asymmetric Dimer Buckling of Ge on Si(111), *Phys. Rev. Lett.* **70**, 2790 (1993).
- Franceschi, F., S. Weinstein, U. Evers, E. Arndt, W. Jahn, H.A.S. Hansen, K. von Bohlen, Z. Berkovitch-Yellin, M. Einstein, I. Agmon, J. Thygesen, N. Volkmann, H. Bartels, F. Schlunzen, A. Zaytzev-Bashan, R. Sharon, I. Levin, A. Dribin, I. Sagi, T. Choli-Papadopoulou, P. Tsiboly, G. Kryger, W.S. Bennett and A. Yonath, Towards Atomic Resolution of Prokaryotic Ribosomes: Crystallographic, Genetic and Biochemical Studies, *The Transition Apparatus*, K. Nierhaus Ed., (1993), 397-410.
- Gu G. and Y.K. Vohra, *Phys. Rev. B*, Phase Stability and Equation of State of the Transition Metal Alloy Mo-Re at High Pressure, *Rapid Communications*, **47**, (1993), 11559.
- Guo, H.C., D.R. Madden, M.L. Silver, T.S. Jardetzky, J.C. Gorga, J.L. Strominger, and D.C. Wiley, Comparison of the P2 Specificity Pocket in Three Human Histocompatibility Antigens: HLA-A\*6801, HLA-A\*0201, and HLA-B8\*2705, *Proc.Natl. Acad. Sci, USA*, **90**, 8053-8057.
- Haller, G.L. and G. Larsen, Characterization of Pt-Ni/KL-Zeolite Bimetallic Catalysts by Chemisorption, Catalysis and X-ray Absorption, *Proc. 9th Intern. Zeolite Conf*, R. van Ballmoos, J.B. Higgins and M.M.S. Treacy, eds., Butterworth Heinemann, Vol. **2**, (1993), 441.
- Haller, G.L. and G. Larsen, The Effect of Preparation Method on Metal-Support Interaction in Pd/L-zeolite Catalysts, *Proc. 10th Intern. Congr. Catal.*, A. L. Buczi, F. Solymosi, P. Tetenyl eds., (1993).
- Haller, G.L., A. Jentys, and J.A. Lercher, The Formation of Metallic Particles During Temperature Programmed Reduction of Silica Supported Pt and Ni Chlorides, *J. Phys. Chem.*, **97**, (1993).
- Haller, G.L., A. Jentys, M. Englisch and J.A. Lercher, Effects of Adsorbed Oxygen Containing Molecules On the XANES of Pt in Supported Pt/SiO<sub>2</sub> Catalysts, *Cataysis Letters*, **21**, (1993), 303.
- Harms, J., F. Schlunzen, K. von Bohlen, J. Thygesen, S. Meyer, I. Dunkel, B. Donzelmann, H.A.S. Hansen, A. Zaytzev-Bashan, A. Dribin, G. Kryger, G. Thoms, N. Volkmann, H. Bartels, W.S. Bennett and A. Yonath, The Effect of Cryogenic Treatment on the Cell Dimensions of Ribosomal Crystals, *ESF Report*, K. Wilson Ed., (1993), 26-29.
- Headrick, R. L., and J.M. Baribeau, Correlated Roughness in Headrick, R.L. and J. M. Baribeau, Interface Roughness in Ge/Si Superlattices, *J. Vac. Sci. and Technol. B*, **11** (1993), 1514.
- Headrick, R.L., J.M. Baribeau, D.J. Lockwood, T.E. Jackman, and M.J. Bedzyk, X-ray and Raman Scattering Characterization of Ge/Si Buried Layers, *Appl. Phys. Lett.* **62**, (1993), 687.
- Houde-Walter, S.N., J.M. Inman, A.J. Dent, and G.N. Greaves, Sodium and Silver Environments and Ion Exchange Processes in Silicate and Aluminosilicate Glasses, *J. Phys Chem.* **97**, (1993), 9330-9336.
- Huxley, H.E., A. Stewart, H. Sosa, T. Irving, Two Dimensional X-ray Diffraction Diagrams from Contracting Muscle Recorded on Imaging Plates with Millisecond Time Resolution Using Synchrotron Radiation, *Biophys. J.* **64**, (1993), A27.
- Jordan, E.H., S. Ochi, A. Rivera, and D.M. Pease, Internal Strain Measurement Using X-ray Opaque Markers, *Novel Experimental Techniques in Fracture Mechanics*, ed. A. Shukla, ASME WAM, **176**, (1993), 91-100.
- Kim, K.H., P. Willingmann, Z.X. Gong, M.J. Kremer, M.S. Chapman, I. Minor, M.A. Oliveira, M.G. Rossmann, K. Andries, G.D. Diana, F.J. Dutko, M.A. McKinlay, D.C. Pevear, A Comparison of the Anti-rhinoviral Drug Binding Pocket in HRV14 and HRV1A, *J. Mol. Biol.* **230**, (1993) 206-227.
- Koynova, R. and M. Caffrey, Mesophase Transition Temperatures as Measured by Fluorescence and Calorimetry, *Biophys. J.* **65**, (1993), 550.
- Krol, A., Y.L. Soo, S. Huang, Z.H. Ming, and Y.H. Kao, Local Structure About Mu Atoms in l-x Mux As Diluted Magnetic Semiconductors, *Phys. Rev. B* **47:12**, (1993), 7187.
- Kwak, B.S., G. D. Lei and W.M.H. Sachtler, EXAFS Evidence of Interaction Between Ga and Pt in HZSM-5, in *Catalysis in Environmental and Petrochemical Technologies*, Korea-Germany Catalysis Symp. (1993), 199-211.
- Lang, J.C., X.Wang, B.N. Harmon, A.I. Goldman, K.W. Dennis, R.W. McCallum, and K.D. Finkelstein, submitted to *Phys. Rev. B*, Brief Reports (1994).

- Lang, J.C., X.Wang, V.P. Antropov, B.N. Harmon, A.I. Goldman, H. Wan, G.C. Hadjipanayis, and K.D. Finkelstein, *Phys. Rev. B* (1994).
- Liddington R.C. and S.C. Harrison, Structure of Simian Virus 40, *Structure* **0**, (1993), xxii-xxiii.
- Lockwood, D.J., J.M. Baribeau, T.E. Jackman, P. Aebi, T. Tylliszczak, A. P. Hitchcock, and R.L. Headrick, Influence of Annealing on the Interface Structure and Strain Relief in Si/Ge Heterostructures, *Scanning Microscopy*, **7**, (1993),457-473.
- Luo H. and A. Ruoff, X-ray Diffraction Study of Sulfur at 32 GPa; Amorphization at 25 GPa, *Phys. Rev. B* **48**, (1993), 569.
- Madden, D.R., D.N. Garboczi, and D. C. Wiley, The Antigenic Identity of Peptide-MHC complexes: A Comparison of the Conformations of Five Viral Peptides Presented by HLA-A2, *Cell* **75**, (1993), 693-708.
- Mencke, A., A.C. Cheng, and M. Caffrey, A Simple Apparatus for Time-Resolved X-ray Diffraction Studies Utilizing Static Pressures and Pressure-jumps Up to 300MPa, *Rev. Sci. Instr.* **64**, (1993), 383-389.
- Oliveira, M.A., R. Zhao, W.M. Lee, M.J. Kremer, I. Minor, R.R. Rueckert, G.D. Diana, D.C. Pevear, F.J. Dutko, M.A. McKinlay, M.G. Rossmann, The Structure of Human Rhinovirus 16, *Structure* **1** (1993), 51-68.
- Rossmann, M.G., T.J. Smith, R.R. Rueckert, The Structure of Human Rhinovirus 14, *Structure*, Introductory issue: xxiv-xxv, (1993).
- Ruoff, A., H. Luo, C. Vanderborgh, H. Xia, K. Brister, V. Arnold, Production and Metrology of 5-mm X-ray Apertures for 100 keV Diffraction Studies in the Diamond Anvil Cell, *Rev. Sci. Instr.* **64**, (1993), 3462-3466.
- Ruoff, A., X-ray and Optical Research to 560 GPa: Metalization of Molecular Solids, Xe, S, O<sub>2</sub> and the Prospects For Metallic Hydrogen, *Strongly Coupled Plasmas* ed. by H.M. Van Horn and S. Schimaris, U. Rochester Press, (1993), 11.
- Sachtler, W.M.H. and Zongchao Zhang, Zeolite Supported Transition Metal Catalysts, *Advances in Catalysts* **39**, (1993), 129-220.
- Sachtler, W.M.H., Z. Zhang, A. Yu. Stakheev, and J.S. Feeley, Transition Metal/Zeolite Catalysts by Design: Nucleation and Growth of Mono-and Bimetallic Particles in Zeolite, *New Frontiers in Catalysis*, L. Guzzi, F. Solymosi, P. Tetenyi eds, Elsevier Science Pubs., (1993), 271-281.
- Shen, Q. and K.D. Finkelstein, *Rev. Sci. Instr.* (1993).
- Shen, Q. and K.D. Finkelstein, A Complete Characterization of X-ray Polarization State by Combination of Single and Multiple Bragg Reflections, *Rev. Sci. Instr.* **64**, (1993), 3451.
- Shen, Q., C.C. Umbach, B. Weselak, and J. M. Blakely, X-ray Diffraction for a Coherently Illuminated Si (001) Grating Surface, *Phys. Rev. B* **48**, (1993), 17967.
- Shen, Q., Effects of a General X-ray Polarization in Multiple-Beam Bragg Diffraction, *Acta Crystallogr.*, **A49**, (1993), 605.
- Sun, W.-Q., T. C. Irving and C. Leopold, Sugars and lipid phase transitions in relation to desiccation tolerance of seeds, to be published in *Physiologia Plantarum*.
- Thiel, D.J., D.H. Bilderback, and A. Lewis, Production of Intense Micrometer-sized X-ray Beams with Tapered Glass Monocapillaries, *Rev. Sci. Instrum.*, Vol. **64**, (1993), 2872.
- Thiel, D.J., P. Livins, E. A. Stern and A. Lewis, Microsecond-resolved XAFS of the triplet excited state of Pt<sub>2</sub>(P<sub>2</sub>O<sub>5</sub>H<sub>2</sub>)<sub>4</sub><sup>+</sup>, *Nature* **362**, 40-43 (1993).
- Tylliszczak, T., P. Aebi, A.P. Hitchcock, T.E. Jackman, J.M. Baribeau, and D.J. Lockwood, Simultaneous Multiple File EXAFS Analysis: Methodology and application to Buried Ge-Si Interfaces, *Jap. J. Appl. Phys.* **32**, (1993), 134-136.
- Vohra, Y.K., Onset of F-Bonding in Actinide and Lanthanide Metals at Ultrahigh Pressures, *Physica B*, **190**, (1993), 1.
- Weir, B.E., "Fabrication and analysis of Boron ordered d-doped layer in Si," submitted to the Physics and Engineering Physics Department at Stevens Institute of Technology, Hoboken NJ.
- Wu, H., M.G. Rossmann, The Canine Parvovirus Empty Capsid Structure, *J. Mol. Biol.*, **233**, (1993), 231-244.
- Wu, H., W. Keller, M.G. Rossmann, Determination and Refinement of the Canine Parvovirus Empty-Capsid Structure, *Acta Crystallogr.*, **D49**, (1993), 572-579.
- Wu, T.C., W.A. Bassett, P.C. Burnley, and M.S. Weathers, Shear-promoted Phase Transitions in Fe<sub>2</sub>SiO<sub>4</sub> and Mg<sub>2</sub>SiO<sub>4</sub> and the Mechanism of Deep Earthquakes, *J. of Geophys. Resch.* **98**, (1993), 19767-19776.
- Xia, H., Q. Xia and A. Ruoff, New High Pressure Structure of Gallium Nitride: Wurtzite to Rocksalt Phase Transition, *Phys. Rev. B*, **47**, (1993), 12925.
- Xia, H., Q. Xia, and A. Ruoff, BP at Megabar Pressures and its Equation of State to 110 GPa, *J. Appl. Phys.* **74**, (1993), 1660.
- Xia, Q., H. Xia, and A. Ruoff, Pressure Induced Rocksalt Phase of Aluminum Nitride: A Metastable Structure at Ambient Conditions, *J. Appl. Phys.*, **73**, (1993), 8198.
- Yonath A. and F. Franceschi, Structural Aspects of Ribosnucleo-protein Interactions in Ribosomes, *Current Opinion in Structural Biology* **3**, (1993), 45.
- Zhu T. and M. Caffrey, Thermodynamics, Thermomechanical and Structure Properties of an Asymmetric Phosphatidylcholine, *Biophys. J.* **65**, (1993), 939-954.
- Zlotnick, A., B.R. McKinney, S. Munshi, J. Bibler, M.G. Rossmann, J. E. Johnson, A Monoclinic Crystal with R32 Pseudo-symmetry: a Preliminary Report of Nodamura Virus Structure Determination, *Acta Crystallogr.* **D49**, (1993), 580-587.



CHES

**Cornell High Energy  
Synchrotron Source**

Wilson Laboratory  
Cornell University  
Ithaca, N.Y. 14853-8001